

# Single Molecule Conductance of Oligothiophene Derivatives

Emma J. Dell

Submitted in partial fulfillment of the requirements

for the degree of Doctor of Philosophy in the

Graduate School of Arts and Sciences

COLUMBIA UNIVERSITY

2015

© 2015

Emma J. Dell

All rights reserved

# **Abstract**

## **Single Molecule Conductance of Oligothiophene Derivatives**

**Emma J. Dell**

This thesis studies the electronic properties of small organic molecules based on the thiophene motif. If we are to build next-generation devices, advanced materials must be designed which possess requisite electronic functionality. Molecules present attractive candidates for these advanced materials since nanoscale devices are particularly sought after. However, selecting a molecule that is suited to a certain electronic function remains a challenge, and characterization of electronic behavior is therefore critical. Single molecule conductance measurements are a powerful tool to determine properties on the nanoscale and, as such, can be used to investigate novel building blocks that may fulfill the design requirements of next-generation devices. Combining these conductance results with strategic chemical synthesis allows for the development of new families of molecules that show attractive properties for future electronic devices. Since thiophene rings are the fruitflies of organic semiconductors on the bulk scale, they present an intriguing starting point for building functional materials on the nanoscale, and therefore form the structural basis of all molecules studied herein.

First, the single-molecule conductance of a family of bithiophene derivatives was measured. A broad distribution in the single-molecule conductance of bithiophene was found compared with that of a biphenyl. This increased breadth in the conductance distribution was shown to be explained by the difference in 5-fold symmetry of thiophene rings as compared to the 6-fold symmetry of benzene rings. The reduced symmetry of thiophene rings results in a restriction on the torsion angle space available to these molecules when bound between two metal electrodes

in a junction, causing each molecular junction to sample a different set of conformers in the conductance measurements. By contrast, the rotations of biphenyl are essentially unimpeded by junction binding, allowing each molecular junction to sample similar conformers. This work demonstrates that the conductance of bithiophene displays a strong dependence on the conformational fluctuations accessible within a given junction configuration, and that the symmetry of such small molecules can significantly influence their conductance behavior.

Next, the single-molecule conductance of a family of oligothiophenes comprising one to six thiophene units was measured. An anomalous behavior was found: the peak of the conductance histogram distribution did not follow a clear exponential decay with increasing number of thiophene units in the chain. The electronic properties of the materials were characterized by optical spectroscopy and electrochemistry to gain an understanding of the factors affecting the conductance of these molecules. Different conformers in the junction were postulated to be a contributing factor to the anomalous trend in the observed conductance as a function of molecule length.

Then, the electronic properties of the thiophene-1,1-dioxide unit were investigated. These motifs have become synthetically accessible in the last decade, due to Rozen's unprecedentedly potent oxidizing reagent -  $\text{HOF}\cdot\text{CH}_3\text{CN}$  - which has been shown to be powerful yet selective enough to oxidize thiophenes in various environments. The resulting thiophene-1,1-dioxides show great promise for electronic devices. The oxidation chemistry of thiophenes was expanded and tuning of the frontier energy levels was demonstrated through combining electron poor and electron rich units.

Finally, charge carriers in single-molecule junctions were shown to be tunable within a family

of molecules containing these thiophene-1,1-dioxide (TDO) building blocks. Oligomers of TDO were designed in order to increase electron affinity, maintain delocalized frontier orbitals, while significantly decreasing the transport gap. Through thermopower measurements, the dominant charge carriers were shown to change from holes to electrons as the number of TDO units was increased. This resulted in a unique system in which the charge carrier depends on backbone length, providing a new means to tune p- and n-type transport in organic materials.

Taken together, the results presented in this thesis offer an insight into how molecular symmetry and the accessible conformers within a junction have important consequences on conductance behavior. Additionally, thiophene-1,1-dioxide is shown to be an exciting unit for single molecule devices, especially when combined with electron rich thiophene flanking groups. By demonstrating, for the first time, a change in conductance pathway with molecular length, this work provides a framework for using frontier orbital levels to strategically design electronic building blocks.

# Contents

<b>List of Figures</b>	<b>iv</b>
<b>1 Introduction</b>	<b>1</b>
1.1 Motivation . . . . .	1
1.2 Scanning tunneling microscope break junction technique . . . . .	2
1.3 The thiophene moiety . . . . .	6
1.4 The thiophene-1,1-dioxide moiety . . . . .	7
1.5 Efforts in this thesis . . . . .	8
<b>2 Impact of molecular symmetry on conductance</b>	<b>11</b>
2.1 Preface . . . . .	11
2.2 Introduction . . . . .	11
2.3 Bithiophene vs Biphenyl . . . . .	12
2.4 Rotations in the Junction . . . . .	15
2.5 Rotational “snapshots” . . . . .	16
2.6 Calculations . . . . .	17
2.7 Conclusion . . . . .	20
2.8 Experimental section . . . . .	21
<b>3 Length-Dependent Conductance of Oligothiophenes</b>	<b>28</b>
3.1 Preface . . . . .	28
3.2 Introduction . . . . .	28
3.3 Synthesis of Oligothiophene Family <b>T<sub>n</sub></b> . . . . .	29

3.4	Unusual Length Dependence . . . . .	31
3.5	Frontier Energy Levels . . . . .	32
3.6	Coherent Tunneling Model . . . . .	33
3.7	Aggregation Studies . . . . .	36
3.8	Solvation Shell Studies . . . . .	38
3.9	Elongation Studies . . . . .	38
3.10	Conclusion . . . . .	40
3.11	Experimental Section . . . . .	42
<b>4</b>	<b>The Conductance of Thiophene-1,1-Dioxide Oligomers</b>	<b>48</b>
4.1	Preface . . . . .	48
4.2	Introduction . . . . .	48
4.3	Traditional Thiophene Oxidation . . . . .	49
4.4	Rozen's Reagent . . . . .	50
4.5	Synthesis of the <b>TDO<sub>n</sub></b> Family . . . . .	51
4.6	Single Molecule Conductance of the <b>TDO<sub>n</sub></b> Family . . . . .	55
4.7	Conclusion . . . . .	58
4.8	Experimental Section . . . . .	59
<b>5</b>	<b>Changing the Charge Carriers with Molecular Length</b>	<b>67</b>
5.1	Preface . . . . .	67
5.2	Introduction . . . . .	67
5.3	Oxidation Lowers the LUMO . . . . .	70
5.4	Thermopower Measurements . . . . .	71

5.5 Conclusion . . . . .	77
<b>6 NMR Characterization</b>	<b>78</b>
<b>Bibliography</b>	<b>94</b>

## List of Figures

1	Representation of the steps during the STM-BJ technique. a. The STM tip and gold substrate. b. The tip is brought into contact with the substrate and then pulled away. c. At a certain displacement, the gold contact ruptures. d. A molecule can bridge the junction. . . . .	3
2	Examples of conductance data. A. Sample conductance trace for gold-gold contacts with no molecules present. The top arrow shows the step at $1G_0$ when the gold wire is atomically thin. The bottom arrow shows the exponential decay of conductance after the junction breaks. B. Sample conductance trace when a molecule is present. The arrow shows the plateau corresponding to the molecular conductance. C. Two-dimensional conductance histogram. D. One-dimensional logarithmically binned histogram. . . . .	5
3	The different rotational symmetries of the 6-membered phenyl ring ( <b>P2</b> , top) as compared to the 5-membered thiophene ring ( <b>T2</b> , bottom) are reflected in their respective conductance measurements. . . . .	12
4	Synthesis of <b>T2</b> from 2,2'-bithiophene . . . . .	13
5	Sample conductance traces measured for <b>P2</b> and <b>T2</b> at 90 mV bias voltage. . . .	13
6	Logarithmically-binned conductance histograms of A. Biphenyl ( <b>P2</b> ); B. Bithiophene ( <b>T2</b> ); C. <b>T2-twist</b> ; D. <b>T2-flat</b> showing a Gaussian fit with full width at half maximum indicated by the arrows. . . . .	14
7	Schematic illustrating how ring symmetry impacts rotations for <b>P2</b> (left) and <b>T2</b> (right) when bound in a junction. . . . .	16

8	Synthesis of <b>T2-twist</b> . . . . .	17
9	Synthesis of <b>T2-flat</b> . . . . .	17
10	A-D. Calculated unrestricted (solid) and restricted (dashed) potential energy curves as a function of internal torsion angle. E-H. The distributions of torsion angles sampled during the first 10 restricted MD simulations (out of 500), where the distance between their Au-binding sulfur atoms is restricted to its initial value to reproduce the constraints imposed on each molecule when it binds in the break junction. Each curve represents the torsion angle distribution from an individual run. . . . .	18
11	Schematic of the <b>Tn</b> family where n = 1 - 6. Hexyl chains are installed on the longer oligomers for solubility as described in the experimental section. . . . .	29
12	Synthesis of <b>T3</b> . . . . .	29
13	Synthesis of <b>T5</b> . . . . .	30
14	Synthesis of <b>T6</b> . . . . .	30
15	A. Log-binned conductance histograms for the oligothiophenes <b>T1-T6</b> (100 bins/decade). B. Plot of the conductance as a function of the length of the molecules <b>T1-T6</b> . Conductances for <b>T1-T3</b> have a decay constant $\beta = 0.30 \text{ \AA}^{-1}$ and <b>T4-T6</b> have a decay constant $\beta = 0.71 \text{ \AA}^{-1}$ . . . . .	31
16	One dimensional conductance histograms for the <b>Tn</b> family. . . . .	32

17	A. Cyclic voltammograms performed in dichloromethane (DCM) with Ag/AgCl reference electrode, 0.1 M tetra butyl ammonium hexafluorophosphate as the electrolyte and a scan rate of 50 mVs <sup>-1</sup> for <b>T2-T6</b> . B. Solution UV-vis absorption spectra of <b>T2-T6</b> dissolved in DCM. C. HOMO/LUMO levels for <b>T2-T6</b> (HOMO levels obtained from the cyclic voltammetry data, and LUMO levels calculated using the UV-vis absorption spectra and the relationship $\Delta E_g = E_{HOMO} - E_{LUMO}$ )	33
18	a. Schematic of the tunneling model employed for transport calculations. b. Calculated low-bias transmission, showing qualitatively correct behavior for <b>T1-T4</b> , but not <b>T5</b> and <b>T6</b> . c. Calculated gating dependence of the transmission for <b>T3</b> and <b>T4</b> . d. Difference in energy between the molecular HOMO and the Fermi energy of the gold electrodes.	35
19	A. UV-vis absorption data taken in 1,2,4 trichlorobenzene (TCB) for <b>T4</b> at temperatures from 17°C to 55°C. B. UV-vis absorption data taken in TCB for <b>T5</b> at different concentrations, normalized to allow comparison of the onset of absorption. C. UV-vis absorption data for <b>T4</b> taken in different solvents. D. Conductance histograms for <b>T4</b> in three solvents: tetradecane (C14), 1,2,4 trichlorobenzene (TCB), and 1,2-dichlorobenzene (DCB).	37
20	Conductance histograms for <b>T4</b> in both ambient conditions and under argon.	38

21	A. Two-dimensional conductance histograms of <b>T3</b> , <b>T4</b> and <b>T5</b> . B. Plot of the conductance obtained from the 2D plot for a fully elongated junction (demarcated by the dashed lines in A) as a function of the length of the molecules <b>T1-T6</b> . Conductances for <b>T1-T3</b> have a decay constant $\beta = 0.46 \text{ \AA}^{-1}$ for <b>T1-T3</b> , and <b>T4-T6</b> have a decay constant $\beta = 0.60 \text{ \AA}^{-1}$ .	39
22	Comparison of the oxidation of different thiophene derivatives with traditional oxidizing agents (left) and Rozen's reagent (right).	50
23	Synthesis of bithiophene dioxide and terthiophene dioxide.	51
24	Normalized UV-vis absorption spectra taken in dichloromethane for unoxidized dibromo-bithiophene ( <b>4a</b> ) and dibromo-terthiophene ( <b>4b</b> ) together with their fully oxidized analogs ( <b>4c</b> and <b>4d</b> respectively).	52
25	Schematic of the <b>TDO<sub>n</sub></b> family where n = 1 - 4. Hexyl chains are installed on the longer oligomers for solubility as described in the experimental section.	52
26	Synthesis of <b>TDO1</b>	53
27	Normalized UV-vis absorption spectra taken in dichloromethane for terthiophene derivatives with different extents of oxidation.	53
28	Treatment of this quaterthiophene derivative with Rozen's reagent oxidizes just the middle two units resulting in <b>4.3</b> after the Stille coupling instead of <b>TDO4</b> .	55
29	Synthesis of <b>TDO4</b> .	55

30	A. Sample conductance versus displacement traces, laterally offset, for the <b>TDO<sub>n</sub></b> series. These traces display molecule-specific conductance features, which persist for longer displacements as the molecular length increases. B. One-dimensional log-binned conductance histograms, each composed of 20,000 traces, for <b>TDO1-TDO4</b> measured at a 10 mV bias in 1-octylbenzene. Arrows indicate peak conductance positions. Inset: Plot of conductance as a function of the number of oxidised thiophene monomer units ( <i>n</i> ) in <b>TDO1-TDO4</b> . Using $G \sim e^{-\beta L}$ , we obtain a decay constant of 1.04/n. (c) Two-dimensional conductance-displacement histogram for <b>TDO3</b> created by aligning all traces at the point where conductance crosses 0.5 $G_0$ , and then overlaying them. The color bar indicates number of counts per 1000 traces. . . . .	56
31	Two-dimensional conductance versus displacement histograms for the <b>TDO<sub>n</sub></b> series. . . . .	57
32	Semilog plot showing the decay in conductance for the <b>TDO<sub>n</sub></b> and <b>Tn</b> families with molecule length. . . . .	58
33	Crystal structure of <b>4.3</b> provided by Serge Ruccolo in Prof. Gerard Parkin's group. . . . .	63
34	Schematic demonstrating a HOMO-conducting molecule (left) and a LUMO-conducting molecule (right). The conductance pathway depends on which orbital aligns better with the Fermi level of gold ( $E_F$ ). . . . .	68
35	A. Normalized UV-vis absorption spectra for the <b>TDO<sub>n</sub></b> family measured in dichloromethane. B. Colors of the <b>TDO<sub>n</sub></b> family in solution. . . . .	69

36	A. Cyclic voltammograms for <b>TDO<sub>n</sub></b> performed in dichloromethane with Ag/AgCl reference electrode, 0.1 M tetrabutyl ammonium hexafluorophosphate as the electrolyte and a scan rate of 50 mVs <sup>-1</sup> . B. HOMO and LUMO levels in eV for the <b>TDO<sub>n</sub></b> family calculated from the cyclic voltammetry data as shown in Table 1.	70
37	Example of a transmission function that determines the probability that an electron of a given energy will tunnel through the molecular junction. Highlighted are sections in which $E_F$ aligns closer to the HOMO or LUMO of the molecule. The Seebeck coefficient is proportional to the slope of the transmission function and thus yields positive or negative values depending on the alignment. . . . .	72
38	Schematic of the scanning tunneling microscope break junction set up for simultaneous measurements of molecular conductance and thermopower. . . . .	73
39	Sample trace for thermopower measurements. Top panel: Sample piezo ramp used in collecting thermopower data, showing the motion of the tip away from the substrate over time. The hold is shown in the gray shaded area. Bottom panel: Sample current vs displacement trace (red) and voltage vs displacement trace (blue) for <b>TDO<sub>3</sub></b> . . . . .	74

40 A. STM-BJ measurements are taken with a temperature difference of 16 K between the gold tip and the substrate. While the molecule is bridged across the junction, the applied bias is dropped to zero and the current is measured. Seebeck coefficients for each junction are calculated using this current and compiled into the 1D histograms shown. The black curves are Gaussian fits to the Seebeck distributions. B. Plot of Seebeck coefficient as a function of molecular length for the **TDO**<sub>n</sub> family with error bars reflecting the standard deviation of the Gaussian fits. A shift from positive to negative Seebeck values is seen with increasing length, indicating a change in the charge carriers from holes to electrons. . . . . 75

This thesis was written with the unending support of my wonderful mum

and Charli XCX on loop

# 1 Introduction

## 1.1 Motivation

The birth of quantum mechanics at the dawn of the twentieth century tore apart the foundations of classical physics. Gone was the notion that objects at the nanoscale behave simply as smaller versions of their macroscopic counterparts. The quantum realm became ripe for discovery, and discovery abounded. Materials thinned to a single sheet were transformed from their bulk parents.<sup>1</sup> Crystals cut into smaller and smaller pieces suddenly changed color.<sup>2</sup>

This thesis focuses on one aspect of the quantum world: the behavior of a single molecule when wired into a circuit. Motivation is two-pronged; the fundamental interest in explicating the extraordinary behavior on this scale, and the more practical desire to miniaturize electronic components.<sup>3</sup> The latter is particularly important since our current silicon-based technology imposes a limit on transistor size of approximately 4 nm.<sup>4</sup> Bottom-up circuitry composed of individual molecules wired together entices as a means of circumventing this limit, and thus creating smaller, more complex devices.<sup>5</sup> In addition to their inherent nano-size, molecules are attractive components for electronic devices as a result of their easy chemical modification and purification.<sup>6–9</sup> The promise of molecular devices, however, depends upon the success of measuring and controlling the current flowing through a single molecule.<sup>10</sup> The central question thus becomes: how can we determine the conductance of a molecule?

## 1.2 Scanning tunneling microscope break junction technique

The conductance of a molecule,  $G$ , is defined as:

$$G = I/V \quad (1)$$

For  $G$  to be determined, a molecule must be wired into a circuit. The essential requirements for this are: a molecule-sized gap in a circuit, a way of incorporating a molecule into this gap, and a means of replicating the results so as to be statistically meaningful. To this end, a variety of metal-molecule-metal junctions have been designed over the last two decades which involve creating a sub-10 nm gap between two metals and the subsequent bridging of a molecule across that gap.<sup>11-14</sup> Good electronic coupling between the molecule and the metal electrodes is ensured through installing aurophilic linker groups such as amines or thiols at either end of the molecule.<sup>15-17</sup> All molecules in this thesis utilize methyl sulfide linkers. These groups form donor-acceptor bonds with the electrodes through the delocalization of the lone pair of electrons on the sulfur in SMe to an under coordinated gold atom.

The work in this thesis centers around one of these metal-molecule-metal junction techniques - the Scanning Tunneling Microscope Break Junction (STM-BJ). The STM-BJ technique was developed by Xu and Tao who demonstrated that molecular junction conductance could be measured by a gold scanning tunneling microscope tip that repeatedly makes and breaks contact with a gold substrate electrode surrounded by a solution of the sample molecules.<sup>11</sup>

The process is explained as follows: First, imagine the system with just the gold electrodes and no solution. A sharp gold tip is arranged above a gold substrate on a piezoelectric positioner (Figure 1a) and a small bias ( $\sim 100$  mV) is applied between them. Current is measured as a

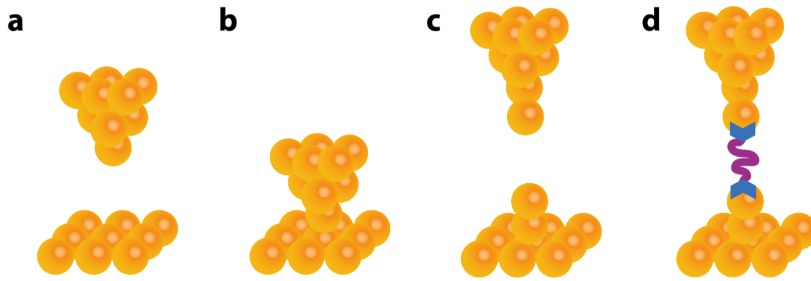


Figure 1: Representation of the steps during the STM-BJ technique. a. The STM tip and gold substrate. b. The tip is brought into contact with the substrate and then pulled away. c. At a certain displacement, the gold contact ruptures. d. A molecule can bridge the junction.

function of the tip distance above the substrate. As the tip is brought down to the substrate, a gold-gold contact is formed, completing the circuit (Figure 1b). The tip is then pulled away from the malleable surface at a rate of 10 nm/s, drawing a chain of gold atoms with it, and the conductance decreases as this emerging gold wire grows in length and thus resistance. At first, this decrease is linear in accordance with Ohm's law, but as the gold wire becomes atomically thin, the conductance becomes quantized. Stepwise drops in integer values of the quantum of conductance,  $G_0$  ( $2e^2/h = 77.4 \mu\text{S}$ , where  $e$  is the electron charge,  $h$  is the Planck constant, and S is the conductance unit), are therefore observed, down to a conductance of  $1G_0$  for a single-atom thick wire. At a certain displacement of tip and substrate, this chain of atoms ruptures, forming a gap in the circuit across which conductance decays exponentially (Figure 1c).

If molecules are present in solution on the substrate electrode, then this picture is altered slightly. The molecules may be initially bound through one of their end linker groups to the gold substrate. As the tip is brought into contact with this substrate, one or more molecules may bind to it using the linker group at their other end. When the tip is pulled away from the substrate, and the gold contact ruptures, a molecule may be left spanning this gap. The molecular conductance can therefore be measured (Figure 1d). Since the conductance quantum

unit,  $G_0$ , corresponds to complete transmission of electrons through the point contact between the electrodes, by measuring the molecular conductance in units of  $G_0$  we obtain a measure of how conductive the molecule is compared to a gold atom. As the tip is pulled further away, this molecular junction is also broken, and the process is then repeated.

The STM-BJ technique, therefore, allows for the rapid creation and measurement of thousands of molecular junctions. Additionally, several factors can be tuned during this process to allow for further exploration of electronic properties. Possible variables include the speed at which the tip is retracted, the bias across the junction, and whether or not the molecule is held in the junction for a period of time.

Example data that can be obtained using the STM-BJ technique are shown in Figure 2. An example trace for gold-gold contact rupture is shown in Figure 2A. As described, the conductance decreases as the tip is pulled further away from the substrate (displacement), and quantized conductance plateaus are seen until the point at which the junction breaks, after which the conductance decays exponentially. When molecules are present in solution around the gold-gold contacts, additional plateaus may be seen due to the formation of metal-molecule-metal junctions (Figure 2B).

To determine statistically meaningful molecular transport data, it is critical to average over thousands of these traces. For instance, the traces can be compiled together, using the  $1G_0$  rupture event as a point of alignment, to form a two-dimensional histogram as shown in Figure 2C. These two-dimensional histograms provide information about how the junction evolves with elongation, and thus its stability, and the feature length helps to confirm the identity of the molecule.

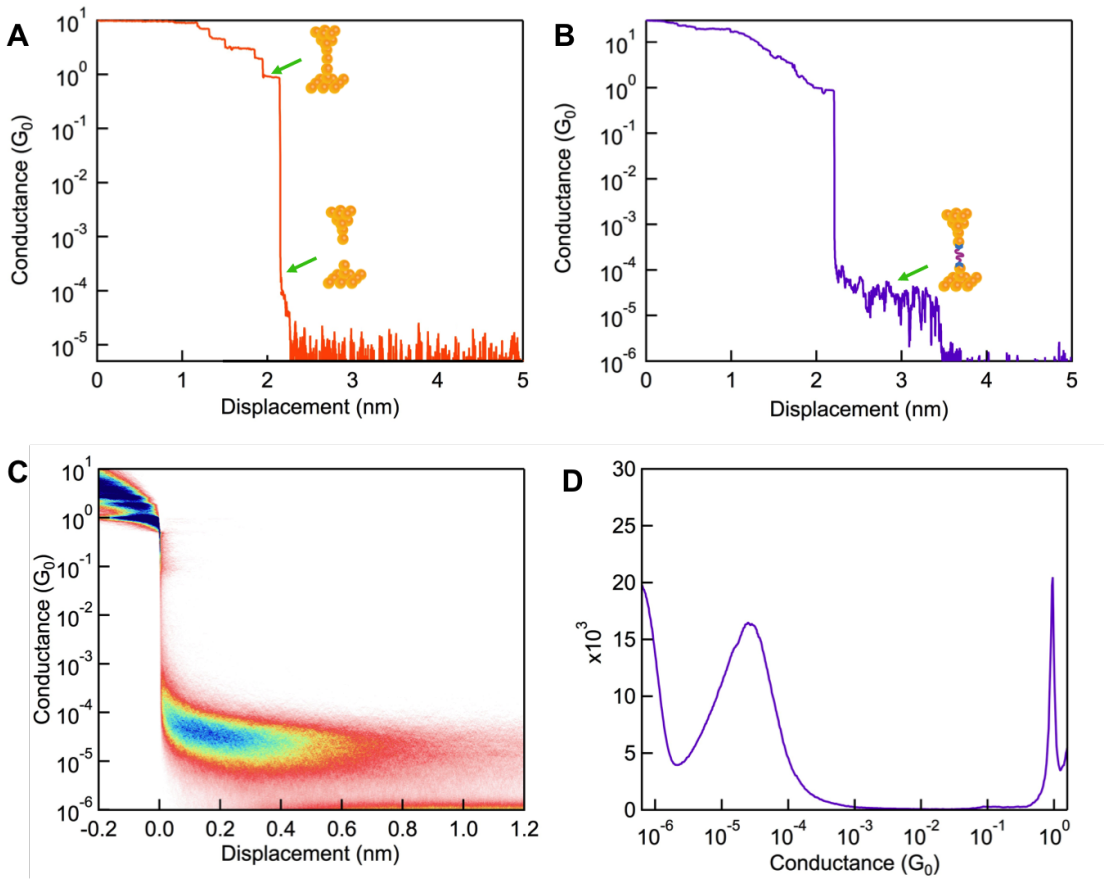


Figure 2: Examples of conductance data. A. Sample conductance trace for gold-gold contacts with no molecules present. The top arrow shows the step at  $1G_0$  when the gold wire is atomically thin. The bottom arrow shows the exponential decay of conductance after the junction breaks. B. Sample conductance trace when a molecule is present. The arrow shows the plateau corresponding to the molecular conductance. C. Two-dimensional conductance histogram. D. One-dimensional logarithmically binned histogram.

Additionally, data points can be binned along the conductance axis to form a one-dimensional histogram as shown in Figure 2D. These histograms show well defined molecular peaks, which can be fit using a Gaussian function to extract the most probable conductance value. Furthermore, if a family of molecules is measured with a common motif that increases in length, conductance changes across the series can be measured. For tunneling transport, conductance is expected to decrease exponentially with chain length. This decrease is characterized by the tunneling decay constant  $\beta$  which depends on the metal, the nature of the metal-molecule interface, and

the conductance pathway, and thus provides further information about the molecular transport properties.

### 1.3 The thiophene moiety

With the characterization tool established, we turn to the molecular substrates of interest. Poly- and oligothiophenes are ubiquitous throughout organic electronics as semiconducting electron-rich  $\pi$ -systems.<sup>18–22</sup> They have been incorporated into photovoltaic devices, light-emitting diodes, and thin-film transistors, to name just a few. Historically, polythiophenes were first prepared and demonstrated to be one-dimensional linear conjugated systems in 1980.<sup>23</sup> Oligothiophenes joined them as semiconductor powerhouses in 1989 when  $\alpha$ -sexithiophene was incorporated into field-effect transistors for the first time.<sup>24</sup> Work with polythiophenes flourished in particular after regioselective syntheses to soluble products were discovered,<sup>25</sup> and poly(3-hexylthiophene) remains the archetypical hole-transporting organic semiconductor.<sup>26</sup>



So why are these structures so frequently investigated? Their dominance stems firstly from their ease of chemical synthesis. Thiophene chemistry dates back to 1883,<sup>27</sup> and there are multiple straightforward methods with which to modify its structure.<sup>28</sup> Importantly, thiophenes are also ideal for metal-catalyzed cross-coupling reactions.<sup>29</sup> This synthetic versatility makes thiophene a highly tunable building block. Secondly, thiophene-based materials have favorable chemical stability, both in the conducting and the semiconducting state, in part due to the high polarizability of the sulfur atom, making them suitable for real-world applications.<sup>18</sup> Thirdly, their electronic properties are outstanding, with high electron mobilities and good on/off ratios.<sup>30</sup> Substituted polythiophenes have demonstrated high organizational capabilities and their

crystalline packing in the solid state strongly correlates with electron mobilities.<sup>31,32</sup>

The thiophene moiety is therefore well-established as an excellent candidate for bulk-scale electronics, so we were intrigued as to its behavior on the single-molecule scale. Up to now, oligothiophenes have received sparse attention in the realm of single-molecule studies.<sup>33-35</sup> Although previous work has demonstrated that oligothiophenes are conducting, a thorough investigation of the relationship between their molecular structure and conductance at the single-molecule level was lacking. Conductance measurements have the possibility to not only reveal the potential of thiophenes as building blocks for molecular devices, but also to act as a powerful characterization tool that could explicate structure-property relationships.

#### 1.4 The thiophene-1,1-dioxide moiety

In addition to investigating the single molecule conductance properties of oligothiophenes, we were also interested in how tuning the chemistry of these materials could affect their electronic behavior. In particular, we wanted to look at oxidized thiophene derivatives. The thiophene-1,1-dioxide moiety is a fledgling player in organic electronics, but yet it intrigues. In 1998, Barbarella and co-workers first explored the idea of exploiting the hypervalent nature of the sulfur atom in the thiophene unit to improve bulk electronic properties.<sup>36</sup> Their oxidation of the thienyl sulfurs to synthesize oligothiophene-1,1-dioxides for the first time opened the gateway to a new family of thiophene-based materials.<sup>37,38</sup> Underpinning this work is the rationale that oxidizing the thiophene moiety reduces its aromaticity. Thiophene is a  $6\pi$  aromatic system; two of the  $\pi$  electrons come from the lone pairs on the sulfur atom. After oxidation, sulfur's electrons are all engaged in covalent bonding, and the ring no longer fulfills Hückel aromaticity. In a system of consecutive oxidized rings, this reduced aromaticity



leads to increased delocalization along the molecular backbone, which is predicted to be concomitant with a decrease in the band gap.<sup>39</sup> Since narrow band-gaps and high backbone mobility are both key factors for organic electronics, thiophene-1,1-dioxide seemed very promising.

A major drawback, however, is that until recently, thiophene oxidation was extremely chemically challenging. Traditional oxidizing agents require long timescales, give poor yields and are unable to oxidize three or more adjacent thiophene units, stalling the progress of devices based upon thiophene-1,1-dioxide.<sup>40</sup> However, in 2005, Rozen and co-workers showed that a stabilized form of hypofluorous acid,  $\text{HOF}\cdot\text{CH}_3\text{CN}$ , could oxidize thiophenes at room temperature, in a matter of minutes and in high yields, opening up the possibility of incorporating the thiophene-1,1,-dioxide moiety into a host of materials.<sup>41</sup> We wanted to use this powerful oxidizing agent to synthesize thiophene-1,1-dioxide containing oligomers and study their single molecule conductance behavior. Since thiophene-1,1-dioxide is known to have dramatically altered frontier orbital energies as a result of the reduced aromaticity compared to thiophene, would this be reflected in the conductance?

## 1.5 Efforts in this thesis

This study proposed using the STM-BJ technique to investigate the single molecule conductance of oligothiophenes and their oxidized analogs. In Chapter 2, the conductance of a family of bithiophene derivatives terminated with methyl sulfide gold-binding linkers is investigated. The single molecule conductance of bithiophene shows a broad distribution compared with that of a methyl sulfide terminated biphenyl. It is demonstrated that this increased breadth in the conductance distribution may be explained by the difference in symmetry and thus rotational freedom of the 5-membered thiophene ring as compared to the 6-membered benzene ring. When

a bithiophene is bound between two metal electrodes in a junction, its rotational freedom is restricted, causing each molecular junction to sample a different set of conformers in the conductance measurements. This is not the case for biphenyl. This work highlights the impact of structure on conductance and shows that for bithiophene derivatives there is a strong dependence of conductance on the conformational fluctuations accessible within a given junction configuration, and that the symmetry of such molecules can significantly influence their conductance behaviors.

In Chapter 3, the single-molecule conductance of a family of oligothiophenes comprising one to six thiophene moieties terminated with methyl sulfide linkers is measured. The most fundamental study of the single molecule conductance length dependence of oligothiophenes was unknown in the literature. An anomalous behavior was observed in this study: the molecular conductances do not show a simple exponential decay with increasing chain length. Rather, the quaterthiophene derivative shows an unexpectedly high conductance. Optical spectroscopy and electrochemistry were used to determine the frontier orbital levels for these molecules. A number of factors including these energies, as well as aggregation and solvent effects are discussed to rationalize this odd behavior, and it is postulated that junction conformation may be a contributing factor.

In Chapter 4, the synthesis of a family of molecules containing the thiophene-1,1-dioxide moiety using Rozen’s reagent ( $\text{HOF}\cdot\text{CH}_3\text{CN}$ ) is described. Rozen and coworkers showed that this oxidation narrows the band gap of the molecules, and in particular, lowers the LUMO (lowest unoccupied molecular orbital),<sup>42</sup> and our family of molecules displays similar trends. Furthermore, single molecule conductance measurements are carried out on thiophene-1,1-dioxide containing

molecules for the first time. This family displays much higher conductance values than their unoxidized counterparts which is attributed to the increased conjugation through the molecular backbone. Additionally, using thermopower measurements,<sup>43,44</sup> in Chapter 5 it is shown that the conductance carriers changes from holes to electrons as the number of thiophene-1,1-dioxide units is increased. This is the first time that a change from HOMO (highest occupied molecular orbital) to LUMO conductance has been achieved simply by modulating the number of repeat units in a molecule, demonstrating how precise control over molecular design can have significant impact on the resultant electronic properties.

## 2 Impact of molecular symmetry on conductance

### 2.1 Preface

This chapter is based on a manuscript entitled *Impact of Molecular Symmetry on Single-Molecule Conductance* by Emma J. Dell†, Brian Capozzi†, Kateri H. DuBay, Timothy C. Berkelbach, Jose Ricardo Moreno, David R. Reichman, Latha Venkataraman, and Luis M. Campos published in the *Journal of the American Chemical Society*<sup>45</sup> (†equal contributions). The single molecule conductance experimental work was conducted by Brian Capozzi in Prof. Latha Venkataraman's group. Theoretical work was conducted by Dr. Kateri H. DuBay and Dr. Timothy C. Berkelback in Prof. David R. Reichman's group. Chemical synthesis was assisted by Jose Ricardo Moreno in Prof. Luis M. Campos' group.

### 2.2 Introduction

As the Scanning Tunneling Microscope Break Junction technique has grown in prominence as a tool to probe molecular conductance, several factors that affect the measurements have been elucidated. Although we use the term “molecular conductance” to describe the results obtained using this technique, these measurements are not carried out on a molecule in isolation. Rather, the molecule is bound between two metal electrodes through the aurophilic linker groups at its ends, and this binding influences its physical and electronic environment. The measured conductance therefore reflects both the molecule and its surroundings. Thus, in order to fully understand conductance measurements, one must be aware of these environmental factors.

It is well known that the conductance is sensitive to the properties of the electrodes, the orientation of the molecule-metal bonds, and the conformation of the molecular backbone.<sup>46–54</sup>

We show here that conductance is dependent on a further factor - the degree of symmetry afforded by the molecular backbone in a metal-molecule-metal junction. In order to do this, we compare the charge transport of molecules possessing different degrees of symmetry - a bithiophene derivative and a biphenyl derivative. The differences in ring symmetry are shown to impact the rotational freedom of the molecule in the junction, which in turn influences the molecular conductance distribution.<sup>45</sup>

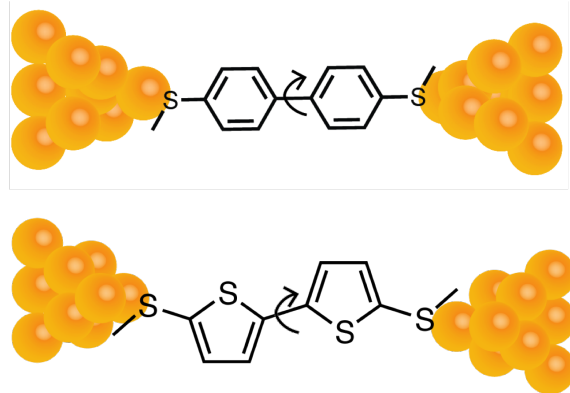


Figure 3: The different rotational symmetries of the 6-membered phenyl ring (**P2**, top) as compared to the 5-membered thiophene ring (**T2**, bottom) are reflected in their respective conductance measurements.

### 2.3 Bithiophene vs Biphenyl

We chose to compare thiophene, our particular motif of interest, with benzene, a similarly sized, aromatic unit, but of contrasting symmetry. The dimers of these rings were prepared bearing methyl sulfide end groups as a means of binding to the gold electrodes (the Au-S bond is known to provide effective electronic coupling in the STM-BJ set-up<sup>55</sup>). 5,5'-bisthiomethyl-2,2'-bithiophene (**T2**) was prepared as shown in Figure 4. The aurophilic methyl sulfide end groups were introduced through deprotonation with *n*-butyllithium, followed by nucleophilic reaction with dimethyl sulfide. The biphenyl analog, 4,4'-bis-(methyl sulfide)biphenyl (**P2**) was

purchased from Sigma Aldrich and used without purification.

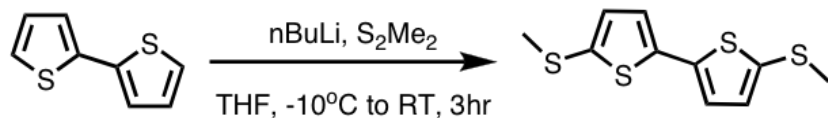


Figure 4: Synthesis of **T2** from 2,2'-bithiophene

The conductances of these two molecules were measured using the STM-BJ technique described in Chapter 1.<sup>11,12</sup> In short, gold atomic point contacts are repeatedly formed and then broken by driving a gold tip in and out of contact with a gold-on-mica substrate. (The gold tip is made from 0.25 mm high purity gold wire, and the substrate from 100 nm of high-purity gold evaporated onto freshly cleaved mica.) Individual molecular junctions are formed when the gold point contacts are broken in a solution of the target molecule (10 mM concentration, 90 mV bias voltage) in 1,2,4-trichlorobenzene. Thousands of conductance-displacement traces were collected for both **P2** and **T2**. These traces display plateaus close to integer multiples of the quantum of conductance,  $G_0$  ( $2e^2/h$ ), and an additional plateau at a conductance value lower than  $G_0$  (Figure 5). These additional plateaus are attributed to a molecule bridging the metal electrodes after the gold point contact is broken.

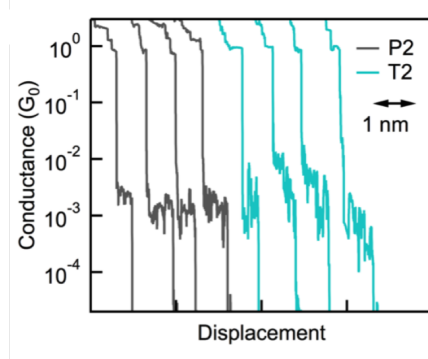


Figure 5: Sample conductance traces measured for **P2** and **T2** at 90 mV bias voltage.

All the conductance traces are compiled into logarithmically binned one-dimensional his-

tograms in order to determine the most frequently measured conductance value for these two molecules. Although the peak conductance positions of both molecules are similar, we were struck by the large full width at half maximum of the conductance histogram for **T2** when compared with that of the **P2** histogram (Figure 6 A and B).

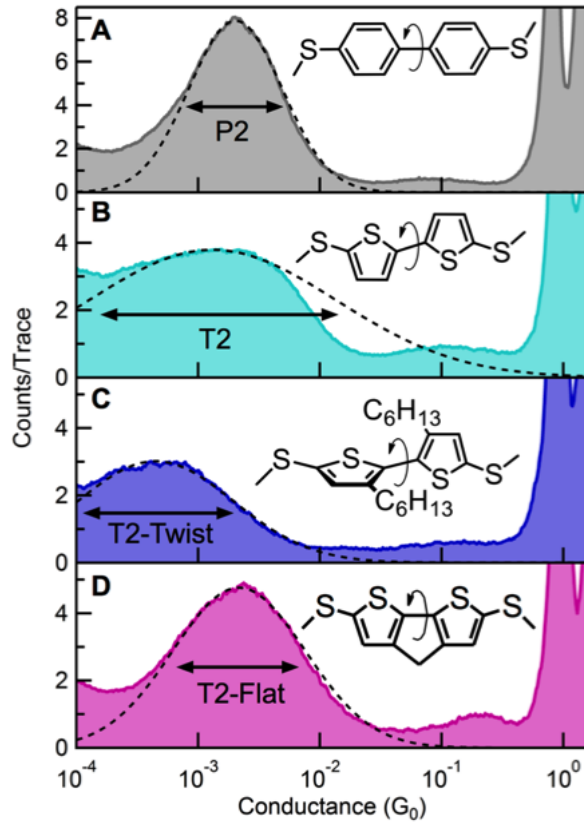


Figure 6: Logarithmically-binned conductance histograms of A. Biphenyl (**P2**); B. Bithiophene (**T2**); C. **T2-twist**; D. **T2-flat** showing a Gaussian fit with full width at half maximum indicated by the arrows.

As discussed in the introduction, molecular conductance is sensitive to environmental factors and therefore the conductance histogram will never display a perfectly sharp peak; there is always some inherent variation between each conductance measurement. The metal-molecule-metal contact geometry is dependent on the atomic-scale geometry of the electrodes which changes each time the tip smashes into the gold substrate, as well as the particular type of binding site

and the orientation of the Au-S-C donor-acceptor bonds relative to the molecular backbone.<sup>53</sup> These factors all lead to variation. However, since the **P2** and **T2** systems share the same electrodes and the same methyl sulfide binding groups, there is clearly an additional factor at play for the latter which leads to a much greater conductance distribution.

## 2.4 Rotations in the Junction

In solutions of **P2** and **T2** at room temperature, both the phenyl rings and the thiophene rings are able to freely rotate due to thermal fluctuations. For **P2**, containment between the electrodes has little effect on these rotations. Biphenyl has a C<sub>2</sub> axis of symmetry running through the molecule so rotations are blind to the restriction of the methyl sulfide end groups in a junction (Figure 7). Since the timescale of these rotations is significantly faster than the timescale of the measurements (100  $\mu$ s), the conductances of the various conformers that are energetically accessible in the junction are averaged. For the 5-fold thiophene system, however, the rotational degrees of freedom in solution differ from the junction when the linker groups are attached to the gold electrodes. The bithiophene does not contain a C<sub>2</sub> axis of symmetry through the molecule and therefore when it is bound in a junction, the barrier to rotation is increased; if the central bond is to rotate by 180°, either one of the electrodes is required to move laterally, or the rest of the structure is required to deform to accommodate the change (Figure 7).

Thus, for **T2**, the molecule is “stuck” in the conformation in which it enters the junction since its rotational freedom is limited. This in turn means that the conductance is strongly dependent on the molecule’s conformation imposed by the binding geometry. This is in contrast to the case for **P2**, where the conductance is independent of the conformation. This difference yields a conductance distribution for **T2** that has a full width at half maximum almost twice

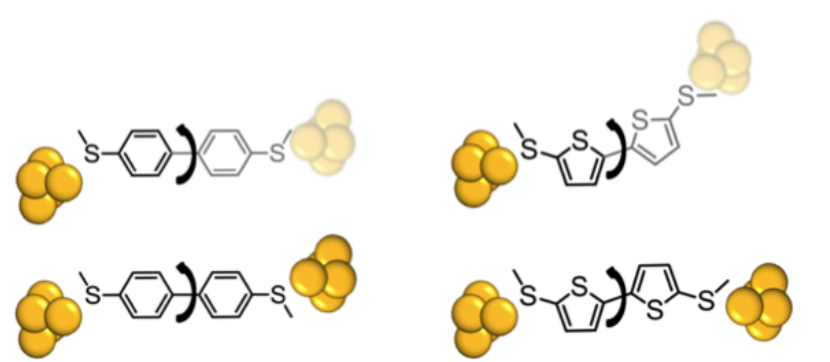


Figure 7: Schematic illustrating how ring symmetry impacts rotations for **P2** (left) and **T2** (right) when bound in a junction.

that of **P2**.

## 2.5 Rotational “snapshots”

In order to experimentally test this hypothesis that conductance is influenced by the allowed rotations for **T2**, we decided to synthesize two other bithiophene derivatives that represent “frozen snapshots” of the rotation in **T2**. **T2-twist**, a bithiophene derivative with hexyl chains installed at the 3,3’ positions was synthesized as shown in Figure 8. Direct deprotonation of 3-hexyl thiophene would occur regioselectively in the 5 position.<sup>56</sup> Bromination, on the other hand, occurs regioselectively at the 2 position. Thus, to install the boronic ester group at the 2 position, bromination is carried out first, followed by lithium halogen exchange under kinetic control in the second step. Suzuki coupling is then used to fuse the two thiophene rings together,<sup>57</sup> followed by installation of the methyl sulfide linker groups as before.

In **T2-twist**, the steric bulk of the alkyl chains forces the molecule to adopt a twisted conformation. Another bithiophene derivative, **T2-flat** was synthesized as shown in Figure 9.

In **T2-flat**, the internal rotation between the aromatic rings is locked by a saturated methylene linker. Due to their structural features, **T2-flat** and **T2-twist** already have restricted rotational freedom around the inter-ring torsion in solution, and therefore it is predicted that

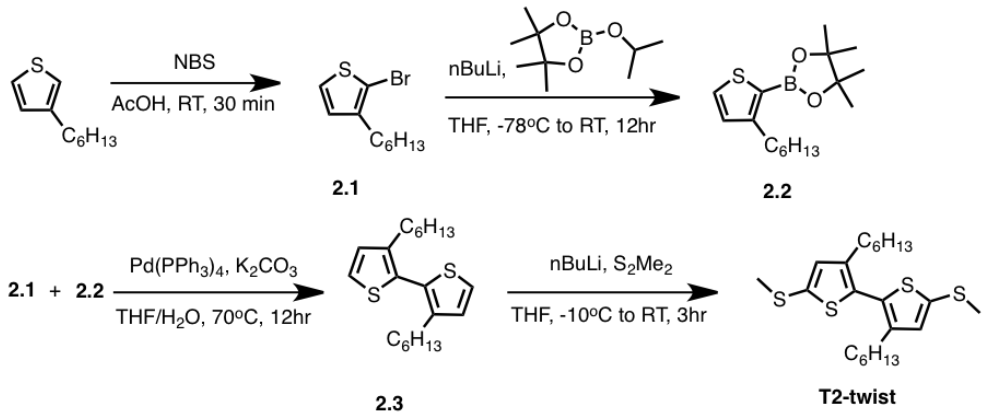


Figure 8: Synthesis of **T2-twist**

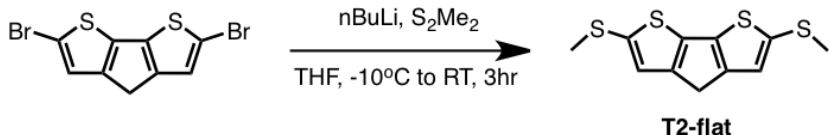


Figure 9: Synthesis of **T2-flat**

they will have fewer energetically accessible conformers that could be present in the junction as compared to **T2**. We measured the conductance of these molecules and we see that the conductance distributions for both the twisted and planar bithiophene derivatives are considerably narrower than that of **T2** (Figure 6 C and D). In addition, the conductance peak of **T2-flat** overlaps the higher-conducting portion of the conductance peak of **T2**, which would be expected from its enhanced electronic conjugation due to the forced planarity. By contrast, the peak of **T2-twist** overlaps the lower-conductance portion of the **T2** peak as expected from its reduced conjugation.

## 2.6 Calculations

To further probe this relationship between conductance and symmetry, we calculated the torsional potential energy curves for biphenyl and the bithiophene derivatives using OPLS-SB-T, a classical force field that has been specifically designed to correctly represent the effects of

conjugation in such biaryl systems.<sup>58</sup> For each system, the minimum energy unbound structure was determined while restricting the torsional angle,  $\theta$ , to a value between  $0^\circ$  to  $180^\circ$  in steps of  $10^\circ$ . This resulted in the solid potential energy curves shown in Figure 10 A - D.

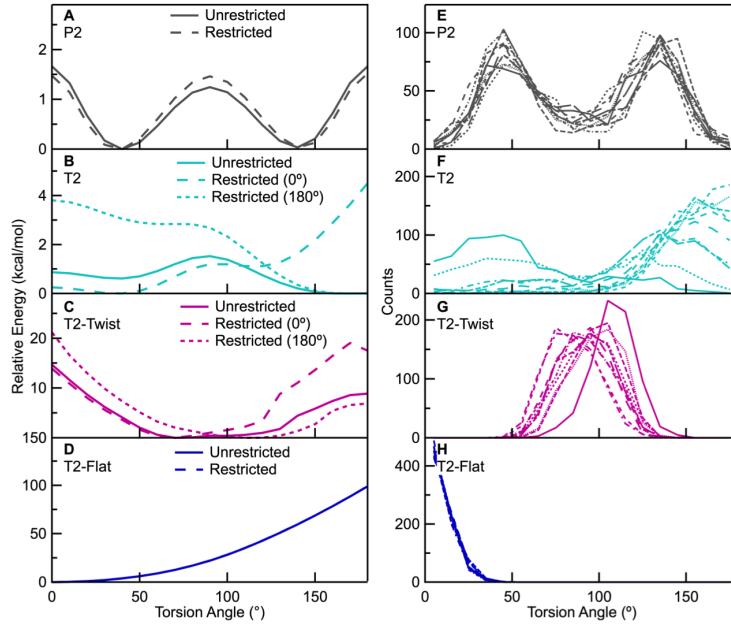


Figure 10: A-D. Calculated unrestricted (solid) and restricted (dashed) potential energy curves as a function of internal torsion angle. E-H. The distributions of torsion angles sampled during the first 10 restricted MD simulations (out of 500), where the distance between their Au-binding sulfur atoms is restricted to its initial value to reproduce the constraints imposed on each molecule when it binds in the break junction. Each curve represents the torsion angle distribution from an individual run.

In order to explore the additional barriers to torsional fluctuations that could be induced upon binding in the junction, the structures were then minimized with an additional restriction on the distance between the two sulfur atoms that act as Au-attachment sites. For **P2** and **T2-flat**, these atoms were frozen in their optimal positions when  $\theta = 0^\circ$  (as obtained from the minimized structure in the first step). For **T2** and **T2-twist**, these atoms were frozen in their optimal positions both when  $\theta = 0^\circ$  and when  $\theta = 180^\circ$ . The  $\theta = 180^\circ$  case was not investigated for **P2**, as it is identical to the  $\theta = 0^\circ$  case, or for **T2-flat** as it is clearly an inaccessible configuration. The potential energy curves calculated in the presence of these

additional restrictions are shown in Figure 10 A - D as dashed lines.

We see that for **P2** the restricted and unrestricted geometry potential energy curves are quite similar (Figure 10A), suggesting that junction binding should not bias the distribution of inter-ring torsional angles sampled during a conductance measurement. In contrast, the torsional potential of **T2** is significantly modified when the Au-binding S atoms are restricted, as evident in Figure 10B. This is due to the 5-fold symmetry of the thiophene ring, which imposes a constraint as discussed above. Given the heights of the barriers introduced when the distance between the Au-binding S atoms is fixed, which are several times the expected thermal fluctuations of the system at room temperature, the observed distribution of torsion angles in bithiophene will be significantly biased by the binding orientation of each molecule in the break junction. Since every measurement run has a different electrode structure (and this structure is changed as the junction is elongated), we expect the distributions of bithiophene torsional angles to vary significantly from junction to junction, and possibly also within each junction as it is elongated. As a result, the conductance measurements capture variations in junction binding, widening the measured conductance peak.

To further understand how the trapping of molecules in a junction might slow or restrict inter-ring rotations, we carried out room temperature molecular dynamics (MD) simulations of the four molecules. These simulations were run using DESMOND<sup>59</sup> and OPLS-SB-T. Each simulation consisted of a single molecule in a vacuum. Sampling was done within the NVT ensemble at 300 K, utilizing a Nose-Hoover thermostat. No cutoffs were implemented. In the initial step, all atoms were allowed to move without restriction, as would be the case for the molecules prior to their binding in the junction. This 51 ns simulation was allowed to equilibrate

for 1 ns and then starting configurations for the next set of simulations were collected every 100 ps, providing a total of 500 sample configurations that might be expected to “jump” into the junction. Then, in the second step, the distance between the molecules’ terminal sulfurs was held fixed in order to simulate the binding event (the pulling forces were not represented in this model). These simulations were run for 2 ns. The molecule was allowed to equilibrate for the first 1 ns, and then the position of  $\theta$  (the inter-ring dihedral angle) was recorded every 2 ps during the next ns, yielding 500  $\theta$ -values for each of the 500 different “bound” runs. Figure 10 E - H displays histograms of the inter-ring torsion angles sampled for the first 10 restricted MD simulations for all molecules. It is evident that the distributions are nearly identical for all biphenyl runs, whereas the distributions vary significantly from run to run for bithiophene. This further demonstrates that the conductance measured in a single bithiophene trace is limited to distinct sets of conformers dependent on the molecule’s various geometries as the junction extends.

## 2.7 Conclusion

Bithiophene exhibits a broad conductance distribution as compared to biphenyl. The reduced symmetry of bithiophene leads to a restriction of its interring torsion rotations when confined in a junction. This means that the conductance measured in a single bithiophene trace is dependent on the particular molecular conformation in the junction, whereas in a single biphenyl trace, the conformations are averaged through free rapid rotation. This is further exemplified by the conductance traces of **T2** derivatives that have structurally controlled reduced rotational freedom. Both **T2-twist** and **T2-flat** show conductance histograms with narrower full widths at half maximum. This work demonstrates the importance of considering the molecular backbone

symmetry when designing functional conducting molecular devices and also shows that current can be used to probe the structure of a molecule in a junction, expanding the scope of the characterization potential of the STM-BJ technique.

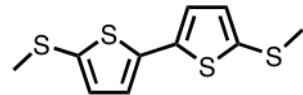
## 2.8 Experimental section

### General

All reactions were performed in oven-dried round bottom flasks. The flasks were fitted with rubber septa and reactions were conducted under a positive pressure of argon, unless otherwise noted. Anhydrous solvents were obtained from a Schlenk manifold with purification columns packed with activated alumina and supported copper catalyst (Glass Contour, Irvine, CA). Stainless steel syringes or cannulae were used to transfer air- and moisture-sensitive liquids. Flash column chromatography was performed employing 32-63  $\mu\text{m}$  silica gel (Dynamic Adsorbents Inc). Thin-layer chromatography (TLC) was performed on silica gel 60  $F_{254}$  plates (EMD). Commercial reagents were used without further purification with the exception of N-bromosuccinimide which was recrystallized from hot water. Commercial reagents purchased from Sigma Aldrich include *n*-butyllithium (2.5 M in hexanes), potassium carbonate, 5,5'-dibromo-2,2'-bithiophene, 2,2'-bithiophene, 2,2':5',2"-terthiophene, thiophene, 3-hexylthiophene, N-bromosuccinimide, 2-Isopropoxy-4,4,5,5-tetramethyl-1,3,2-dioxaborolane, triethylamine, 4,4'-bis-methylsulfanyl-biphenyl. Commercial reagents purchased from Strem Chemicals include Tetrakis (triphenylphosphine) palladium(0). Commercial reagents purchased from Acros Organics include tributyltin chloride, 2,5-dibromothiophene, dimethyl disulfide, 3,4-dibromo thiophene, n-hexyl magnesium bromide. Commercial reagents purchased from Lumtec include 2,6-Dibromo-4H-cyclopenta [2,1-b:3,4-b'] dithiophene. Proton nuclear magnetic resonance ( $^1\text{H}$  NMR) spectra

and carbon nuclear magnetic resonance ( $^{13}\text{C}$  NMR) spectra were recorded on a Bruker DRX300 (300 MHz) and a Bruker DRX400 (400 MHz) spectrometer. Chemical shifts for protons are reported in parts per million downfield from tetramethylsilane and are referenced to residual protium in the NMR solvent ( $\text{CDCl}_3$ :  $\delta$  77.0). Data are represented as follows: chemical shift, multiplicity (app = apparent, br = broad, s = singlet, d = doublet, t = triplet, q = quartet, m = multiplet), coupling constants in Hertz (Hz), and integration. The mass spectroscopic data were obtained at the Columbia University mass spectrometry facility using a JEOL JMSHX110A/110A tandem mass spectrometer. Absorption spectra were taken on a Shimadzu UV-1800 spectrophotometer. Electrochemical data were taken on a CH Instruments Electrochemical analyzer potentiostat assembly with a single cell. Samples were dissolved in dichloromethane containing 0.1 M of supporting electrolyte, tetra butyl ammonium hexafluorophosphate (TBAPF<sub>6</sub>). The measurements were carried out with a glassy carbon working electrode, a platinum wire counter electrode and a Ag/AgCl reference electrode. The potentials were measured against a Ag/AgCl reference electrode and each measurement was calibrated using ferrocene/ferrocenium (Fer) redox system.

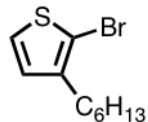
### 5,5'-bisthiomethyl 2,2'-bithiophene (T2)



An oven-dried 50 mL round bottom flask and stir bar were cooled under Ar. 2,2'-Bithiophene was added (500 mg, 3.01 mmol, 1 eq) and dissolved in 20 ml THF. The flask was cooled to -10°C. *n*-Butyllithium (2.5 M in hexanes, 2.4 mL, 6.01 mmol, 2 eq) was added dropwise by

syringe. The solution turned turquoise. The reaction was stirred at -10°C for 1 hour. Dimethyl disulfide (0.53 mL, 6.01 mmol, 2 eq) was added dropwise by syringe. The solution turned a milky yellow. The reaction was stirred at -10°C for 30 minutes and then allowed to warm to room temperature and stirred for another 2 hours. The reaction was quenched with water. The biphasic mixture was poured into a separatory funnel and the organic and aqueous layers were separated. The aqueous layer was extracted two times with diethyl ether (2 x 25 mL) and the combined organic layers were washed with water (30 mL) and brine (30 mL) and dried over magnesium sulfate. After filtration, the organic layer was concentrated under reduced pressure. Purification by column chromatography in 100% hexanes ( $R_f = 0.17$ ) yielded the product as a pale yellow solid (460 mg, 60% yield).  $^1\text{H}$  NMR (400 MHz,  $\text{CDCl}_3$ )  $\delta$  6.96 (s, 4H), 2.51 (s, 6H).  $^{13}\text{C}$  NMR (400 MHz,  $\text{CDCl}_3$ )  $\delta$  131.86, 123.94, 22.24. HRMS (FAB+) calculated for  $\text{C}_{10}\text{H}_{10}\text{S}_4$  258.45, found 258.78.

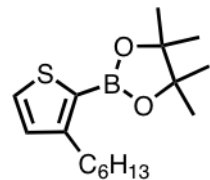
### **2-bromo, 3-hexyl thiophene (2.1)**



An oven-dried 50 mL round bottom flask and stir bar were cooled under Ar. 3-hexylthiophene (3 g, 17.8 mmol, 1 eq) was added and dissolved in 45 ml of acetic acid. N-bromosuccinimide (3.17 g, 17.8 mmol, 1 eq) was added and the solution was stirred for 30 minutes in the dark at room temperature. 45 mL of water was added and then the organic layer was extracted with diethyl ether (2 x 50 mL), washed with sodium hydrogen carbonate (2 x 50 mL), water (2 x 50 mL) and brine (50 mL) and dried over magnesium sulfate. After filtration, the organic layer was

concentrated under reduced pressure to yield a colorless oil (4.15 g, 94%). This crude product was used in the next stage without further purification.  $^1\text{H}$  NMR (400 MHz,  $\text{CDCl}_3$ )  $\delta$  7.19 (d,  $J = 5.6$  Hz, 1H), 6.81 (d,  $J = 5.6$  Hz, 1H), 2.58 (t,  $J = 7.7$  Hz, 2H), 1.62-1.56 (m, 2H), 1.36-1.30 (m, 6H), 0.94-0.90 (t, 3H).  $^{13}\text{C}$  NMR (400 MHz,  $\text{CDCl}_3$ )  $\delta$  142.09, 128.35, 125.24, 108.93, 31.77, 29.85, 29.54, 29.04, 22.75, 14.23. LRMS (ESI+) calculated for  $\text{C}_{10}\text{H}_{15}\text{BrS}$  247.20, found 246.01.

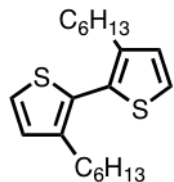
### **3-hexyl thiophene-2-boronic acid pinacol (2.2)**



An oven-dried 100 mL round bottom flask and stir bar were cooled under Ar. **3a** (3 g, 12 mmol, 1 eq) was added and dissolved in 40 mL THF. The solution was cooled to -78 °C. *n*-Butyllithium (2.5 M in hexanes, 5.5 mL, 13 mmol, 1.1 eq) was added dropwise by syringe and the solution was stirred for 30 minutes at -78°C. 2-Isopropoxy-4,4,5,5-tetramethyl-1,3,2-dioxaborolane (2.48 g, 13 mmol, 1.1 eq) was added dropwise by syringe. The solution was allowed to warm to room temperature and stirred overnight. The reaction was quenched by adding 30 mL of water. The organic layer was extracted with diethyl ether (2 x 40 mL), washed with water (50 mL) and brine (50 mL) and dried over magnesium sulfate. After filtration, the organic layer was concentrated under reduced pressure to yield a yellow oil (3.3 g, 92% yield). This crude product was used in the next stage without further purification.  $^1\text{H}$  NMR (400 MHz,  $\text{CDCl}_3$ )  $\delta$  7.47 (d,  $J = 4.6$  Hz, 1H), 7.01 (d,  $J = 4.7$  Hz, 1H), 2.89 (t,  $J = 7.7$  Hz, 2H), 1.65-1.57 (m, 2H), 1.33 (s, 12H), 1.29 (m, 6H), 0.91-0.89 (t, 3H).  $^{13}\text{C}$  NMR (400 MHz,  $\text{CDCl}_3$ )  $\delta$  154.83, 148.34, 131.39,

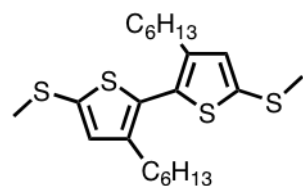
130.42, 83.65, 31.91, 31.81, 30.26, 29.11, 24.93, 22.76, 14.26. LRMS (APCI+) calculated for C<sub>16</sub>H<sub>27</sub>BO<sub>2</sub>S 294.26, found 294.23.

**3-3'dihexyl-2,2'-bithiophene (2.3)**



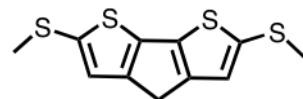
An oven-dried 2 necked 50 mL round bottom flask and stir bar were fitted with a condenser and cooled under Ar. **3a** (200 mg, 0.81 mmol, 1 eq) was added and dissolved in 5 mL of THF that had been sparged with Ar for 20 minutes. Potassium carbonate (112 mg, 0.81 mmol, 1 eq) dissolved in 5 mL of water that had been sparged with Ar for 20 minutes was added by cannula. Tetrakis(triphenylphosphine) palladium(0) (94 mg, 0.081 mmol, 0.1 eq) was added and the solution was heated to 70°C. **3b** (238 mg, 0.81 mmol, 1 eq) was added dropwise and the solution was refluxed at 70°C overnight. The solution was allowed to cool and then the organic layer was extracted with CHCl<sub>3</sub> (2 x 15 mL) and washed with water (20 mL) and brine (20 mL) and dried over magnesium sulfate. After filtration, the organic layer was concentrated under reduced pressure. Purification by column chromatography in 100% hexanes ( $R_f = 0.39$ ) yielded the product as a yellow oil (260 mg, 96% yield). <sup>1</sup>H NMR (400 MHz, CDCl<sub>3</sub>) δ 7.29 (d, J = 5.3 Hz, 2H), 6.97 (d, J = 5.2 Hz, 2H), 2.53 (t, 4H), 1.58-1.55 (m, 4H), 1.29-1.25 (m, 12H), 0.92-0.88 (t, 6H). <sup>13</sup>C NMR (400 MHz, CDCl<sub>3</sub>) δ 14.0, 22.6, 28.8, 29.1, 30.7, 31.6, 125.2, 128.5, 128.7, 142.3 LRMS (APCI+) calculated for C<sub>20</sub>H<sub>30</sub>S<sub>2</sub> 334.58, found 334.11.

**5,5' bisthiomethyl 3,3' dimethyl 2,2' bithiophene (T2-twist)**



The title compound was prepared on a 0.30 mmol scale according to the procedure for compound **2** with the following modification: **3c** (100 mg, 0.30 mmol) was used instead of 2,2'-bithiophene. Purification by column chromatography in 100% hexanes ( $R_f = 0.16$ ) yielded the product as a yellow oil (59 mg, 46% yield).  $^1\text{H}$  NMR (400 MHz,  $\text{CDCl}_3$ )  $\delta$  6.89 (s, 2H), 2.51 (s, 6H), 2.42 (t, 4H), 1.52 (m, 4H), 1.21 (m, 12H), 0.86 (t, 6H).  $^{13}\text{C}$  NMR (400 MHz,  $\text{CDCl}_3$ )  $\delta$  143.11, 137.09, 131.83, 130.29, 31.75, 30.71, 29.21, 29.03, 22.71, 21.66, 14.22. LRMS (APCI+) calculated for  $\text{C}_{22}\text{H}_{34}\text{S}_4$  426.77, found 425.82.

**2,6-dithiomethyl-4H-cyclopenta[2,1-b:3,4-b']dithiophene (T2-flat)**



An oven-dried 25 mL round bottom flask and stir bar were cooled under Ar. 2,6-Dibromo-4H-cyclopenta[2,1-b:3,4-b']dithiophene (100 mg, 0.29 mmol, 1 eq) was added and dissolved in 7 mL THF. The solution was cooled to -78°C. *n*-Butyllithium (1 M in hexanes, 0.60 mL, 0.59 mmol, 2 eq) was added dropwise by syringe and the solution was stirred for 10 minutes at -78°C. The solution turned yellow upon addition of *n*-butyllithium. Dimethyl disulfide (56 mg, 0.59 mmol, 2 eq) was added dropwise by syringe and the solution turned a brighter yellow. The solution was allowed to warm to room temperature and stirred overnight. The solution was washed with water

(2 x 20ml), dried over magnesium sulfate. After filtration, the organic layer was concentrated under reduced pressure. Purification by column chromatography in 100% hexanes ( $R_f = 0.23$ ) yielded the product as a pale orange powder (20 mg, 25% yield).  $^1\text{H}$  NMR (400 MHz,  $\text{CDCl}_3$ )  $\delta$  7.14 (s, 2H), 3.48 (s, 2H), 2.50 (s, 6H).  $^{13}\text{C}$  NMR (400 MHz,  $\text{CDCl}_3$ )  $\delta$  148.53, 141.34, 136.65, 128.79, 32.48, 23.33. HRMS (ESI+) calculated for  $\text{C}_{11}\text{H}_{10}\text{S}_4$  270.46, found 270.08.

### 3 Length-Dependent Conductance of Oligothiophenes

#### 3.1 Preface

This chapter is based on a manuscript entitled *Length-Dependent Conductance of Oligothiophene* by Brian Capozzi†, Emma J. Dell†, Timothy C. Berkelbach, David R. Reichman, Latha Venkataraman, and Luis M. Campos published in the *Journal of the American Chemical Society*<sup>60</sup> (†equal contributions). The single molecule conductance experimental work was conducted by Brian Capozzi in Prof. Latha Venkataraman’s group. Theoretical work was conducted by Dr. Timothy C. Berkelback in Prof. David R. Reichman’s group.

#### 3.2 Introduction

Following on from our study investigating how the rotational properties of bithiophenes affect their molecular conductance, we wanted to characterize the length dependent conductance behavior of a whole series of oligothiophenes. Oligothiophenes have received surprisingly scant attention in single-molecule studies despite being behemoths in the semiconducting world. A small body of work has shown that oligothiophenes are conducting, but a thorough investigation into the relationship between their molecule structure and conductance is lacking in these systems. Prior studies on small oligothiophene chains focussed on molecules with an aliphatic methylene carbon separating the rings from the linker groups and thus interrupting the  $\pi$  conducting system.<sup>33,35</sup> Longer oligothiophene molecular wires, surrounded by alkylsilyl groups, starting at five repeat units were investigated by Tada and coworkers,<sup>34,61</sup> in addition to wires completely encapsulated by fluorene units.<sup>62</sup> These functional groups along the backbone may affect conformational and electronic properties.

A study of bare oligothiophene wires containing gold-binding linkers directly attached to the thiophene moieties had not been carried out. Tao and coworkers compared the conductance properties of two oligothiophene derivatives: the ter- and quaterthiophene analogs.<sup>33</sup> They demonstrated that the latter shows a higher conductance, and they attribute this to quaterthiophene's HOMO's level being better aligned with the Fermi level of gold than terthiophene. Inspired by this result and wanting to place it into the context of a whole family of oligothiophenes, we set out to study molecules containing one to six repeat thiophene units (Figure 11). Through this work, we uncover an unusual length-dependent conductance for the oligothiophenes, and we focus on understanding the unexpectedly high conductance of quaterthiophene.<sup>60</sup>

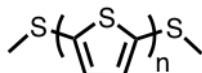


Figure 11: Schematic of the **T<sub>n</sub>** family where  $n = 1 - 6$ . Hexyl chains are installed on the longer oligomers for solubility as described in the experimental section.

### 3.3 Synthesis of Oligothiophene Family T<sub>n</sub>

We synthesized a family of methyl-sulfide terminated oligothiophene with one to six repeat units. Thiophene rings were coupled together through Stille reactions.<sup>63</sup> The synthesis of the three-membered oligomer, **T3**, is shown in Figure 12. 2,5-Dibromothiophene is reacted with one

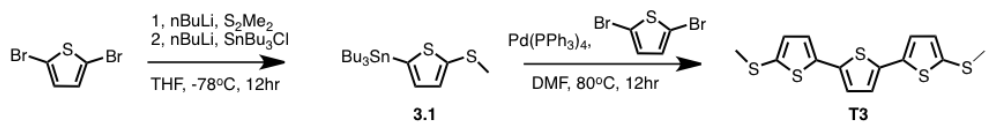


Figure 12: Synthesis of **T3**.

equivalent of *n*-butyllithium and the resultant anion then reacts with dimethyl disulfide to install the methyl sulfide linker groups. This is followed by a second equivalent of *n*-butyllithium and a nucleophilic reaction with tributyltin chloride to form the stannane, **3.1**. This stannane is used

as a generic coupling partner to form both **T3** and **T4** through palladium catalyzed coupling reactions. The synthesis of **T5** follows a similar pattern, except a bithiophene stannane (**3.2**)

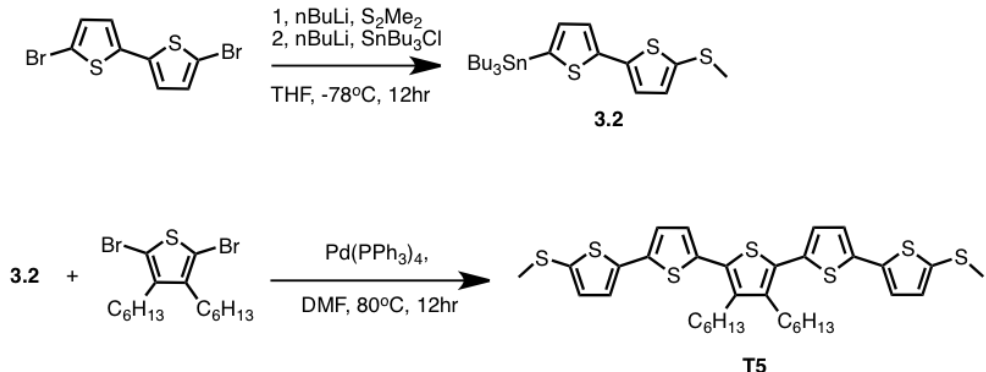


Figure 13: Synthesis of **T5**.

is used and hexyl groups are introduced on the middle thiophene ring to improve solubility (Figure 13). The synthesis of **T6** again uses the bithiophene stannane (**3.2**) as one of the coupling partners, and uses 5,5'-dibromo-4,4'-dihexyl-2,2'-bithiophene (**3.3**) as the aryl halide partner (Figure 14). Again, two hexyl groups are introduced onto this dihalide for solubility. **3.3** is synthesized through a palladium-catalyzed homocoupling reaction.<sup>64</sup> 2-Bromo 3-hexyl thiophene (**2.1**) is treated with silver (I) nitrate and potassium fluoride in the presence of  $\text{PdCl}_2(\text{PhCN})_2$  resulting in coupling at the C-H bond adjacent to the sulfur atom.

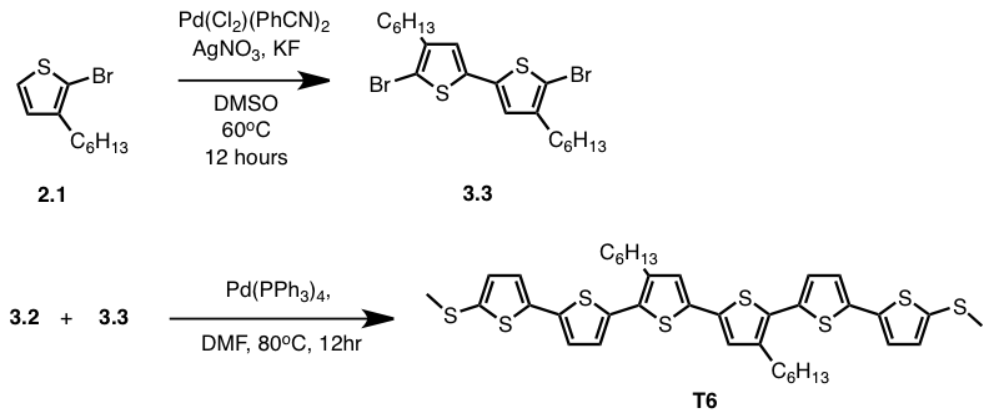


Figure 14: Synthesis of **T6**.

### 3.4 Unusual Length Dependence

The single molecule conductances of the **Tn** family were measured. The results show an unusual conductance trend. We do not see a clear exponential decrease of conductance with oligomer length, as would be expected for coherent tunneling (Figure 15).<sup>65</sup> The shorter **T1-T3** fall on

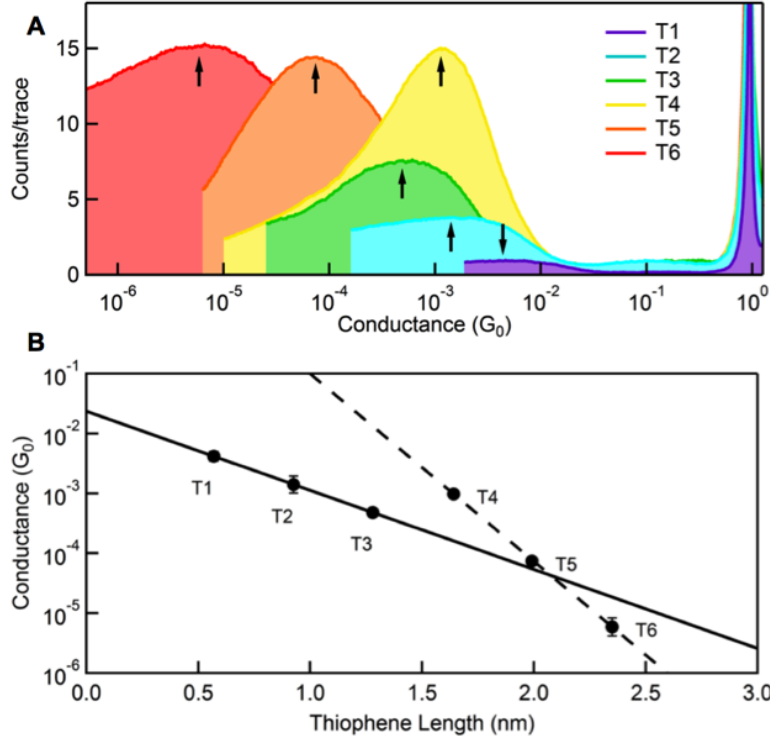


Figure 15: A. Log-binned conductance histograms for the oligothiophenes **T1-T6** (100 bins/decade). B. Plot of the conductance as a function of the length of the molecules **T1-T6**. Conductances for **T1-T3** have a decay constant  $\beta = 0.30 \text{ \AA}^{-1}$  and **T4-T6** have a decay constant  $\beta = 0.71 \text{ \AA}^{-1}$ .

an exponential (i.e.  $G \sim e^{-\beta L}$ ) with a decay constant of  $0.30 \text{ \AA}^{-1}$ , a value that is close to that of other conjugated systems.<sup>66,67</sup> However, **T4** appears to have a higher conductance than **T3**, and the longer oligomers show a larger decay ( $0.71 \text{ \AA}^{-1}$ ), closer to those seen for saturated systems. This result is in contrast to measurements of alkanes<sup>55,68-70</sup> or oligoenes<sup>71,72</sup>, where the conductance of oligomers can be fit with a single exponential. (Individual one-dimensional histograms for the **Tn** series are shown in Figure 16.)

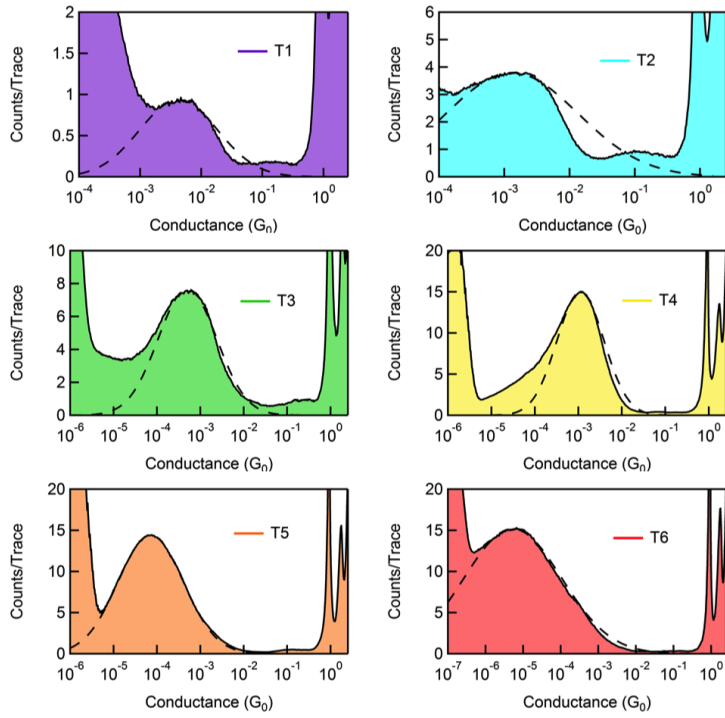


Figure 16: One dimensional conductance histograms for the **T<sub>n</sub>** family.

### 3.5 Frontier Energy Levels

As discussed in the introduction, a higher conductance for **T4** as compared to **T3** has been observed before.<sup>33</sup> Since this behavior was attributed to the HOMO of quaterthiophene being closer to the gold Fermi level than that of terthiophene, we wanted to ascertain the numerical values of the HOMO levels. We therefore performed cyclic voltammetry (CV) and UV-vis absorption measurements on **T2-T6** in order to determine the frontier energy levels of the oligomers (Figure 17). The HOMO was determined from the oxidation potential ( $E_{ox}$ ) by CV, and the LUMO was deduced from  $E_{ox}$  and the optical energy gap at the wavelength absorption onset from the UV-vis spectrum. We observe that the changes in the HOMO level as the number of thiophenes increases are fairly small, indicating that the anomalously high conductance may not solely be due to changes in the energy level alignment of **T4**. In fact, **T5** and **T6** show almost

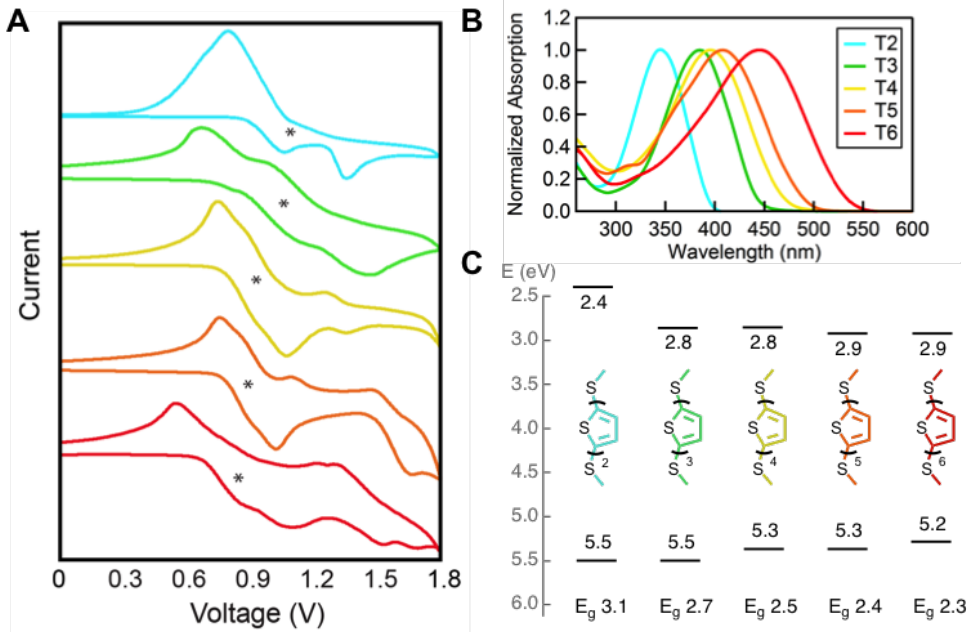


Figure 17: A. Cyclic voltammograms performed in dichloromethane (DCM) with Ag/AgCl reference electrode, 0.1 M tetra butyl ammonium hexafluorophosphate as the electrolyte and a scan rate of  $50 \text{ mVs}^{-1}$  for **T2-T6**. B. Solution UV-vis absorption spectra of **T2-T6** dissolved in DCM. C. HOMO/LUMO levels for **T2-T6** (HOMO levels obtained from the cyclic voltammetry data, and LUMO levels calculated using the UV-vis absorption spectra and the relationship  $\Delta E_g = E_{\text{HOMO}} - E_{\text{LUMO}}$ )

the same oxidation potential as **T4**, which suggests that the HOMO does not get significantly closer to the Fermi level as the molecular length is increased. Had this been the factor that explains the anomaly, we would expect **T5** and **T6** to display conductance values similar to (or larger than) that of **T4**, contrary to what is seen experimentally.

### 3.6 Coherent Tunneling Model

Further insight into this hypothesis can be obtained from a coherent tunneling model. Since these molecules conduct through the HOMO, we construct a simplified Hamiltonian describing an oligomeric molecule ( $M$ ) with  $N$  bridge sites, each representing the HOMO of a single thiophene unit ( $N = 1-6$  for **T1-T6**) to elucidate the effect of increasing molecular length on the transmission characteristics (the linker gateway state is neglected for simplicity). The Hamil-

tonian also includes the coupling to the left ( $L$ ) and right  $R$ ) gold electrodes. Specifically, we use:

$$H = H_L + H_R + H_M + H_{ML} + H_{MR} \quad (2)$$

with:

$$H_M = \sum_{n=1}^N \epsilon_H |n\rangle\langle n| + \sum_{n=1}^{N-1} t_H (|n\rangle\langle n+1| + HC) \quad (3)$$

$$H_L + H_R = \epsilon_s (|L\rangle\langle L| + |R\rangle\langle R|) \quad (4)$$

$$H_{ML} + H_{MR} = t_s (|L\rangle\langle 1| + |N\rangle\langle R|) + HC \quad (5)$$

where  $HC$  denotes the Hermitian conjugate of preceding terms. In the above equation,  $\epsilon_s$  is the gold s-orbital energy,  $t_s$  is the coupling between the molecule and the gold,  $\epsilon_H$  is the single-site HOMO energy, and  $t_H$  is the intersite HOMO coupling. The model system is shown schematically in Figure 18A.

The transmission coefficient,  $T(E)$ , is calculated using standard Green's function techniques, accounting for hybridization with the electrodes via an imaginary constant self energy  $\Sigma = -i\Gamma/2(|L\rangle\langle L| + |R\rangle\langle R|)$ , yielding  $T(E) = \Gamma^2 |G_{L,R}(E)|^2$ , where  $G_{L,R}(E) = L|(E - H - \Sigma)^{-1}|R$ . The energy-dependent transmission coefficient is evaluated at the Fermi energy, which assumes low bias transport.

Using reasonable approximations for the HOMO electronic coupling and the electrode hybridization, we considered the effect of varying the offset between the HOMO site energies and the electrode Fermi energy. Through this procedure, we are simply seeking to identify a regime where we can observe an increased conductance for **T4** compared to **T3**. When far from res-

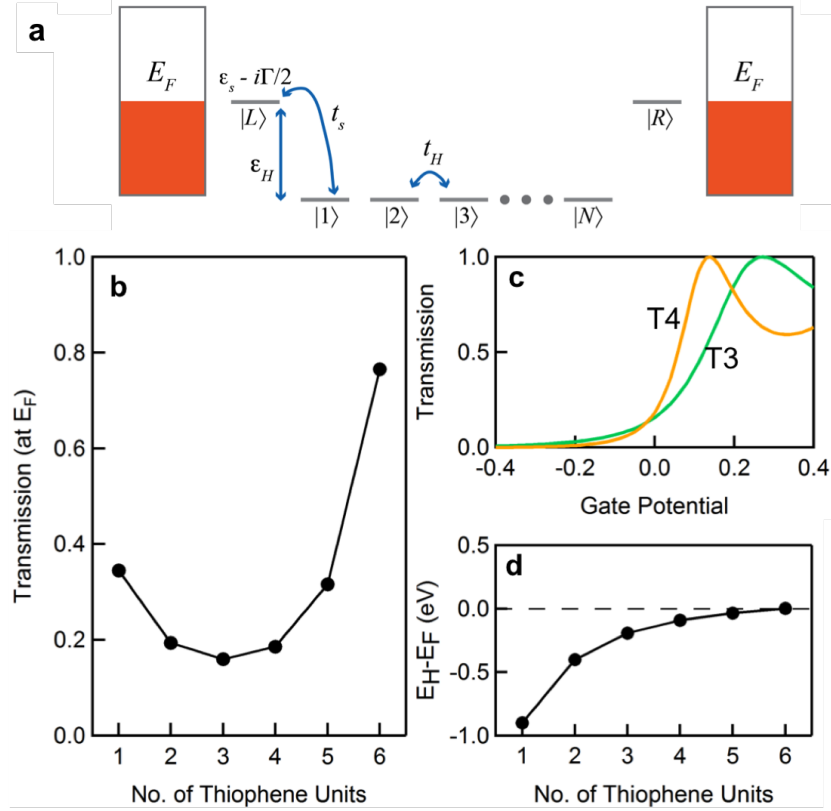


Figure 18: a. Schematic of the tunneling model employed for transport calculations. b. Calculated low-bias transmission, showing qualitatively correct behavior for **T1-T4**, but not **T5** and **T6**. c. Calculated gating dependence of the transmission for **T3** and **T4**. d. Difference in energy between the molecular HOMO and the Fermi energy of the gold electrodes.

onance, the transmission coefficient displays purely exponential behavior with the number of bridge sites, as typically observed.<sup>73,74</sup> By raising the HOMO site energy, one can realize a situation whereby the transmission decays for **T1-T3**, but increases for **T4**, as observed experimentally (Figure 18B). The parameters required for this behavior also qualitatively reproduce the gating dependence observed by Tao and coworkers for **T3** and **T4** (Figure 18C). However, this resonance effect persists for **T5** and even more so for **T6**, predicting a continued increase in the conductance, contrary to what is seen experimental. This behavior can be understood by tracking the molecule's HOMO energy  $E_H$  as a function of length, which demonstrates the increased resonance for **T5** and **T6** (Figure 18D). The evolution of the molecular HOMO energy

is seen to be in good agreement with the CV results (Figure 17). However, the lack of agreement between the measured and predicted conductance trends for **T3-T6** indicate that in a molecular junction, the HOMO is not getting significantly closer to  $E_F$ . Thus, transport in these systems is due to a far off-resonance tunneling mechanism. In this regime, small changes in the location of  $E_H$  relative to  $E_F$  have a negligible impact on the trend in conductance as a function of molecular length. This simple model presented here fails to explain the data, confirming our proposition that the experimental behavior is not due to enhanced resonance effects.

### 3.7 Aggregation Studies

A second possible explanation for the non-exponential decay in conductance could be that the **T4** molecules are forming  $\pi$ -aggregates in solution leading to a higher conductance pathway. It has been postulated previously that oligothiophenes may form such  $\pi$ -aggregates in solution and Tada and coworkers have synthesized oligomers bearing groups that can hinder such aggregation.<sup>62</sup> However, oligothiophenes are known to pack in a herringbone structure in the solid-state, and such a packing would not enhance the conductance of molecular junctions.<sup>75-77</sup> Nonetheless, we investigated whether the molecules formed aggregates in solution by studying the temperature, concentration, and solvent dependence on their UV-vis absorption spectra. Solutions of the oligothiophenes in 1,2,4 trichlorobenzene, TCB, (the same solvent used for the conductance measurements) were cooled from 55°C to 17°C. During cooling, no change (bathochromic or hypsochromic) is seen in the onset of absorption of the oligothiophenes (Figure 19A). Solutions of aggregates typically show reductions in their extinction coefficients and blue shifts on the order of 50 nm upon cooling.<sup>78-80</sup> Thus, the spectra are indicative of free molecules in solution. Changes in concentration should also affect the spectra of aggregates since at lower con-

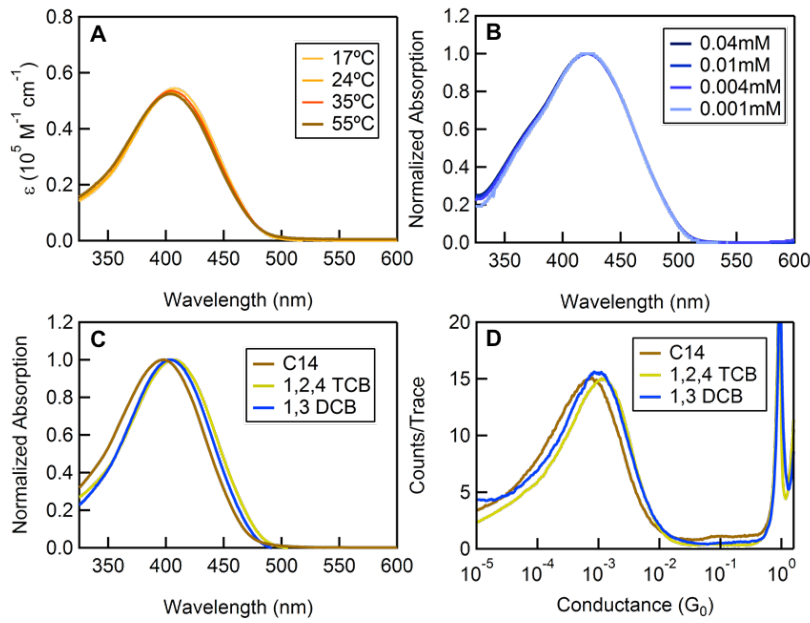


Figure 19: A. UV-vis absorption data taken in 1,2,4 trichlorobenzene (TCB) for **T4** at temperatures from 17°C to 55°C. B. UV-vis absorption data taken in TCB for **T5** at different concentrations, normalized to allow comparison of the onset of absorption. C. UV-vis absorption data for **T4** taken in different solvents. D. Conductance histograms for **T4** in three solvents: tetradecane (C14), 1,2,4 trichlorobenzene (TCB), and 1,2-dichlorobenzene (DCB).

centration aggregation is less likely. We varied the concentration of oligothiophenes in TCB and again saw no change in the positions of the onset of absorption or  $\lambda_{max}$  (Figure 19B). Molecules prone to aggregation display different behavior in “good” and “poor” solvents. When the solvent is varied, we note only a slight change in the onset of absorption and  $\lambda_{max}$  from non-polar tetradecane (C14) to the slightly polar dichlorobenzene (Figure 19C). However, these changes, on the order of 5-10 nm, are minor compared to those of 50-70 nm reported as evidence of oligothiophene aggregates in solution.<sup>79</sup> Furthermore, there is no change in the shape of the absorption curve, and these curves are typical for fully dissolved oligothiophenes.

We also measured the conductance of **T4** in various solvents and saw no difference in the width of the histograms (Figure 19D). Thus, we can rule out the possibility that  $\pi$ -stacked aggregates are formed in the junction, and we cannot attribute the unusual decay trend to the

sampling of multiple molecules or aggregates in the junction.

### 3.8 Solvation Shell Studies

A third plausible explanation for the non-exponential decay in conductance seen here could be due to a water gating effect. Recent studies show that water solvation shells around the backbone of a molecule can change transport resonances and therefore increase conductance; this effect was found to be particularly strong for long molecules.<sup>35</sup> To investigate whether the high conductance of **T4** is a result of such a gating effect, we measured the conductance of **T4** in an argon environment. We find that the conductance of **T4** in argon is slightly higher than that in air (Figure 20), but within the width of the histograms. Therefore, water gating cannot explain the higher conductance of **T4** compared to **T3** that we observe in our measurements.

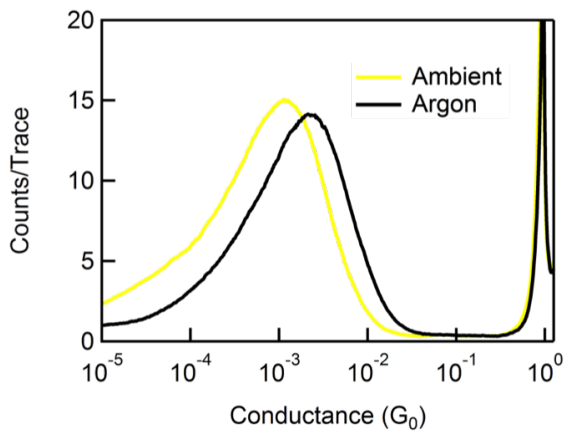


Figure 20: Conductance histograms for **T4** in both ambient conditions and under argon.

### 3.9 Elongation Studies

Having ruled out HOMO-Fermi level resonance, aggregation, and water gating as explanations for the high conductance of **T4**, we further analyzed two-dimensional (2D) conductance histograms to extract information on the length dependent behavior, which can correlate to con-

formational changes, on the conductance of the oligothiophene family. Since the length of the thiophene in the junction can depend on the orientation of the thiophene units relative to each other, we constructed 2D conductance-displacement histograms, without data selection so as to include all possible junction conformations in the statistical analysis, to understand how the molecular conductance evolves with junction elongation.<sup>81</sup>

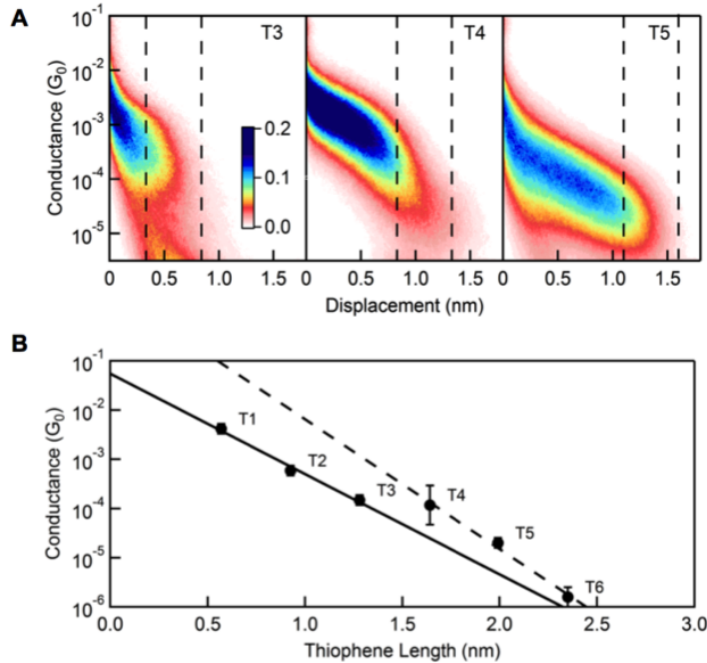


Figure 21: A. Two-dimensional conductance histograms of **T3**, **T4** and **T5**. B. Plot of the conductance obtained from the 2D plot for a fully elongated junction (demarcated by the dashed lines in A) as a function of the length of the molecules **T1-T6**. Conductances for **T1-T3** have a decay constant  $\beta = 0.46 \text{ \AA}^{-1}$  for **T1-T3**, and **T4-T6** have a decay constant  $\beta = 0.60 \text{ \AA}^{-1}$ .

Figure 21A shows these 2D histograms for **T3**, **T4** and **T5**. In these plots, we see a conductance feature that extends to longer displacements with increasing number of thiophene units. This indicates that the conductance plateau length in individual traces scales with the molecular length of the backbone, as has been found in other STM-BJ experiments. These results thus provide additional conclusive evidence that stable molecular junctions are formed with these oligothiophenes. Furthermore, a detailed comparison of the 2D histograms for **T3** and **T4** (Fig-

ure 21A) indicate that the conductance of **T4** is high for small displacements (relative to the point where the Au contact breaks). It is possible that for **T4**, the  $\pi$ -system couples directly to the gold electrodes at small electrode separation,<sup>73</sup> enhancing conductance, though it is not clear why **T5** does not show a similar effect. The 2D histograms also show that the conductance of a fully elongated **T4** junction is comparable to that of a **T3** junction.

To isolate and analyze the data of fully extended junctions, we determined the conductance from a subset of the 2D histograms within a 0.5 nm window demarcated by the dashed lines in Figure 21A. We integrated all counts within this window to generate a conductance profile<sup>82</sup> and fit a Gaussian to determine a peak conductance value. These values are plotted against molecular length in Figure 21B, which are again fit to two exponential decays with  $\beta = 0.46 \text{ \AA}^{-1}$  for **T1-T3** and  $\beta = 0.60 \text{ \AA}^{-1}$  for **T4-T6**. Although the difference between the two  $\beta$ s has diminished, the conductance values still do not lie on a single exponential. Note that the decay constants determined here for **T1-T3** are also different from that found by Yamada et. al. ( $0.1 \text{ \AA}^{-1}$ ).<sup>34</sup> However, their measurements were for alkylsilylamino-substituted oligomers of 8 or more units where conductance could be through a hopping mechanism rather than tunneling.<sup>61</sup> Therefore, we see that this conductance trend is not entirely due to trapping molecular conformations that have shorter overall lengths.

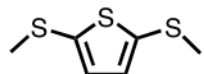
### 3.10 Conclusion

In summary, we have carried out single molecule conductance measurements on a family of methyl sulfide-terminated oligothiophenes using the scanning tunneling microscope based break-junction technique. We find that the peak of the conductance histogram distribution does not follow a clear exponential decay with increasing number of thiophene units in the chain, though

some care must be taken in accounting for molecular elongation effects. We postulate that different conformers in the junction are a contributing factor to the anomalous trends in the observed conductance as a function of molecule length. We point out that our findings have been qualitatively analyzed within a coherent tunneling model, as has been successfully employed for other organic molecules.<sup>83</sup> However, this point of view precludes more complex effects, such as Coulomb interactions on the molecule, hopping transport, and strong electron-phonon coupling. All of these effects are to be expected in conjugated polymers, especially with increasing length. Again, we have demonstrated that the molecular conformations in the junction play a critical role in the conductance behavior of oligothiophenes.

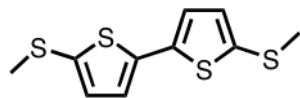
### 3.11 Experimental Section

#### 2,5-bisthiomethylthiophene (**T1**)



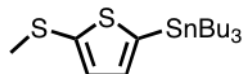
The title compound was prepared according to published procedures,<sup>84</sup> yielding the product as a yellow oil (1.11 g, 55% yield). <sup>1</sup>H NMR (400 MHz, CDCl<sub>3</sub>) δ 6.90 (s, 2H), 2.48 (s, 6H). <sup>13</sup>C NMR (400 MHz, CDCl<sub>3</sub>) δ 139.19, 131.03, 22.16. LRMS (APCI+) calculated for C<sub>6</sub>H<sub>8</sub>S<sub>3</sub> 176.32, found 175.98.

#### 5,5'-bisthiomethyl 2,2'-bithiophene (**T2**)



Synthesis described in Chapter 2.

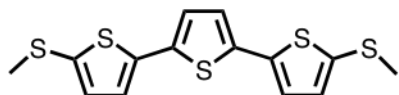
#### 2-tributylstanny 5-thiomethyl thiophene (**3.1**)



An oven-dried 100 mL round bottom flask and stir bar were cooled under Ar. 2,5 dibromothiophene (1 g, 4.13 mmol, 1 eq) was added and dissolved in 50 mL THF. The solution was cooled to -78°C. *n*-Butyllithium (2.4 M in hexanes, 1.89 mL, 4.5 mmol, 1.1 eq) was added dropwise by syringe and the solution was stirred for 30 minutes at -78°C. Dimethyl disulfide (0.39 g, 4.13 mmol, 1 eq) was added dropwise by syringe and the solution was allowed to warm to room temperature and stirred for one hour. The solution was then cooled back down to -78°C. *n*-

Butyllithium (2.4 M in hexanes, 1.89 mL, 4.5 mmol, 1.1 eq) was added dropwise by syringe and the solution was stirred for 30 minutes at -78°C. Tributyl tin chloride (1.34 g, 4.13 mmol, 1 eq) was added dropwise by syringe and the solution was allowed to warm to room temperature and stirred overnight. The mixture was added to 25 mL water. The organic layer was extracted with diethyl ether (2 x 50 mL), and the combined organic layers were washed with water (100 mL) and brine (100 mL) and dried over magnesium sulfate. After filtration, the organic layer was concentrated under reduced pressure to yield the product as a dark brown oil (1.6 g, 92% yield). The crude product was used in the next step without further purification.  $^1\text{H}$  NMR (400 MHz,  $\text{CDCl}_3$ )  $\delta$  7.15 (d,  $J = 3.3$  Hz, 1H), 7.02 (d,  $J = 3.3$  Hz, 1H), 2.50 (s, 3H), 1.56 (m, 8H), 1.34 (m, 8H), 1.09 (m, 8H), 0.90 (m, 12H).  $^{13}\text{C}$  NMR (400 MHz,  $\text{CDCl}_3$ )  $\delta$  141.85, 140.18, 135.51, 131.07, 28.76, 26.99, 21.76, 13.48, 10.70. HRMS (ESI+) calculated for  $\text{C}_{17}\text{H}_{32}\text{S}_2\text{Sn}$  419.28, found 419.28.

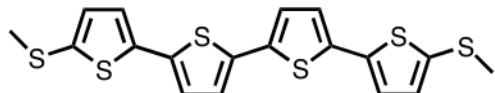
### 5,5'' bisthiomethyl-2,2':5',2''-terthiophene (T3)



An oven-dried two necked 50 mL round bottom flask and stir bar was fitted with a condenser and cooled under Ar. 2,5 Dibromothiophene (433 mg, 1.79 mmol, 1 eq) was added and dissolved in 15 mL DMF. The solution was sparged with Ar for 20 minutes. Tetrakis(triphenylphosphine) palladium(0) (207 mg, 0.179 mmol, 0.1 eq) was added and the solution was heated to 80°C. **3.1** (1.50 g, 3.58 mmol, 2 eq) was added dropwise and the solution was heated at 80°C overnight. The reaction mixture was cooled and passed through a silica plug with  $\text{CHCl}_3$  and 1% triethylamine, to remove any remaining stannane. The eluent was poured into 100 mL  $\text{CHCl}_3$  and

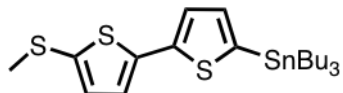
washed with water (5 x 100 mL) and brine (100 mL), and dried over magnesium sulfate. After filtration, the organic layer was concentrated under reduced pressure. Purification by column chromatography in 100% hexanes yielded the product as a bright yellow solid (420 mg, 69% yield).  $^1\text{H}$  NMR (400 MHz,  $\text{CDCl}_3$ )  $\delta$  7.01 (m, 4H), 6.97 (d,  $J = 3.8\text{Hz}$ , 2H), 2.52 (s, 6H).  $^{13}\text{C}$  NMR (400 MHz,  $\text{CDCl}_3$ )  $\delta$  131.88, 124.44, 123.95, 22.23. LRMS (APCI+) calculated for  $\text{C}_{14}\text{H}_{12}\text{S}_5$  340.57, found 341.25.

#### **5,5''' bisthiomethyl-2,2':5',2'':5'',2'''-quaterthiophene (T4)**



The title compound was prepared on a 0.62 mmol scale according to the procedure for compound **T3** with the following modifications: 5,5'-dibromo 2,2'-bithiophene (200 mg, 0.62 mmol, 1 eq) was used instead of 2,5-dibromothiophene. After heating overnight the product had crashed out of solution. This orange solid was filtered off and washed with methylene chloride, and recrystallized from  $\text{CHCl}_3$  to yield pure product (158 mg, 60% yield).  $^1\text{H}$  NMR (400 MHz,  $\text{CDCl}_3$ )  $\delta$  7.07 (d,  $J = 3.7\text{ Hz}$ , 2H), 7.04 (d,  $J = 3.7\text{ Hz}$ , 2H), 7.01 (d,  $J = 3.6\text{ Hz}$ , 2H), 6.97 (d,  $J = 3.6\text{ Hz}$ , 2H), 2.52 (s, 6H). LRMS (EI+) calculated for  $\text{C}_{18}\text{H}_{14}\text{S}_6$  422.69, found 422.2.

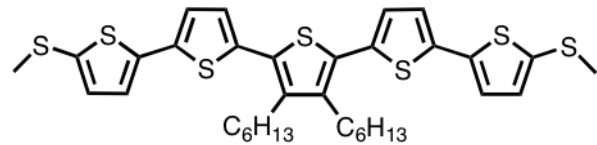
#### **5-thiomethyl-5'-tributylstannyl-2,2'-bithiophene (3.2)**



An oven-dried 50 mL round bottom flask and stir bar were cooled under Ar. 5,5'-dibromo 2,2'-

bithiophene (350 mg, 1.65 mmol, 1 eq) was added and dissolved in 20 mL THF. The solution was cooled to -78°C. *n*-Butyllithium (2.5 M in hexanes, 0.66 mL, 1.65 mmol, 1 eq) was added dropwise by syringe and the solution was stirred for 30 minutes at -78°C. The solution turned royal blue upon addition of *n*-butyllithium. Tributyl tin chloride (540 mg, 1.65 mmol, 1 eq) was added dropwise by syringe and the solution turned yellow. The solution was allowed to warm to room temperature and stirred overnight. The solution was washed with water (2 x 20ml), dried over magnesium sulfate. After filtration, the organic layer was concentrated under reduced pressure to yield a yellow oil (610 mg, 75% yield). In our hands, organotin compounds have shown considerable decomposition during column chromatography, so the crude material was taken to the next step without further purification.  $^1\text{H}$  NMR (300 MHz,  $\text{CDCl}_3$ )  $\delta$  7.25 (d,  $J = 3.4$  Hz, 1H), 7.05 (d,  $J = 3.4$  Hz, 1H), 7.01 (d,  $J = 3.7$  Hz, 1H), 6.98 (d,  $J = 3.7$  Hz, 1H), 2.50 (s, 3H), 1.63-1.55 (m, 8H), 1.42-1.34 (m, 8H), 1.17-1.11 (m, 8H), 0.90 (t,  $J = 7.3$  Hz, 12H).  $^{13}\text{C}$  NMR (400 MHz,  $\text{CDCl}_3$ )  $\delta$  136.23, 132.09, 125.08, 123.61, 29.09, 27.39, 22.38, 13.80, 11.05. HRMS (ESI+) calculated for  $\text{C}_{21}\text{H}_{34}\text{S}_3\text{Sn}$  501.40, found 501.97.

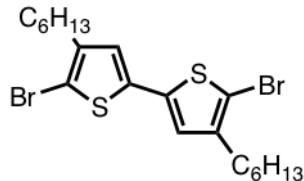
**5,5'''-dithiomethyl-3'',4''-dihexyl-2,2',5',2'',5'',2''',5''',2''''-pentathiophene (T5)**



The title compound was prepared on a 0.37 mmol scale according to the procedure for compound **T3** with the following modifications: 3,4-Dihexyl-1,5-dibromothiophene (150 mg, 0.37 mmol, 1 eq) was used instead of 2,5-dibromothiophene. **3.2** (367 mg, 0.73 mmol, 2 eq) was used instead of 2-tributylstanny-5-thiomethyl-thiophene. Purification by column chromatography in 100%

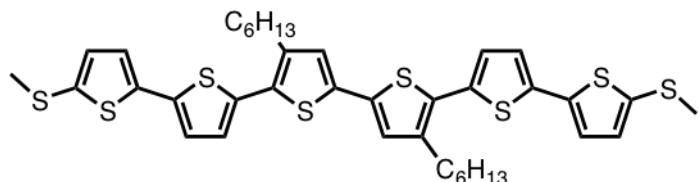
hexanes ( $R_f = 0.19$ ) yielded the product as a bright orangey-red solid (190 mg, 38% yield).  $^1\text{H}$  NMR (400 MHz,  $\text{CDCl}_3$ )  $\delta$  7.08 (d,  $J = 3.8$  Hz, 2H), 7.03 (d,  $J = 2.9$  Hz, 2H), 7.02 (d,  $J = 2.9$  Hz, 2H), 6.99 (d,  $J = 3.7$  Hz, 2H), 2.70 (t, 4H), 2.51 (s, 6H), 1.61-1.57 (m, 4H), 1.45-1.40 (m, 4H), 1.34-1.31 (m, 8H), 0.90 (t, 6H).  $^{13}\text{C}$  NMR (400 MHz,  $\text{CDCl}_3$ )  $\delta$  140.50, 139.32, 136.68, 135.30, 131.90, 129.80, 126.41, 124.05, 123.73, 31.59, 30.72, 29.70, 28.34, 22.76, 22.24, 14.24. LRMS (APCI+) calculated for  $\text{C}_{34}\text{H}_{40}\text{S}_7$  673.14, found 672.3.

### **5,5'-dibromo-4,4'-dihexyl-2,2'-bithiophene (3.3)**



The title compound was prepared on a 0.015 mmol scale according to published procedures<sup>64</sup> yielding the product as a bright yellow oil (2.5g, 70% yield).  $^1\text{H}$  NMR (400 MHz,  $\text{CDCl}_3$ )  $\delta$  6.77 (s, 2H), 2.57 - 2.46 (t, 4H), 1.58 (dd,  $J = 8.6, 5.8$  Hz, 4H), 1.32 (d,  $J = 2.0$  Hz, 12H), 0.90 (s, 6H). LRMS (APCI+) calculated for  $\text{C}_{20}\text{H}_{28}\text{Br}_2\text{S}_2$  492.37, found 491.9.

### **3'',4''-dihexyl-5,5'''- bis(methylthio)- 2,2':5',2'';5'',2''':5''',2'''';5''''- sexithio-phene (T6)**



The title compound was prepared on a 0.32 mmol scale according to the procedure for compound

**T3** with the following modifications: 5,5'-dibromo-4,4'- dihexyl-2,2'-bithiophene (**3.3**) (80 mg, 0.16 mmol, 1 eq) was used instead of 2,5 dibromothiophene and 5-thiomethyl-5'-tributylstanny-2,2'-bithiophene (**3.2**) (163 mg, 0.32 mmol, 2 eq) was used instead of 2-tributylstannyl- 5-thiomethyl-thiophene. Column chromatography in 10% ethyl acetate in hexanes ( $R_f = 0.13$ ) yielded the product as a bright red solid (51 mg, 41% yield).  $^1\text{H}$  NMR (400 MHz,  $\text{CDCl}_3$ )  $\delta$  7.07 (s, 2H), 7.03 (d,  $J = 1.0$  Hz, 4H), 7.00 (d,  $J = 1.0$  Hz, 4H), 2.70 (t, 4H), 2.52 (s, 6H), 1.73-1.61 (m, 4H), 1.45-1.30 (m, 12H), 0.91 (t, 6H).  $^{13}\text{C}$  NMR (400 MHz,  $\text{CDCl}_3$ )  $\delta$  140.99, 139.53, 137.02, 136.92, 135.44, 135.26, 132.16, 129.76, 126.96, 126.67, 124.37, 124.07, 32.01, 30.78, 29.87, 29.58, 22.96, 22.47, 14.44. LRMS (APCI+) calculated for  $\text{C}_{38}\text{H}_{42}\text{S}_8$  754.11, found 754.5.

## 4 The Conductance of Thiophene-1,1-Dioxide Oligomers

### 4.1 Preface

This chapter is based on a manuscript entitled *Molecular Length Dictates the Nature of Charge Carriers in Single-Molecule Junctions of Oxidized Oligothiophenes* by Emma J. Dell†, Brian Capozzi†, Jianlong Xia, Latha Venkataraman, and Luis M. Campos published in *Nature Chemistry*<sup>85</sup> (†equal contributions). The single molecule conductance experimental work was conducted by Brian Capozzi in Prof. Latha Venkataraman’s group. Chemical synthesis was assisted by Dr. Jianlong Xia in Prof. Luis M. Campos’ group.

### 4.2 Introduction

Having investigated the rotational and length dependence of the conductance of oligothiophenes, we were motivated to probe how chemical modifications of their structure would influence their electrical behavior. In particular, we wanted to devise a strategy for increasing the molecular conductance. On a bulk scale, general strategies for tuning electrical properties of thiophene-based materials have included incorporating various electron-withdrawing substituents at the  $\alpha$  and  $\beta$  positions, copolymerizing thiophene units with electron deficient units, and architectural modifications.<sup>86,87</sup> However, an alternative strategy exists - utilizing sulfur’s hypervalency - a strategy first explored by Barbarella and co-workers.<sup>36</sup> Thiophene can be oxidized to thiophene-1,1-dioxide. This process engages sulfur’s lone pairs in bonding, and thus reduces the aromaticity of the system, favoring the quinoidal form. This, in turn, increases the conjugation along a chain of connected oxidized thiophene units, and thus is predicted to lower the HOMO-LUMO gap of the oligomer. Barbarella and co-workers’ studies showed that the maximum

wavelength absorption of oligothiophene dioxides displayed a 60-110 nm red shift in comparison to their unoxidized analogs. Cyclic voltammetry data indicate that the oxidation process lowers the energy of both the HOMO and the LUMO, but that the effect on the electron affinity is much more dramatic than that on the ionization potential leading to an overall reduction in energy gap.<sup>37</sup> Motivated by these exciting electronic properties, we were interested in how these materials would behave at the single molecule level.

### 4.3 Traditional Thiophene Oxidation

Thiophene oxidation is by no means easy to achieve.<sup>88</sup> The aromaticity of the thiophene moiety must be overcome, which traditionally requires high temperatures and long reaction times. At the same time, the non-aromatic product may undergo facile Diels-Alder or elimination reactions under the harsh conditions so needed to drive the process in the first place, and side reactions such as epoxidation of the double bond may occur.<sup>89</sup> Barbarella's group utilized the peracid meta-chloroperoxybenzoic acid (mCPBA) in methylene chloride at room temperature to carry out their oxidations. This method required the presence of silyl groups on the oligomers, limiting the scope of the synthesis. Additionally, the timescale of these reactions was long - up to one week for the quaterthiophene - and resulted in mixtures of products. The oxidation of 2,5'-bisilyl-2,2'-bithiophene afforded mixtures of the mono- and bis-dioxides. They were able to separate these by column chromatography, but the yields were prohibitively low to be used for translational research. Alongside peracids, another orthodox strategy to bring about thiophene oxidation is to use dimethyldioxirane. Again, although this reagent is effective with aliphatic sulfurs, long reaction times and poor yields are seen with thiophene derivatives.

#### 4.4 Rozen's Reagent

The difficulties in oxidizing thiophenes led to a stagnation in this area of research until the discovery by Rozen and coworkers of a strategy to handle hypofluorous acid (HOF), a strong oxidizing agent. They showed that bubbling a diluted fluorine-in-nitrogen gaseous mixture through aqueous acetonitrile ( $\text{CH}_3\text{CN}$ ) generates the  $\text{HOF}\cdot\text{CH}_3\text{CN}$  complex, Rozen's reagent.<sup>90</sup> The oxygen is bonded to a fluorine which imparts on it a partial positive charge and a truly electrophilic nature, resulting in an exceptional oxygen transfer reagent, which has practical applications due to the stability afforded from complexation with acetonitrile.<sup>91</sup> Oxidation processes using Rozen's reagent can take place at room temperature in relatively short times. These mild conditions sidestep competing reactions during the formation of thiophene dioxides.

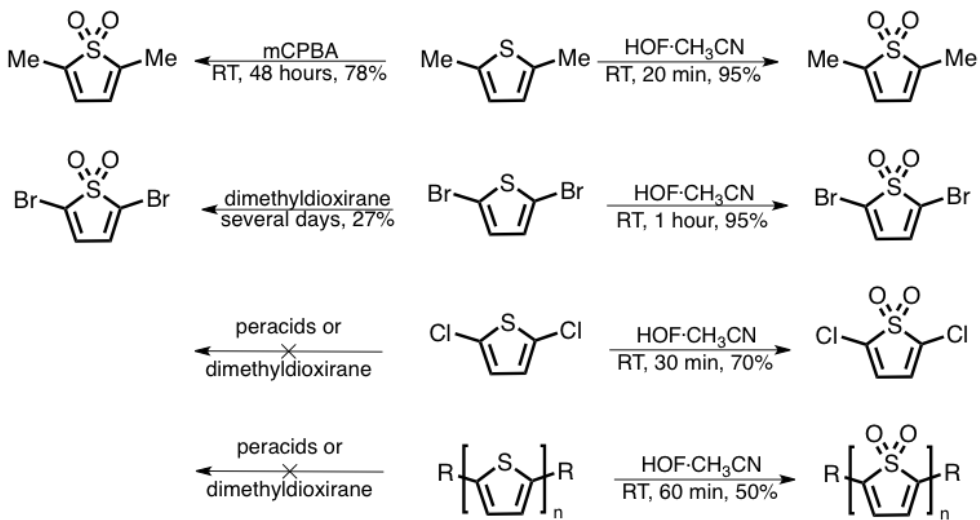


Figure 22: Comparison of the oxidation of different thiophene derivatives with traditional oxidizing agents (left) and Rozen's reagent (right).

Direct comparison of the oxidations between various agents and  $\text{HOF}\cdot\text{CH}_3\text{CN}$  are shown in Figure 22.<sup>92</sup> The peracid mCPBA oxidized 2,5-dimethylthiophene in 48 hours with a 78% yield. With Rozen's reagent, the reaction took a mere 20 minutes and gave near quantitative

yields. As the thiophene ring becomes more electron-depleted, the traditional methods struggle further, with peracids failing to oxidize 2,5-dibromothiophene, and dimethyldioxirane requiring several days to achieve a 27% yield. By contrast, HOF·CH<sub>3</sub>CN gave a 95% yield in one hour. 2,5-Dichlorothiophene cannot be oxidized by traditional methods, but HOF·CH<sub>3</sub>CN could be used to synthesize 2,5-dichlorothiophene-1,1-dioxide for the first time with 70% yield in 30 minutes. The most striking demonstration of the potency of Rozen's reagent was evident using oligothiophenes with up to four repeat units. In cases where traditional oxidation strategies of oligothiophenes yield mixtures of mono and dioxidized products, HOF·CH<sub>3</sub>CN was able to completely oxidize bithiophene, terthiophene and quaterthiophene.

#### 4.5 Synthesis of the TDO<sub>n</sub> Family

We wanted to use Rozen's reagent to oxidize oligothiophene derivatives and then measure their single molecule conductance. As a preliminary study, 5,5'-dibromo-2,2'-bithiophene (**4a**) and 5,5''-dibromo-2,2':5',2''-terthiophene (**4c**) were oxidized using the HOF·CH<sub>3</sub>CN complex to generate the fully oxidized analogs in high yields in just 30 minutes (Figure 23).

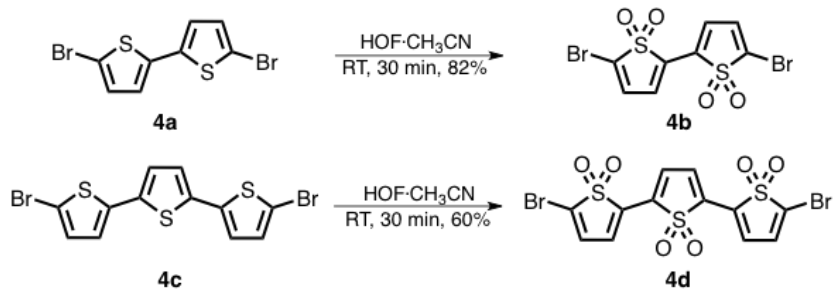


Figure 23: Synthesis of bithiophene dioxide and terthiophene dioxide.

The UV-vis absorption spectra of these molecules show that oxidation has a considerable effect on the electronic properties of the molecules (Figure 24). Both **4b** and **4d** display a

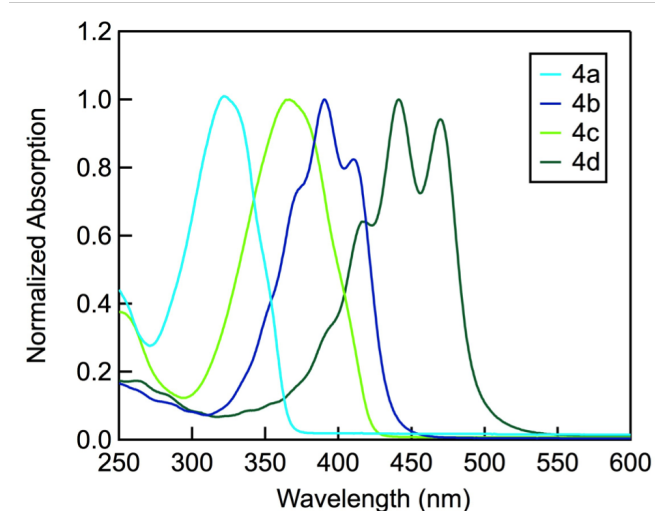


Figure 24: Normalized UV-vis absorption spectra taken in dichloromethane for unoxidized dibromo-bithiophene (**4a**) and dibromo-terthiophene (**4b**) together with their fully oxidized analogs (**4c** and **4d** respectively).

red-shift of approximately 70 nm as compared to their unoxidized analogs. Furthermore, vibronic features appear in the spectra of the oxidized molecules, indicating an increase in the rigidity of the molecular backbone.<sup>93</sup> Both of these observations imply an increase in conjugation along the oxidized molecules, providing substance for the hypothesis that they will display higher conductance values. We decided to investigate the characteristics of a family of molecules that combined these oxidized electron-deficient units with electron-rich unoxidized thiophenes. We designed a series of molecules composed of oligo-thiophene-1,1-dioxide centers coupled to unoxidized thiophenes on both sides - the **TDO<sub>n</sub>** family (Figure 25).

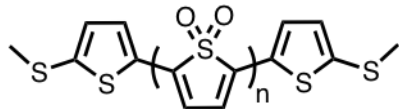


Figure 25: Schematic of the **TDO<sub>n</sub>** family where  $n = 1 - 4$ . Hexyl chains are installed on the longer oligomers for solubility as described in the experimental section.

For the first member of the family, a Stille coupling was performed on 2,5-dibromothiophene-1,1-dioxide (**4.1**) with our generic flanking stannane **3.1** (synthesis described in Chapter 3) to

generate a terthiophene derivative with the middle unit oxidized (Figure 26). We named this compound **TDO1**.

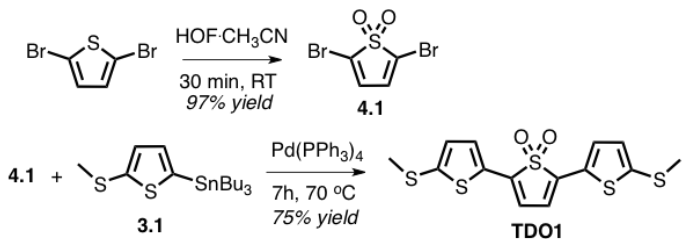


Figure 26: Synthesis of **TDO1**

This particular electron-rich/electron-poor combination yields a drastic reduction in the transport gap. The UV-vis absorption spectrum of **TDO1** was especially interesting since it showed a greater red-shift than that of a fully oxidized terthiophene derivative (Figure 27). This is attributed to a “push-pull” effect between the electron rich and electron poor units.<sup>94,95</sup> When electron rich moieties (such as thiophene rings) are combined with electron poor moieties (such as thiophene-1,1-dioxides), the frontier orbitals hybridize such that the resultant HOMO has mostly the character of the electron rich unit, and the resultant LUMO has mostly the character of the electron poor unit, with a concomitant reduction in the band gap.

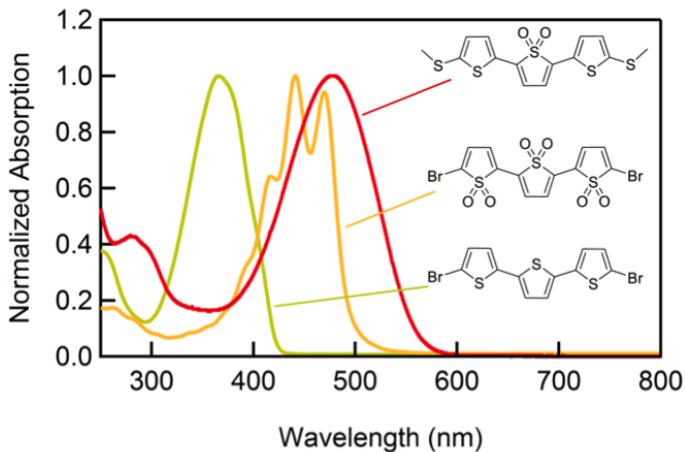


Figure 27: Normalized UV-vis absorption spectra taken in dichloromethane for terthiophene derivatives with different extents of oxidation.

We wanted to investigate how this “push-pull” effect would influence the single-molecule behavior and therefore went on to synthesize a series of **TDO<sub>n</sub>** oligomers with n = 1 to 4. For **TDO<sub>2</sub>** and **TDO<sub>3</sub>**, the synthetic route was very similar to that for **TDO<sub>1</sub>**, shown in Figure 26. The middle oxidized units were prepared first, by oxidizing dibromo derivatives of bi- and ter-thiophenes using HOF·CH<sub>3</sub>CN, with hexyl groups added for solubility as shown in the experimental section. All oxidations took place at room temperature. Then in a second step, the methyl sulfide bearing thiophene rings were added through Stille couplings. It was imperative that both the methyl sulfide groups and the unoxidized thiophene rings were added last, so that they were not also oxidized by Rozen’s reagent. The route to **TDO<sub>4</sub>** was slightly different. Initially, we had tried to prepare **TDO<sub>4</sub>** in the same manner as **TDO<sub>1</sub>**. A quaterthiophene derivative was reacted with an excess of Rozen’s reagent as shown in Figure 28. Unexpectedly, however, even in excess this only resulted in the oxidation of the middle two rings (**4.2**). Due to the symmetry of this molecule, and slight differences in chemical shift between protons on oxidized and unoxidized thiophene rings, **4.2** was initially incorrectly characterized as the fully oxidized derivative, and a Stille coupling was performed with the aim of generating **TDO<sub>4</sub>**. However, compound **4.3** was formed instead, which was shown through both mass spectrometry analysis and X-ray crystallography to only have the middle two units oxidized (see experimental section).

A modified route to **TDO<sub>4</sub>** was proposed (Figure 29). Here, additional hexyl groups were added to the first and last thiophene of the quaterthiophene derivative (**4.5**), since electron-rich units have a greater propensity for oxidation. Secondly, the middle two thiophenes were oxidized in a preliminary step, and once **4.5** had been generated, a second treatment of Rozen’s reagent

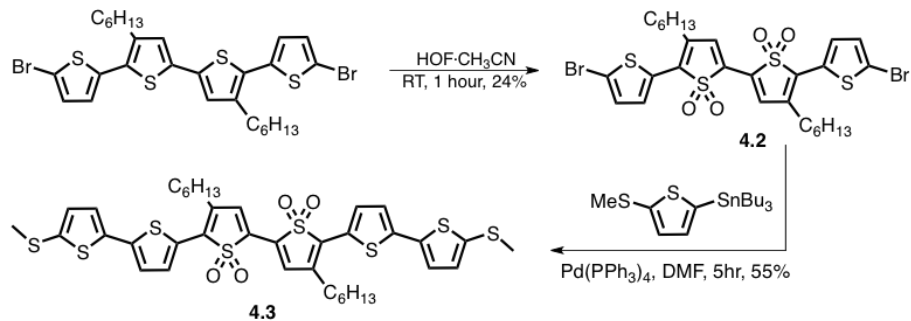


Figure 28: Treatment of this quaterthiophene derivative with Rozen’s reagent oxidizes just the middle two units resulting in **4.3** after the Stille coupling instead of **TDO4**.

oxidized the outer two rings (**4.7**). This fully oxidized quaterthiophene derivative was then subjected to the standard Stille coupling to install the flanking methyl sulfide thiophene units.

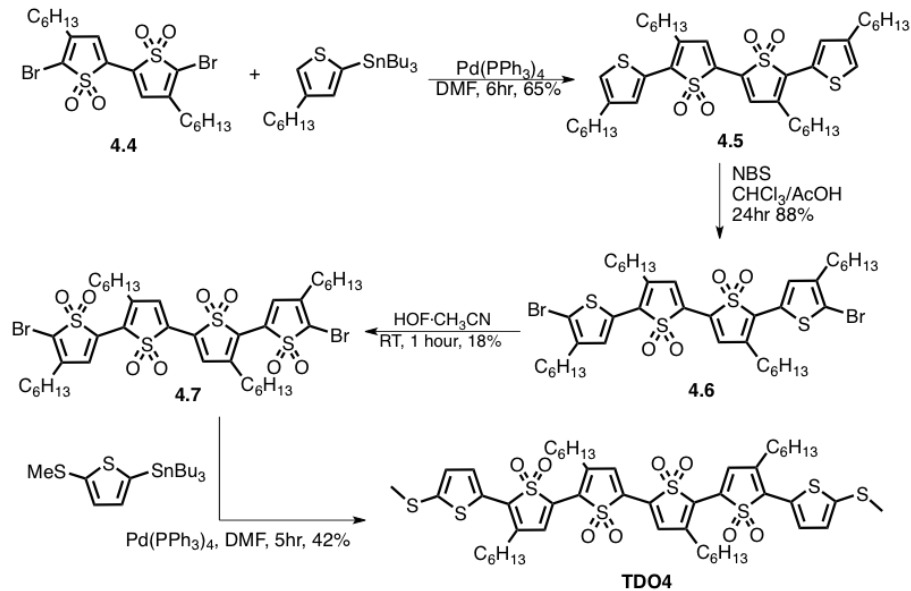


Figure 29: Synthesis of **TDO4**.

#### 4.6 Single Molecule Conductance of the **TDO**<sub>n</sub> Family

Single-molecule conductance measurements on the **TDO**<sub>n</sub> family were then carried out in order to probe how their increased conjugation and smaller optical gaps (as compared to the unoxidized oligothiophene series) impacted charge transport through the molecules. For each molecule in

the series, 20,000 conductance versus displacement traces were collected using the STM-BJ technique. All measured conductance traces were collected and compiled into one-dimensional, logarithmically-binned conductance histograms (100 bins per decade) without data selection and shown in Figure 30B.

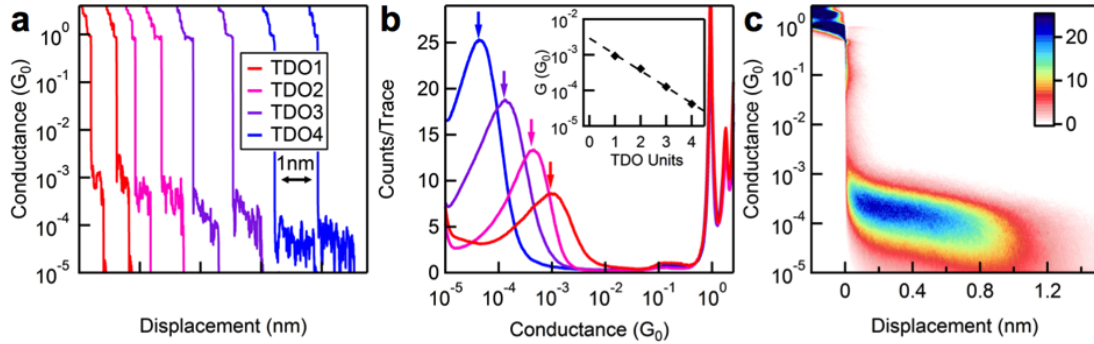


Figure 30: A. Sample conductance versus displacement traces, laterally offset, for the **TDO<sub>n</sub>** series. These traces display molecule-specific conductance features, which persist for longer displacements as the molecular length increases. B. One-dimensional log-binned conductance histograms, each composed of 20,000 traces, for **TDO1-TDO4** measured at a 10 mV bias in 1-octylbenzene. Arrows indicate peak conductance positions. Inset: Plot of conductance as a function of the number of oxidised thiophene monomer units ( $n$ ) in **TDO1-TDO4**. Using  $G \sim e^{-\beta L}$ , we obtain a decay constant of  $1.04/n$ . (c) Two-dimensional conductance-displacement histogram for **TDO3** created by aligning all traces at the point where conductance crosses  $0.5 G_0$ , and then overlaying them. The color bar indicates number of counts per 1000 traces.

These 1D histograms display a clear peak yielding a most probable molecular conductance value that decreases systematically with increasing number of **TDO** monomers (Figure 30B). The relatively narrow breadth of the conductance histogram peaks is indicative of a rather rigid backbone in this class of molecules.<sup>60</sup> A two-dimensional histogram, which retains displacement information, was created from the same data and is shown in Figure 30C for **TDO3**. This 2D histogram demonstrates that these junctions sustain a 1 nm elongation. Comparing 2D histograms across the series we see a clear increase in molecular plateau length with increasing backbone length (Figure 31). This indicates that we probe similar junction structures for all molecules in this series.<sup>81</sup>

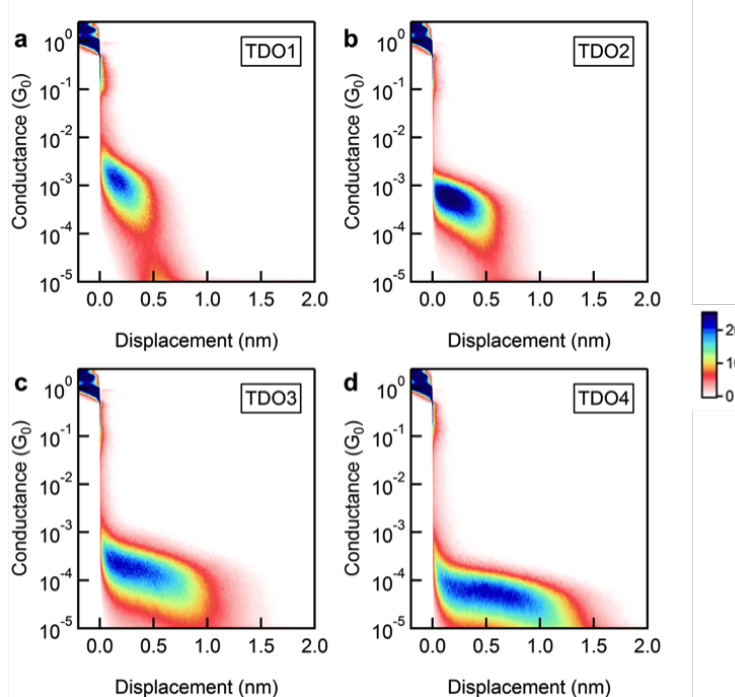


Figure 31: Two-dimensional conductance versus displacement histograms for the **TDO<sub>n</sub>** series.

The inset of Figure 30B gives the peak conductance values on a semi-logarithmic scale plotted against  $n$  (the number of repeat units) showing that conductance decreases exponentially with increasing  $n$  with a decay constant,  $\beta$ , =  $1.04/n$ . Since these **TDO** units are non-aromatic, the conduction path follows that of a chain of alternating double and single bonds across the backbone. We therefore used a through-bond distance of 5.4 Å as opposed to a through-space distance of 3.8 Å to convert the measured  $\beta$  to a decay constant of 0.2/Å. Interestingly, this value compares well with the  $\beta$  determined for oligoene systems,<sup>73,96</sup> and shows that transport across **TDO** oligomers is similar to that across alkene oligomers. Finally, the conductances are relatively high, and are higher than those of the equivalent length unoxidized oligothiopenes (apart from the anomalous **T4** case) (Figure 32). In particular, **TDO4** has a peak conductance an order of magnitude higher than **T6** even though their lengths are nearly equal, demonstrating how the narrow HOMO-LUMO gap has a profound effect on the charge transport.

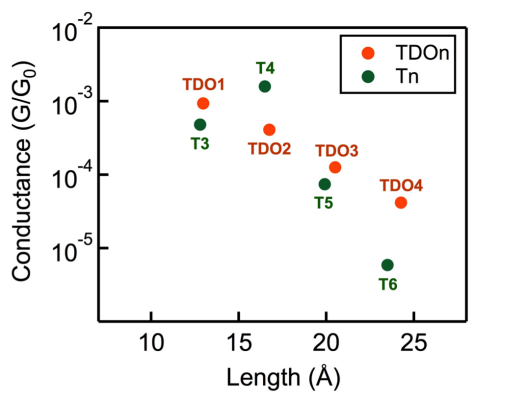


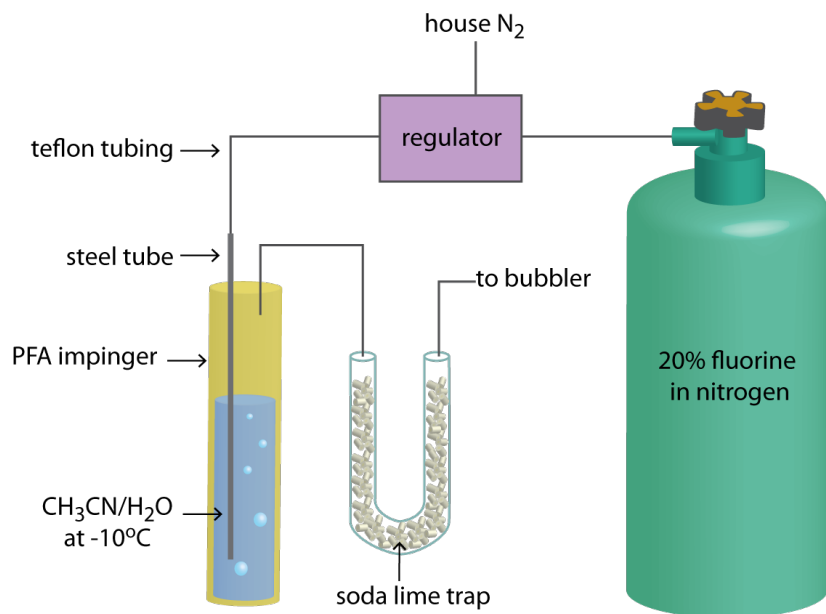
Figure 32: Semilog plot showing the decay in conductance for the **TDOn** and **Tn** families with molecule length.

#### 4.7 Conclusion

We synthesized a family of molecules containing between one and four repeat thiophene-1,1-dioxide units flanked by unoxidized thiophene units - the **TDOn** series. The syntheses were carried out using Rozen's reagent,  $\text{HOF}\cdot\text{CH}_3\text{CN}$ , an extremely potent oxidizing agent. Rozen's reagent is able to oxidize oligothiophenes at room temperature in a matter of minutes, to form products that have a narrowed band gap and increased rigidity along the molecular backbone, as confirmed through UV-vis absorption measurements. Incorporating unoxidized thiophene units on either ends of these molecules reduces the band gap further, through the “push-pull” effect. Using the STM-BJ technique, we show that this family displays narrow 1D histograms, a shallow exponential decay with length, and much higher conductance values than their unoxidized counterparts (apart from **T4**). These observations are attributed to the increased conjugation through the molecular backbone and demonstrate how precise control over molecular design can have significant impact on the resultant electronic properties. However, one optical feature of the **TDOn** family was particularly striking - their lowered LUMO levels, and we wanted to further explore how this feature could impact the charge transport of these molecules, as described in the next chapter.

## 4.8 Experimental Section

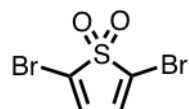
### HOF·CH<sub>3</sub>CN Setup



Fluorine is a very toxic and corrosive gas and must be used with care. With this in mind, whenever in use, the system is monitored for any leaks using damp KI strips which act as a fluorine indicator (white to purple color change). The set up is shown above. A tank of 20% fluorine in nitrogen was purchased from Linde. A 375 mL PFA impinger with two vertical ports was purchased from Savigex. Steel tubing was purchased from McMaster-Carr. A 10:1 mixture of CH<sub>3</sub>CN:H<sub>2</sub>O (total volume usually around 150 mL) is added to the impinger and cooled to -10°C. The system is purged with house N<sub>2</sub> for 20 minutes. 20% fluorine in nitrogen is then bubbled through the system. We monitor the flow rate with the bubbler, and aim for approximately 70 bubbles per minute (like a heart beat). The CH<sub>3</sub>CN:H<sub>2</sub>O mixture is kept at -10°C throughout this process. After about an hour, a 1 mL aliquot of the solution is removed and

added to a few mLs of saturated KI. The liberated I<sub>2</sub> is then titrated against 0.1 M Na<sub>2</sub>S<sub>2</sub>O<sub>3</sub>. The concentration of HOF·CH<sub>3</sub>CN is given by 0.05 x volume of Na<sub>2</sub>S<sub>2</sub>O<sub>3</sub>. We achieved concentrations of around 0.2 M. If the concentration is less than this, the bubbling can be continued for another 30 minutes or so. Once the HOF·CH<sub>3</sub>CN has reached an optimum concentration, it is transferred out of the impinger, ready to be used. The impinger is then filled with a fresh solution of CH<sub>3</sub>CN and the system is purged with house N<sub>2</sub> for 30 minutes. The HOF·CH<sub>3</sub>CN solution is prone to decomposition and should be used within an hour of its formation. HF is a by-product of the formation of HOF·CH<sub>3</sub>CN, and therefore the solution should be treated with care and any excess quenched with saturated NaHCO<sub>3</sub> followed by 1 M NaOH.

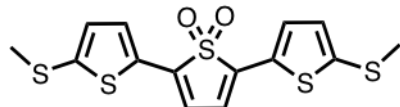
### 2,5-dibromothiophene-1,1-dioxide (4.1)



An oven-dried 100 mL round bottom flask and stir bar were cooled under Ar. 2,5 dibromothiophene (400 mg, 1.65 mmol, 1 eq) was added and dissolved in 10 mL DCM. The solution was cooled to 0°C. HOF·CH<sub>3</sub>CN (55 mL, 0.15 M, 8.27 mmol, 5 eq) was added dropwise. The solution was allowed to warm to room temperature and stirred for 2 hours. The reaction was quenched by adding 30 mL of saturated NaHCO<sub>3</sub> dropwise. The organic layer was extracted with DCM (2 x 50 mL), and the combined organic layers were washed with NaHCO<sub>3</sub> (100 mL) and water (100 mL) and dried over magnesium sulfate. After filtration, the organic layer was concentrated under reduced pressure to yield the product as a white powder (355 mg, 78% yield). The crude product was used in the next step without further purification. <sup>1</sup>H NMR (400 MHz, CDCl<sub>3</sub>)

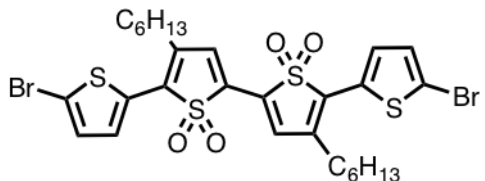
$\delta$  6.86 (s, 2H).  $^{13}\text{C}$  NMR (400 MHz,  $\text{CDCl}_3$ )  $\delta$  128.16, 119.46. LRMS (APCI+) calculated for  $\text{C}_4\text{H}_2\text{O}_2\text{SBr}_2$  273.93, found 274.00.

**5,5"-bis(methylthio)-[2,2':5',2"-terthiophene]-1,1-dioxide (TDO1)**



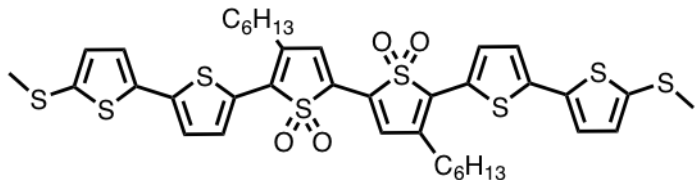
An oven-dried 5 mL round bottom flask and stir bar were cooled under Ar. 2 mL of DMF was added and sparged with Ar for 15 minutes. **4.1** was added (30 mg, 0.11 mmol, 1 eq) together with tetrakis(triphenylphosphine)palladium (6.4 mg, 0.0055 mmol, 0.05 eq). The solution was heated under Ar to 80°C for 5 minutes. **3.1** was added (92 mg, 0.22 mmol, 2 eq) and the solution was stirred at 80°C under Ar for 5 hours, during which time it turned from yellow to a deep red color. The crude mixture was cooled and then passed through a silica plug with DCM and 2% triethylamine. The solution was then washed with water (3 x 75 mL) and dried over magnesium sulfate. After filtration, the organic layer was concentrated under reduced pressure. Purification by column chromatography in 20% ethyl acetate in hexanes ( $R_f = 0.32$ ) yield the product as a deep red/bronze solid (29 mg, 71% yield).  $^1\text{H}$  NMR (400 MHz,  $\text{CDCl}_3$ )  $\delta$  7.47 (d,  $J = 3.9$  Hz, 2H), 7.00 (d,  $J = 3.9$  Hz, 2H), 6.65 (s, 2H), 2.57 (s, 6H).  $^{13}\text{C}$  NMR (400 MHz,  $\text{CDCl}_3$ )  $\delta$  142.76, 135.29, 130.37, 129.87, 128.36, 117.92, 20.77. LRMS (APCI+) calculated for  $\text{C}_{14}\text{H}_{12}\text{O}_2\text{S}_5$  372.57, found 371.94.

**5,5"-dibromo-3',4"-dihexyl- [2,2':5',2":5",2"- quaterthiophene] 1',1',1",1"- tetraoxide (4.2)**



The above compound was synthesized according to published procedures<sup>42</sup> producing a burgundy solid in 24% yield.  $^1H$  NMR (400 MHz,  $CDCl_3$ )  $\delta$  7.45 (d,  $J = 4.0$  Hz, 2H), 7.16 (d,  $J = 4.4$  Hz, 4H), 2.70 - 2.59 (m, 4H), 1.73 - 1.58 (m, 4H), 1.38 - 1.31 (m, 12H), 0.92 - 0.86 (m, 6H).

**3'',4''-dihexyl-5,5'''-bis(methylthio)- [2,2':5',2'':5'',2''':5''',2''''-sexithiophene] 1'',1'',1''',1'''-tetraoxide (4.3)**



The title compound was prepared on a 0.046 mmol scale according to the procedure as **TDO1** with the following modification: **4.2** (35 mg, 0.046 mmol) was used instead of **4.1**. Purification by column chromatography in 10% ethyl acetate in hexanes ( $R_f = 0.16$ ) yielded the product as a purple black solid (12 mg, 32% yield).  $^1H$  NMR (500 MHz,  $CDCl_3$ )  $\delta$  7.64 (d,  $J = 4.0$  Hz, 2H), 7.20 (s, 4H), 7.13 (d,  $J = 3.8$  Hz, 2H), 7.00 (d,  $J = 3.8$  Hz, 2H), 2.76 - 2.70 (m, 4H), 2.55 (s, 6H), 1.70 (s, 4H), 1.47 (d,  $J = 7.7$  Hz, 4H), 1.39 - 1.33 (m, 8H), 0.94 - 0.89 (m, 6H).  $^{13}C$  NMR (400 MHz,  $CDCl_3$ )  $\delta$  141.16, 139.31, 137.64, 134.92, 132.45, 131.35, 130.55, 128.46, 128.02, 127.55, 125.45, 124.67, 31.61, 30.68, 29.45, 27.46, 22.65, 21.83, 14.19. LRMS (MALDI) calculated for  $C_{38}H_{42}O_4S_8$  819.26, found 819.1.

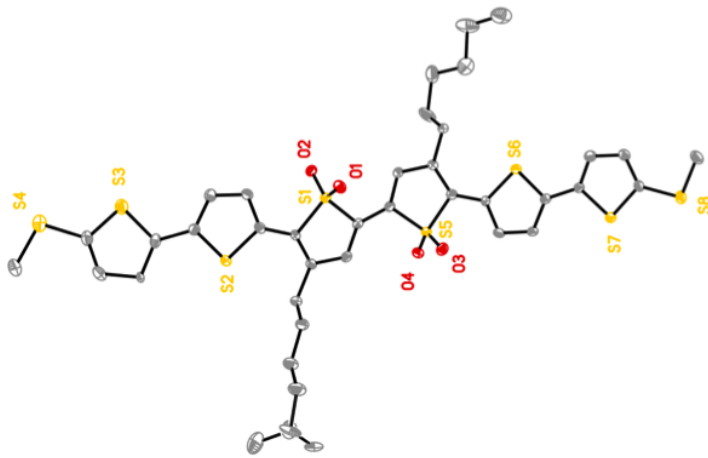
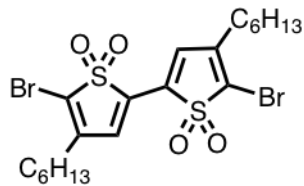


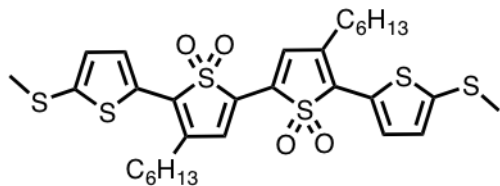
Figure 33: Crystal structure of **4.3** provided by Serge Ruccolo in Prof. Gerard Parkin's group.

#### **5,5'-dibromo-4,4'-dihexyl-[2,2'-bithiophene] 1,1,1',1'-tetraoxide (4.4)**



The above compound was synthesized according to published procedures<sup>42</sup> producing a bright orange solid in 58% yield. <sup>1</sup>H NMR (400 MHz, CDCl<sub>3</sub>) δ 7.12 (s, 2H), 2.47 (t, 4H), 1.55 (m, 4H), 1.34 (m, 12H), 0.90 (t, 6H).

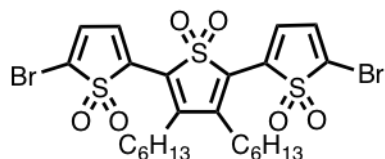
#### **3',4''-dihexyl-5,5''-bis(methylthio)-[2,2':5',2'':5'',2'''- quaterthiophene] 1',1', 1'',1''-tetraoxide (TDO2)**



The title compound was prepared on a 0.064 mmol scale according to the procedure as **TDO1**

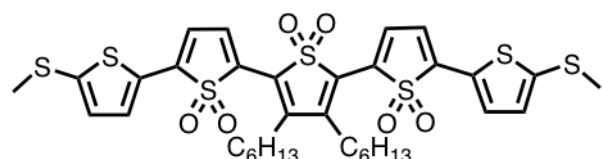
with the following modification: **4.4** (36 mg, 0.064 mmol) was used instead of **4.1**. Purification by column chromatography in 20% ethyl acetate in hexanes ( $R_f = 0.45$ ) yielded the product as a plum purple solid (20 mg, 47% yield).  $^1\text{H}$  NMR (400 MHz,  $\text{CDCl}_3$ )  $\delta$  7.58 (d,  $J = 4.0$  Hz, 2H), 7.17 (s, 2H), 7.07 (d,  $J = 4.0$  Hz, 2H), 2.71 - 2.64 (t, 4H), 2.59 (s, 6H), 1.72 - 1.58 (m, 4H), 1.47 - 1.21 (m, 12H), 0.9 - 0.81 (m, 6H).  $^{13}\text{C}$  NMR (500 MHz,  $\text{CDCl}_3$ )  $\delta$  143.93, 134.72, 132.03, 129.83, 129.51, 129.13, 128.14, 127.84, 31.44, 30.37, 29.27, 27.30, 22.49, 20.77, 14.01. LRMS (APCI+) calculated for  $\text{C}_{30}\text{H}_{38}\text{O}_4\text{S}_6$  655.01, found 654.15.

**5,5"-dibromo-3',4'-dihexyl-[2,2':5',2"-terthiophene] 1,1,1',1',1",1"-hexaoxide (4.8)**



The above compound was synthesized according to published procedures producing a bright orange solid in 48% yield.  $^1\text{H}$  NMR (400 MHz,  $\text{CDCl}_3$ )  $\delta$  7.38 (d,  $J = 5.4$  Hz, 2H), 7.01 (d,  $J = 5.3$  Hz, 2H), 2.86 - 2.77 (t, 4H), 1.62 (m, 4H), 1.34 (m, 12H), 0.91 - 0.85 (m, 6H).

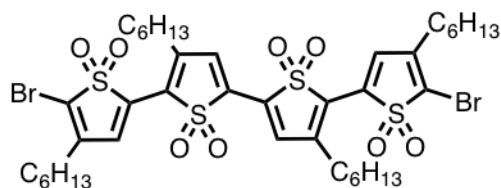
**3",4"-dihexyl-5,5""-bis(methylthio)- [2,2':5',2": 5",2"":5",2""- quinquethiophene] 1',1',1", 1",1",1"- hexaoxide (TDO3)**



The title compound was prepared on a 0.072 mmol scale according to the procedure as **TDO1** with the following modification: **4.8** (48 mg, 0.072 mmol) was used instead of **4.1**. Purification

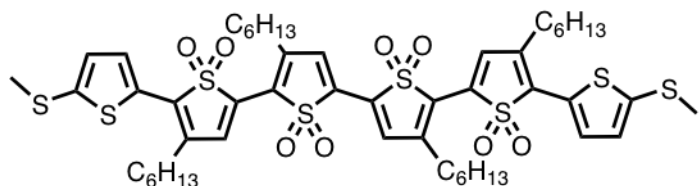
by column chromatography in 30% ethyl acetate in hexanes ( $R_f = 0.17$ ) yielded the product as a deep purple solid (20 mg, 36% yield).  $^1\text{H}$  NMR (400 MHz,  $\text{CDCl}_3$ )  $\delta$  7.55 (d,  $J = 3.9$  Hz, 2H), 7.49 (d,  $J = 5.5$  Hz, 2H), 7.00 (d,  $J = 4.0$  Hz, 2H), 6.69 (d,  $J = 5.6$  Hz, 2H), 2.93 - 2.83 (m, 4H), 2.60 (s, 6H), 1.65 (m, 4H), 1.35 (m, 12H), 0.90 (m, 6H). LRMS (APCI+) calculated for  $\text{C}_{34}\text{H}_{40}\text{O}_6\text{S}_7$  769.13, found 768.3.

**5,5''-dibromo-3',4,4'',4''- tetrahexyl- [2,2':5',2'':5'',2''- quaterthiophene] 1,1,1',1',1'',1'',1'''- octaoxide (4.7)**



The above compound was synthesized according to published procedures producing a dark orange solid in 35% yield.  $^1\text{H}$  NMR (400 MHz,  $\text{CDCl}_3$ )  $\delta$  7.29 (s, 2H), 7.25 (2, 2H), 2.92 (t, 4H), 2.45 (t, 4H), 1.63 (m, 8H), 1.33 (m, 24H), 0.90 (m, 12H).

**3',3'',4''',4''''-tetrahexyl-5,5''''-bis(methylthio)- [2,2':5',2'': 5'',2''':5''',2''''':5''''',2'''''- sexithiophene] 1',1',1'',1'',1''',1''''- octaoxide (TDO4)**



The title compound was prepared on a 0.026 mmol scale according to the procedure as **TDO1** with the following modification: **4.6** (25 mg, 0.026 mmol) was used instead of **4.1**. Purification

by column chromatography in 30% ethyl acetate in hexanes ( $R_f = 0.12$ ) yielded the product as a blue black solid (15 mg, 54% yield).  $^1\text{H}$  NMR (400 MHz,  $\text{CDCl}_3$ )  $\delta$  7.61 (d,  $J = 5.5$  Hz, 2H), 7.39 (s, 2H), 7.26 (s, 2H), 7.07 (d,  $J = 5.4$  Hz, 2H), 2.98 (t, 4H), 2.68 (t, 4H), 2.60 (s, 6H), 1.69 (m, 8H), 1.36 (m, 8H), 1.33 (m, 8H), 1.26 (m, 8H) 0.90 (m, 12H).  $^{13}\text{C}$  NMR (500 MHz,  $\text{CDCl}_3$ )  $\delta$  144.76, 141.32, 133.35, 132.29, 131.65, 130.58, 130.26, 129.75, 129.42, 129.25, 128.89, 126.82, 31.62, 31.48, 31.46, 30.23, 29.71, 29.26, 29.21, 28.78, 27.26, 22.49, 20.59, 14.01. LRMS (MALDI) calculated for  $\text{C}_{50}\text{H}_{66}\text{O}_8\text{S}_8$  1051.57, found 1050.59.

## 5 Changing the Charge Carriers with Molecular Length

### 5.1 Preface

This chapter is based on a manuscript entitled *Molecular Length Dictates the Nature of Charge Carriers in Single-Molecule Junctions of Oxidized Oligothiophenes* by Emma J. Dell†, Brian Capozzi†, Jianlong Xia, Latha Venkataraman, and Luis M. Campos published in *Nature Chemistry*<sup>85</sup> (†equal contributions). The single molecule conductance experimental work was conducted by Brian Capozzi in Prof. Latha Venkataraman’s group. Chemical synthesis was assisted by Dr. Jianlong Xia in Prof. Luis M. Campos’ group.

### 5.2 Introduction

So far we have seen that incorporating electron-poor **TDO** units into our oligomers can narrow their band gaps and increase the molecular conductance. However, we do not know from these small bias conductance measurements what the nature of the orbital that dominates charge transport is i.e. are the molecules hole or electron transporting? The conductance of a molecule depends on the alignment of the molecular energy levels, and in particular the relationship of the highest occupied molecular orbital (HOMO) and the lowest unoccupied molecular orbital (LUMO), with the Fermi level of the gold electrodes.<sup>10</sup> Usually, the Fermi level lies in the HOMO-LUMO gap. (If the Fermi level is very close to either the HOMO or LUMO then electrons will spontaneously transfer between the molecule and the electrode leading to either oxidation or reduction of the molecule.) Whether the molecule is HOMO or LUMO conducting depends on which of the two orbitals is better aligned with the Fermi level (Figure 34). Or, to put it another way, this energy level alignment determines whether the charge carriers are

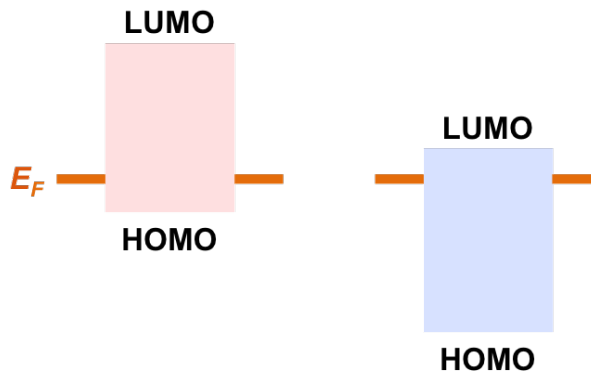


Figure 34: Schematic demonstrating a HOMO-conducting molecule (left) and a LUMO-conducting molecule (right). The conductance pathway depends on which orbital aligns better with the Fermi level of gold ( $E_F$ ).

electrons or holes.

The energy level alignment depends on a number of factors, including the intrinsic electronic properties of the molecule, in addition to the interactions between the molecule and the electrodes in the junction.<sup>74,97–101</sup> In fact, the latter tends to be the dominant factor and so the nature of the linker groups often determines the nature of the charge carriers. For example, amine and sulfide linker groups usually display HOMO conducting behavior, whereas pyridine groups conduct through the LUMO, regardless of the nature of the core molecule.<sup>43</sup> This is perhaps not surprising considering it is the linker groups that are electrically coupled to gold.

All the **Tn** family measured in Chapter 3 are HOMO conducting. Likewise, at the bulk scale, unsubstituted oligothiophenes are large band gap p-type semiconductors.<sup>102,103</sup> The conjugated backbones of these molecules are electron rich with high lying HOMOs well disposed to lose an electron.<sup>30</sup> In order for these species to become electron transporting instead of hole transporting, the LUMO must be lowered and the backbone must become electron deficient. Currently, the most widely used n-type semiconductors are those based on the fullerenes.<sup>28</sup> The soluble C<sub>60</sub> and C<sub>70</sub> derivatives, such as PC<sub>61</sub>BM (phenyl-C<sub>61</sub>-butyric acid methyl ester) in particular,

are commonplace, and provide the electron transporting material in many of the highest efficiency solar cell devices. However, in comparison to the broad range of p-type semiconductors, the field of n-type materials remains limited. Advances in this area using thiophene-based systems have been achieved by introducing electron withdrawing substituents, such as fluorinated moieties.<sup>104–108</sup>

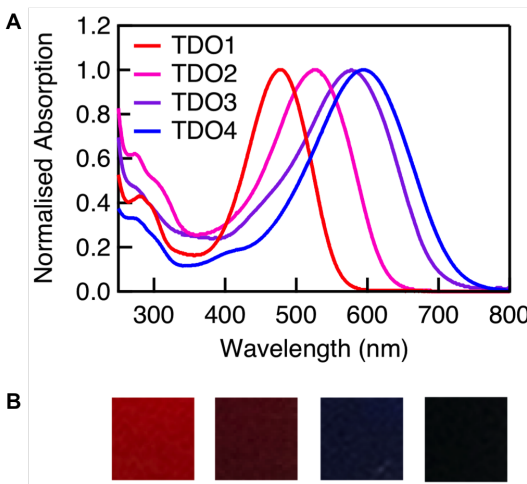


Figure 35: A. Normalized UV-vis absorption spectra for the **TDO<sub>n</sub>** family measured in dichloromethane. B. Colors of the **TDO<sub>n</sub>** family in solution.

We were intrigued as to whether incorporating **TDO** units in the molecule could induce n-type behavior, which might lower the LUMO to such an extent as to override the HOMO-conducting tendency of the methyl-sulfide linkers and thus change the conductance pathway. Compounds containing **TDO** moieties have been found to have low-lying LUMOs and n-type characteristics at the bulk scale.<sup>37,42,88,104,109,110</sup> However, the point at which these materials exhibit n-type behavior as a function of conjugation length is unknown. Since families of n-type materials are underdeveloped in comparison to their p-type counterparts, determining this crossover point is an important fundamental development that can lead to advanced materials design for applications in organic electronics.<sup>102</sup> Characterizing electron transport properties

in these materials is also challenging since bulk transport depends on both intramolecular and intermolecular orbital coupling, the latter being a difficult parameter to control.<sup>104</sup> However, the STM-BJ technique provides a means of probing the fundamental electronic properties at the single-molecule level, rather than in bulk form, sidestepping these issues.<sup>11,99</sup> We therefore wanted to use this technique to probe the nature of the charge carriers in our **TDO<sub>n</sub>** family.

### 5.3 Oxidation Lowers the LUMO

As described in Chapter 4, oxidizing thiophene to its thiophene-1,1-dioxide analog has a dramatic impact on the frontier orbital energy levels. The UV-vis absorption spectra of the **TDO<sub>n</sub>** family show a reduction in the band gap with increasing n, reaching an onset of absorption of 750 nm for **TDO<sub>4</sub>**, accompanied by a deepening of the colors of the molecules in solution from red to dark blue (Figure 35).

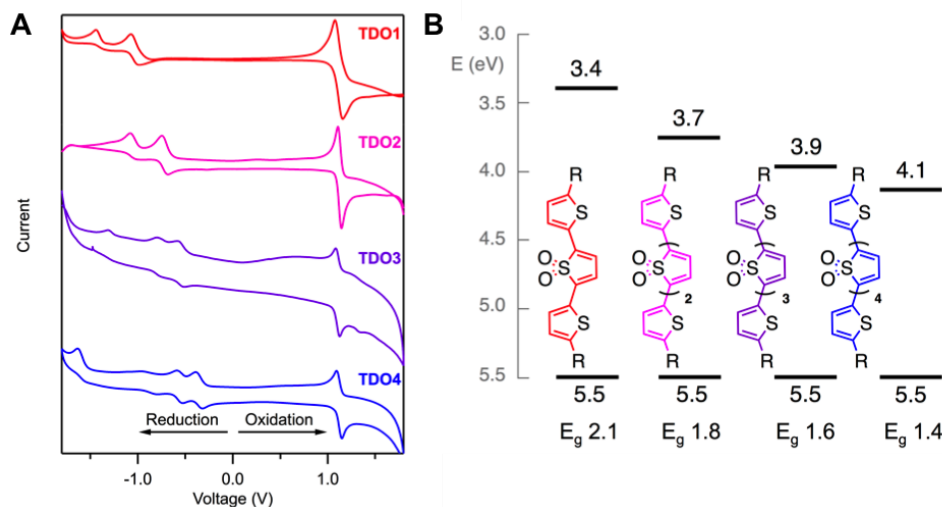


Figure 36: A. Cyclic voltammograms for **TDO<sub>n</sub>** performed in dichloromethane with Ag/AgCl reference electrode, 0.1 M tetrabutyl ammonium hexafluorophosphate as the electrolyte and a scan rate of 50 mVs<sup>-1</sup>. B. HOMO and LUMO levels in eV for the **TDO<sub>n</sub>** family calculated from the cyclic voltammetry data as shown in Table 1.

Cyclic voltammetry measurements were carried out to probe how the HOMO and LUMO levels vary across this series. All the molecules in the series show both oxidation and reduction

peaks in the range -1.8 V to +1.8 V (Figure 36). This is in sharp contrast to the analogous series of all-unoxidized rings, where only oxidation peaks are seen in this solvent window (Figure 17). The cyclic voltammograms indicate that adding thiophene-1,1-dioxide units has a powerful impact on the LUMO of these molecules. The HOMO-LUMO levels for the molecules are shown in Figure 36B, and the LUMO drops from 3.4 eV for **TDO1** to 4.2 eV for **TDO4**. In fact, the value for **TDO4** is nearly that of PC<sub>61</sub>BM, implying possible n-type behavior.<sup>111</sup> We therefore thought that the **TDO****n** family might be good candidates for observing a change in conductance pathway with length.

<b>TDO</b> <b>n</b>	E <sub>ox1/2</sub> (V)	E <sub>red1/2</sub> (V)	E <sub>HOMO</sub> (eV)	E <sub>LUMO</sub>
<b>TDO1</b>	1.12	-1.03	5.5	3.4
<b>TDO2</b>	1.13	-0.72	5.5	3.7
<b>TDO3</b>	1.12	-0.51	5.5	3.9
<b>TDO4</b>	1.12	-0.34	5.5	4.1

Table 1: Frontier orbital energy levels determined from cyclic voltammetry data. E<sub>ox1/2</sub> and E<sub>red1/2</sub> are the midpoints of the first oxidation and reduction peaks respectively in the cyclic voltammograms. E<sub>ox1/2</sub> and E<sub>red1/2</sub> are determined using E<sub>HOMO</sub> = -e[E<sub>ox1/2</sub> + 4.4] and E<sub>LUMO</sub> = -e[E<sub>red1/2</sub> + 4.4] where 4.4 is an empirically derived scale factor for the ferrocene oxidation relative to vacuum.<sup>112,113</sup>

## 5.4 Thermopower Measurements

In order to probe the nature of the orbital alignment between the molecule and the gold electrodes, i.e. whether the HOMO or the LUMO is closer to the Fermi level, we need a handle that will change with the conducting orbital. The Seebeck coefficient is such a handle. To first order, the Seebeck coefficient can be expressed as:<sup>43</sup>

$$S(E_F) = -\frac{\pi^2 k_B^2 T}{3eT(E)} \frac{\partial T(E)}{\partial E} \Big|_{E=E_F} \quad (6)$$

Where,  $k_B$  is Boltzmann's constant,  $T$  is the average temperature of the junction,  $e$  is the charge on an electron, and  $T(E)$  is the transmission function which details the probability that an electron of a given energy is transmitted through the molecular junction. From this expression, it can be seen that the Seebeck coefficient is directly proportional (and opposite in sign) to the slope of the transmission function. This is the key to determining the conducting pathway.

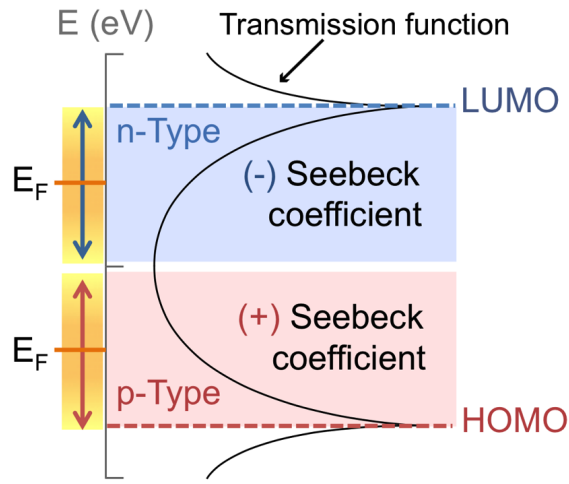


Figure 37: Example of a transmission function that determines the probability that an electron of a given energy will tunnel through the molecular junction. Highlighted are sections in which  $E_F$  aligns closer to the HOMO or LUMO of the molecule. The Seebeck coefficient is proportional to the slope of the transmission function and thus yields positive or negative values depending on the alignment.

As shown in Figure 37, a positive transmission function slope corresponds to LUMO conduction and a negative transmission function slope corresponds to HOMO conduction. Therefore the sign of the Seebeck coefficient can be used as an indicator of which orbital is more closely aligned to the Fermi level.<sup>114</sup> The question though remains of how to experimentally determine the Seebeck coefficient. This is where thermopower measurements prove invaluable.<sup>43,44,115–117</sup> It is known that when a temperature difference is applied across a junction in the presence of an external voltage bias, the expression for the current no longer depends simply on  $G$  and  $V$  as shown in equation 1, but rather expands to include an additional temperature-dependent term

containing the Seebeck coefficient:

$$I = -G\Delta V + GS\Delta T \quad (7)$$

Thus, the Seebeck coefficient can be determined for a single-molecule by applying a temperature difference across the junction and measuring the resulting thermoelectric current (Figure 38).

In this modified STM-BJ setup, the substrate is heated to a temperature of 40°C using a peltier

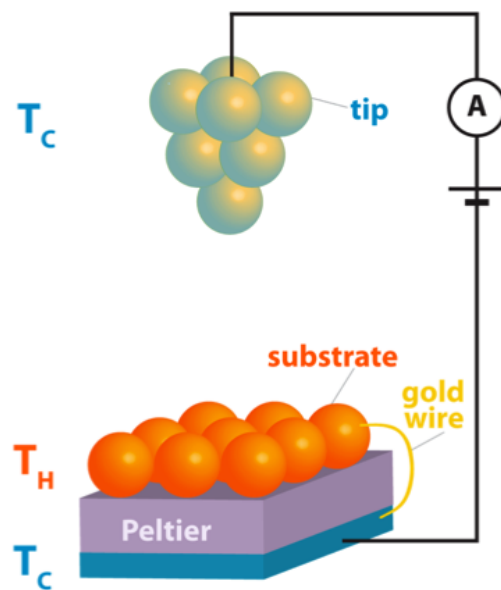


Figure 38: Schematic of the scanning tunneling microscope break junction set up for simultaneous measurements of molecular conductance and thermopower.

while the tip is maintained at room temperature. The tip is brought into contact with the heated substrate while a bias voltage of 10 mV is applied. The tip is pulled away from the substrate and then held fixed at a displacement of 2.2 nm for 150 ms. A 10 mV bias is applied during the pullout and the first and last 25 ms of the hold, but during the middle 100 ms of the hold the bias is dropped to zero (Figure 39).

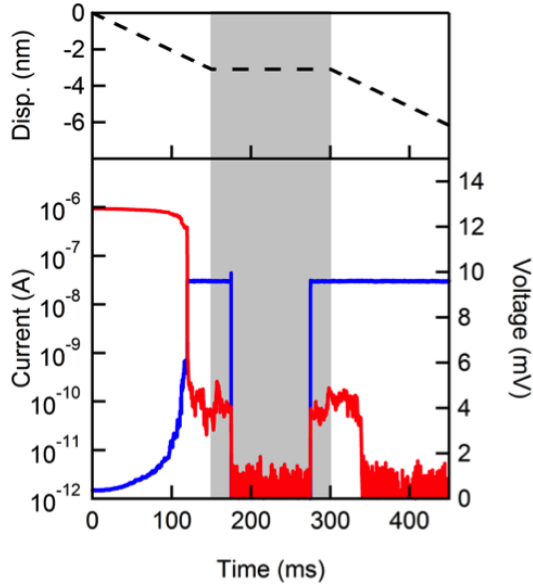


Figure 39: Sample trace for thermopower measurements. Top panel: Sample piezo ramp used in collecting thermopower data, showing the motion of the tip away from the substrate over time. The hold is shown in the gray shaded area. Bottom panel: Sample current vs displacement trace (red) and voltage vs displacement trace (blue) for **TDO3**.

At a 0 mV applied bias, the equation for current simplifies to:

$$I = GS\Delta T \quad (8)$$

The Seebeck coefficient can be extracted by using the thermoelectric current measured at 0 mV together with the known temperature difference and known molecular conductance. Thousands of traces are collected with both a 0 K temperature difference between the tip and the substrate and with a 16 K temperature difference. The control data collected at 0 K are to ensure that there is no thermoelectric current flowing when the temperature gradient is zero. In order to analyze these data, traces are selected where a molecule is present in the junction throughout the hold. These traces are determined by the following process: the conductance at the start and the end of the hold (in the period when the 10 mV bias is applied) is averaged and if this conductance falls within the molecular conductance range (measured in Chapter 4), the

trace is selected. The thermoelectric current measured during the middle portion of the hold in these selected traces is averaged. The thermocurrent values are then used in conjunction with the average molecular conductance (Figure 30B) to compute the average Seebeck coefficient of the given molecular junction using equation 8. We compile these Seebeck coefficients for each molecule into the histograms shown in Figure 40A; these are then fit with a Gaussian function to determine the most frequently measured Seebeck coefficient for each molecule.

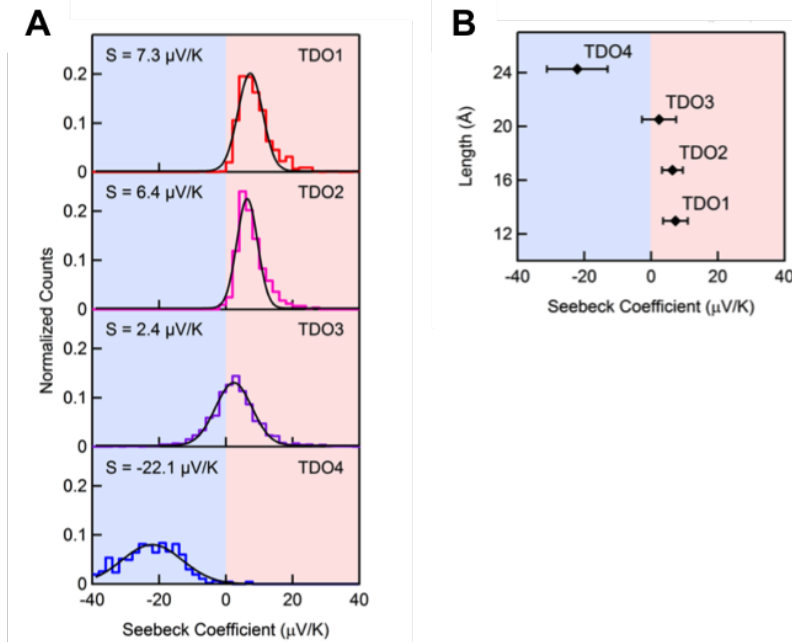


Figure 40: A. STM-BJ measurements are taken with a temperature difference of 16 K between the gold tip and the substrate. While the molecule is bridged across the junction, the applied bias is dropped to zero and the current is measured. Seebeck coefficients for each junction are calculated using this current and compiled into the 1D histograms shown. The black curves are Gaussian fits to the Seebeck distributions. B. Plot of Seebeck coefficient as a function of molecular length for the **TDO<sub>n</sub>** family with error bars reflecting the standard deviation of the Gaussian fits. A shift from positive to negative Seebeck values is seen with increasing length, indicating a change in the charge carriers from holes to electrons.

We plot in Figure 40B the Seebeck coefficient versus the molecular length. For **TDO1-TDO3**, this value is positive and decreases non-linearly with length, while for **TDO4** it is negative and relatively large in magnitude. This trend is contrary to what has been observed in amine, thiol, and trimethyltin-linked oligophenyl series, where the Seebeck coefficient main-

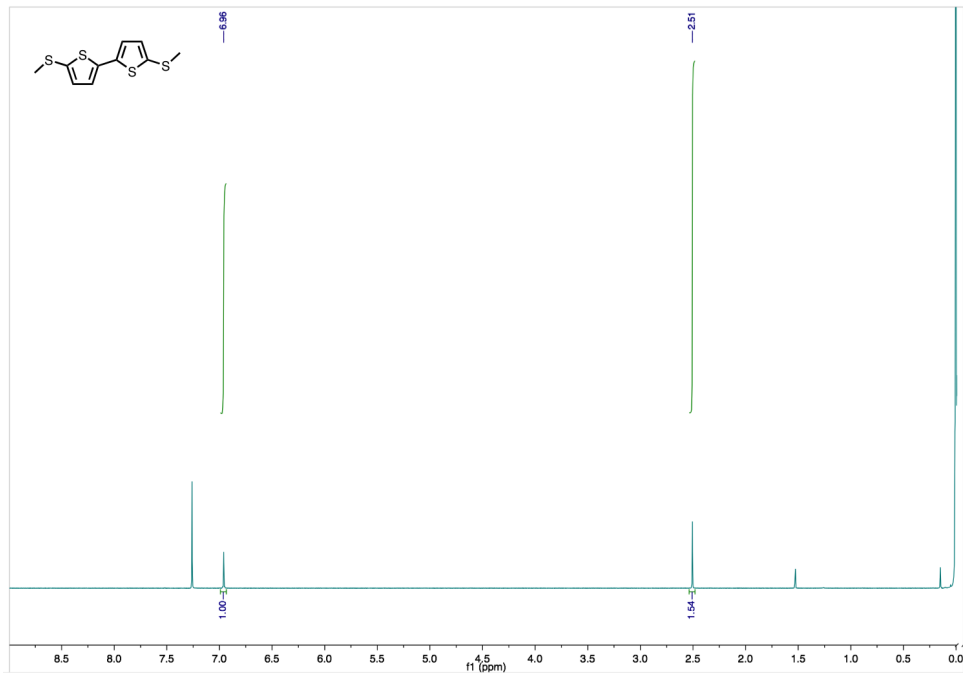
tains the same sign (positive) and increases in magnitude with molecular length.<sup>44,115,117</sup> Such measurements have demonstrated that the oligophenyls conduct via hole transport through the HOMO. The increase in magnitude of S with increasing length in these oligophenyls was attributed to HOMO moving closer to  $E_F$  while simultaneously narrowing as the conducting orbital becomes delocalized over a longer molecule, resulting in a larger slope in the transmission function at  $E_F$ .

Based upon our measurements on the **TDO<sub>n</sub>** series, we infer that transport in **TDO1** is dominated by HOMO, indicating hole-type transport. The large, negative Seebeck coefficient measured for **TDO4** indicates electron-transport dominated by the LUMO. In fact, the magnitude of this value is comparable to that of C<sub>60</sub>, which is among the highest values of organic compounds.<sup>118</sup> The Seebeck coefficient for **TDO2** is smaller in magnitude than **TDO1**; if transport in **TDO2** was dominated by the HOMO, we would expect a larger Seebeck coefficient when compared to **TDO1**. We thus conclude that transport in **TDO2** is not dominated by a single orbital. Finally, the slightly positive but small magnitude Seebeck coefficient measured for **TDO3** suggests that the  $E_F$  lies in the relatively flat region of the transmission function, possibly in the middle of the HOMO-LUMO gap with both orbitals contributing to charge transport. This would imply that the transmission functions for both **TDO2** and **TDO3** do not follow a Lorentzian shape and thus, a direct determination of the level alignment for these two systems is not possible. Taken together, these measurements show that contributions from LUMO to charge transport become increasingly more important as the number of oxidized thiophene units in the molecular backbone is increased.

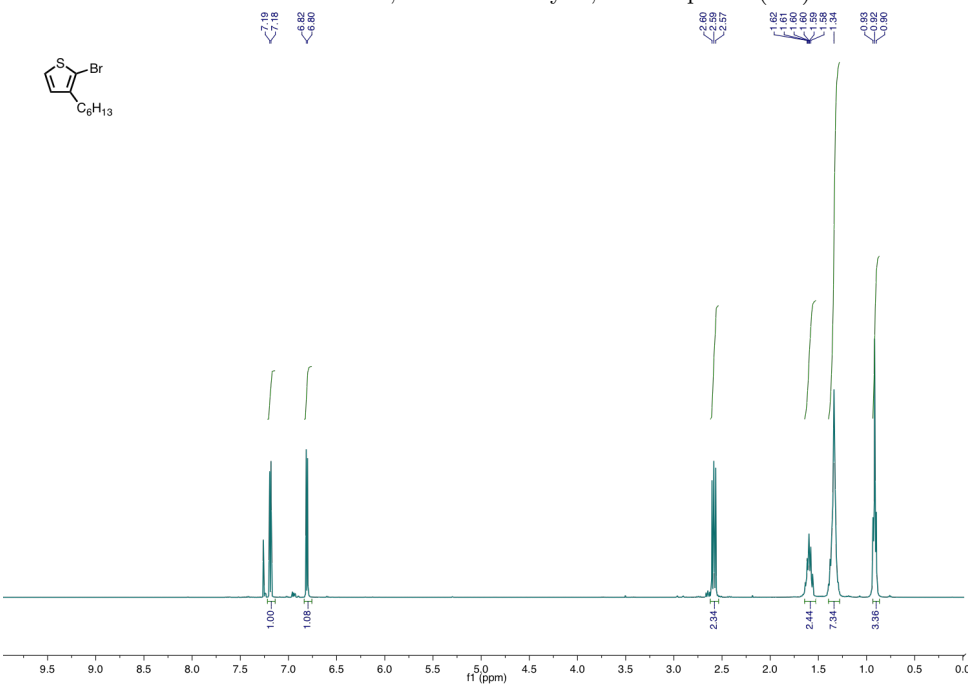
## 5.5 Conclusion

We demonstrated that the **TDO<sub>n</sub>** family show markedly different electronic properties than their unoxidized **Tn** analogs. In particular, they show a narrowed band gap in their absorption spectra. Using cyclic voltammetry measurements we calculated the frontier orbital energy levels for this **TDO<sub>n</sub>** family and showed that this narrowing is primarily due to the LUMO dropping across the series. By performing simultaneous conductance and thermopower measurements we extracted the Seebeck coefficients for these molecules. These showed that for the first two members of the series, the HOMO is better aligned with gold's Fermi level, leading to holes being the charge carriers in the junction. This is the same as for the **Tn** family. However, for **TDO<sub>4</sub>**, the Seebeck coefficient is negative, implying that the LUMO is better aligned with gold's Fermi level and thus electrons are the charge carriers in the junction. While previous studies have shown that the dominant conductive orbital is generally controlled by the aurophilic linker units, control through backbone length is unprecedented. This work, therefore, provides an additional handle with which to tune conductance in single-molecule measurements, and also underscores the promise of thiophene-1,1-dioxide as a powerful electron-deficient motif with a low-lying LUMO to tune to electronic properties in bulk materials.

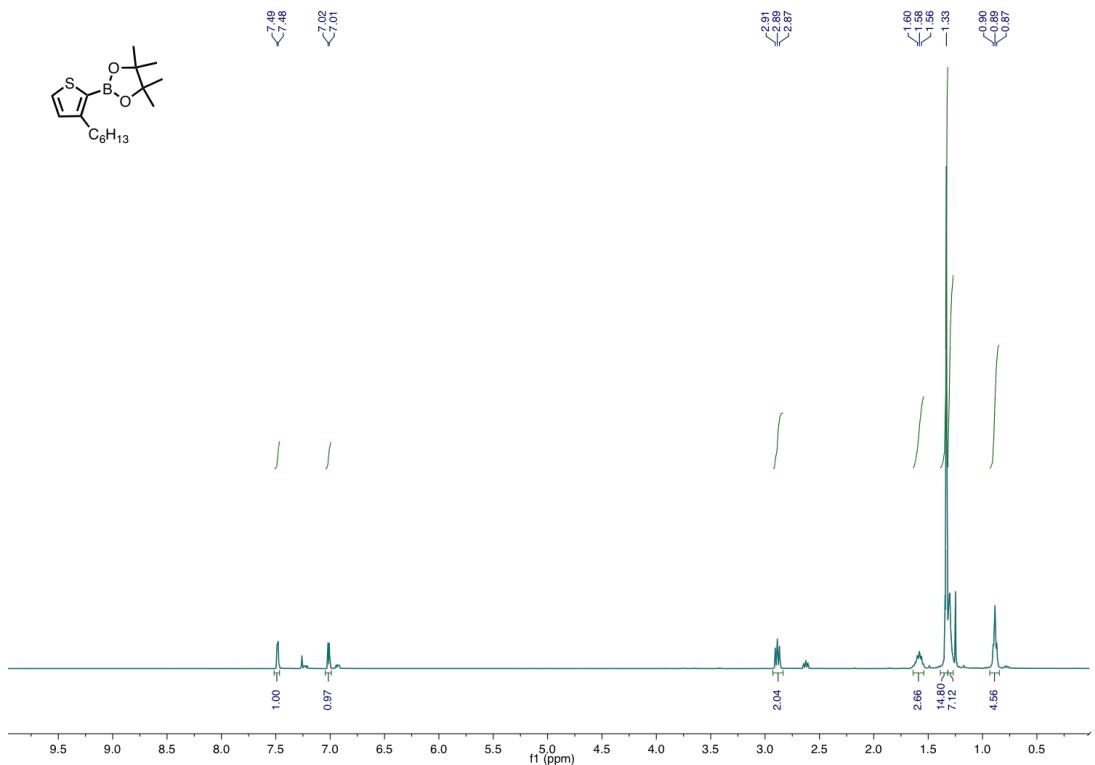
## 6 NMR Characterization



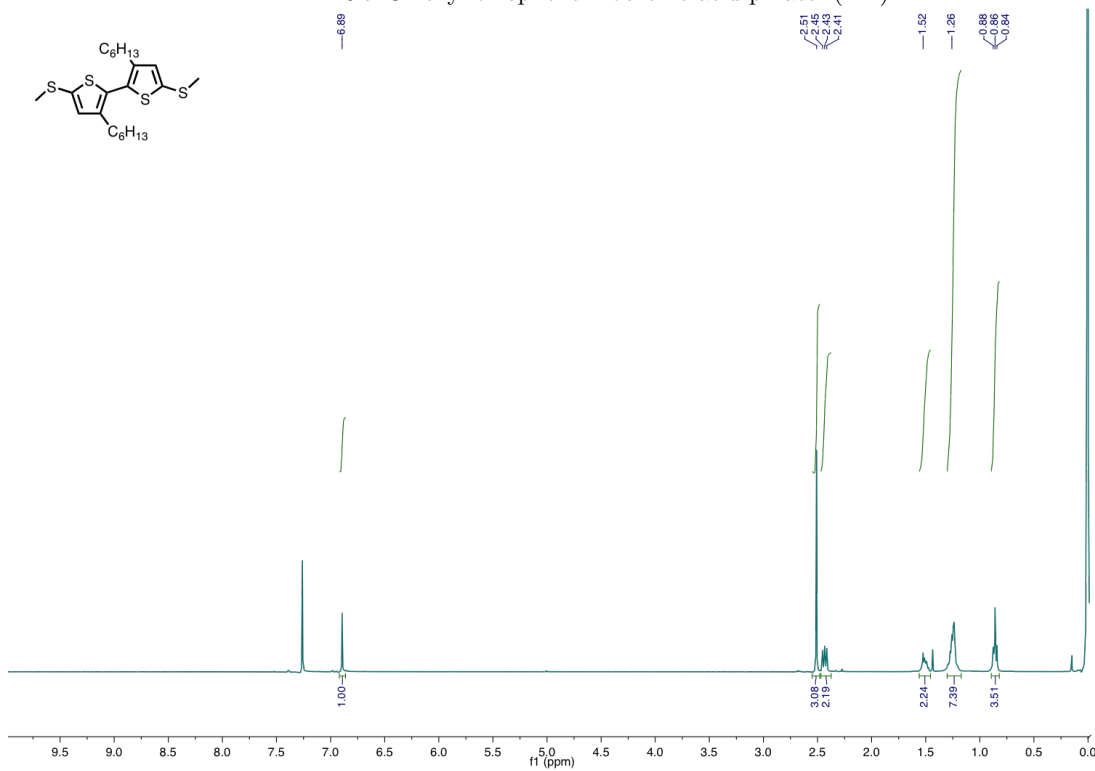
$^1\text{H}$  NMR of 5,5'-bithiomethyl 2,2'-bithiophene (**T2**)



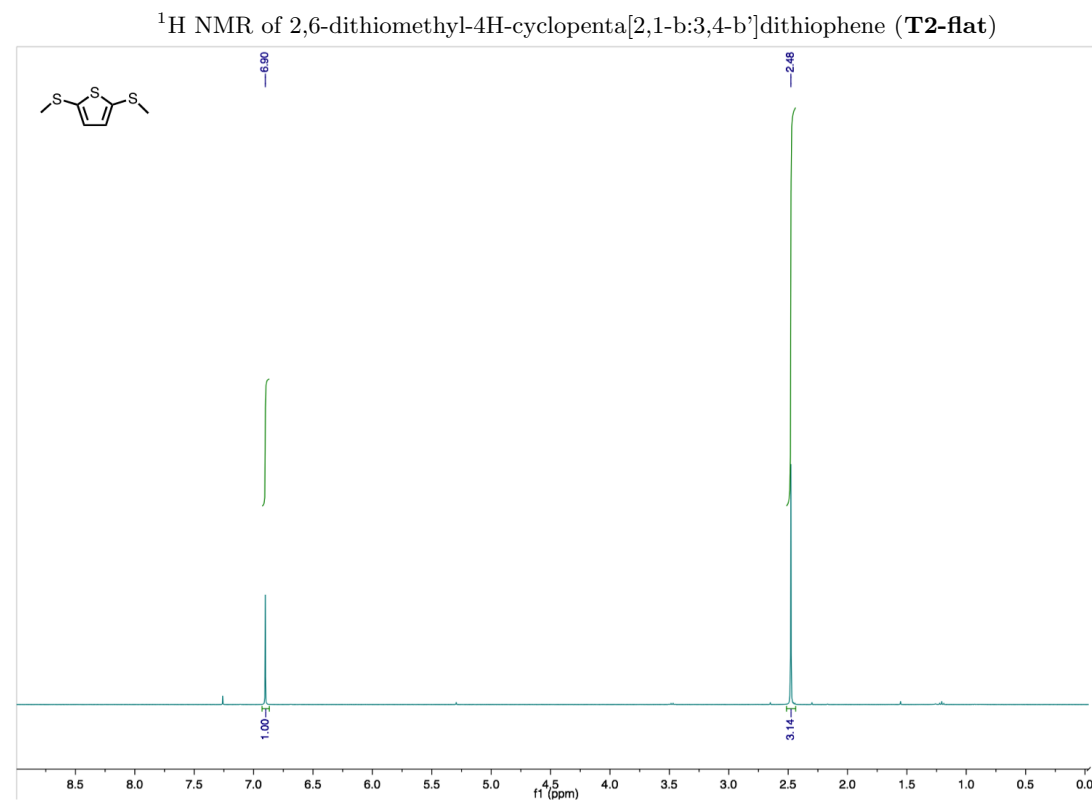
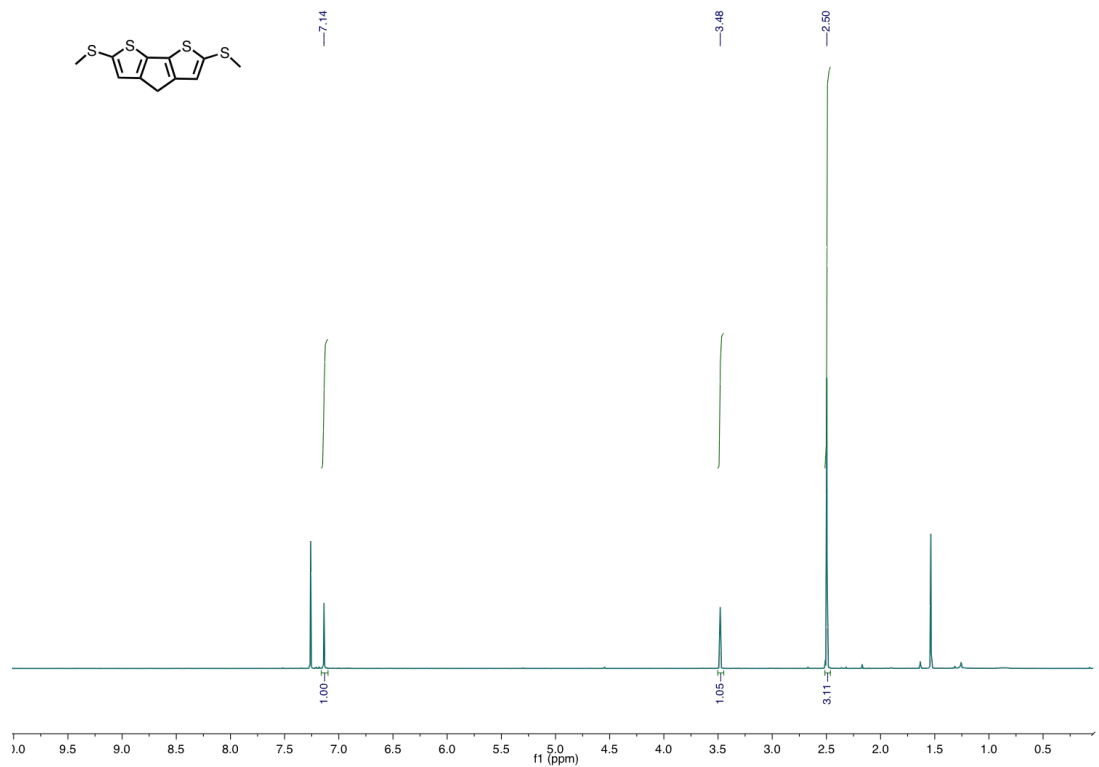
$^1\text{H}$  NMR of 2-bromo, 3-hexyl thiophene (**2.1**)

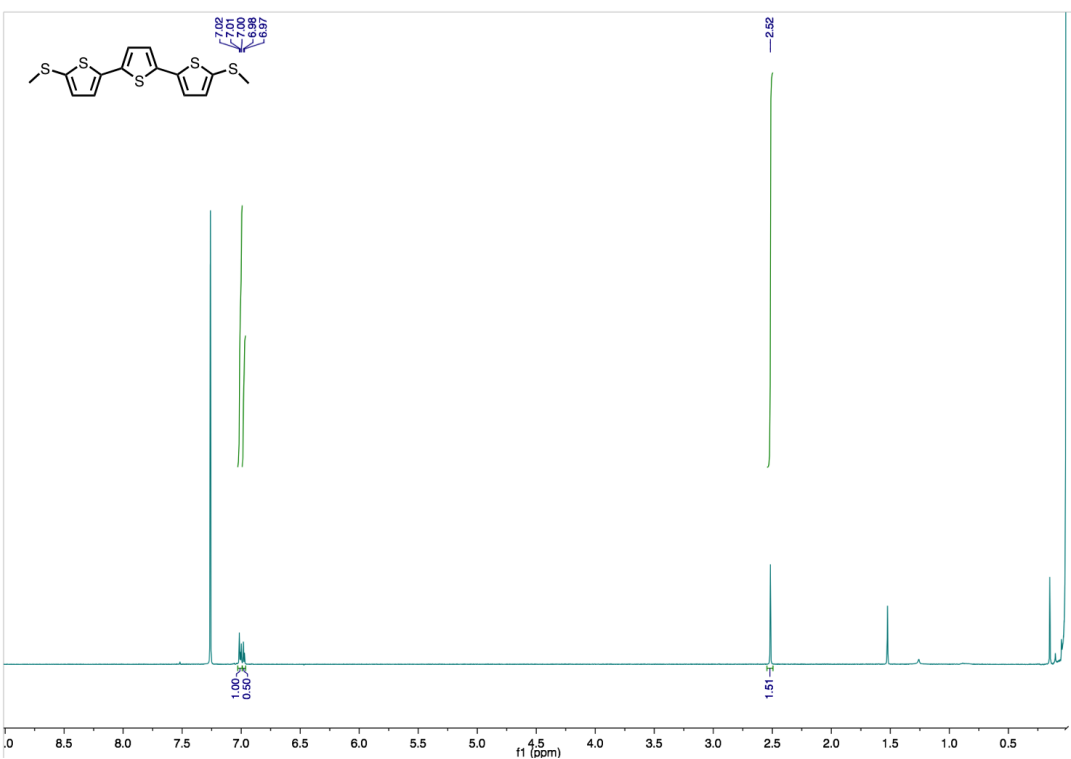


<sup>1</sup>H NMR of 3-hexyl thiophene-2-boronic acid pinacol (**2.2**)

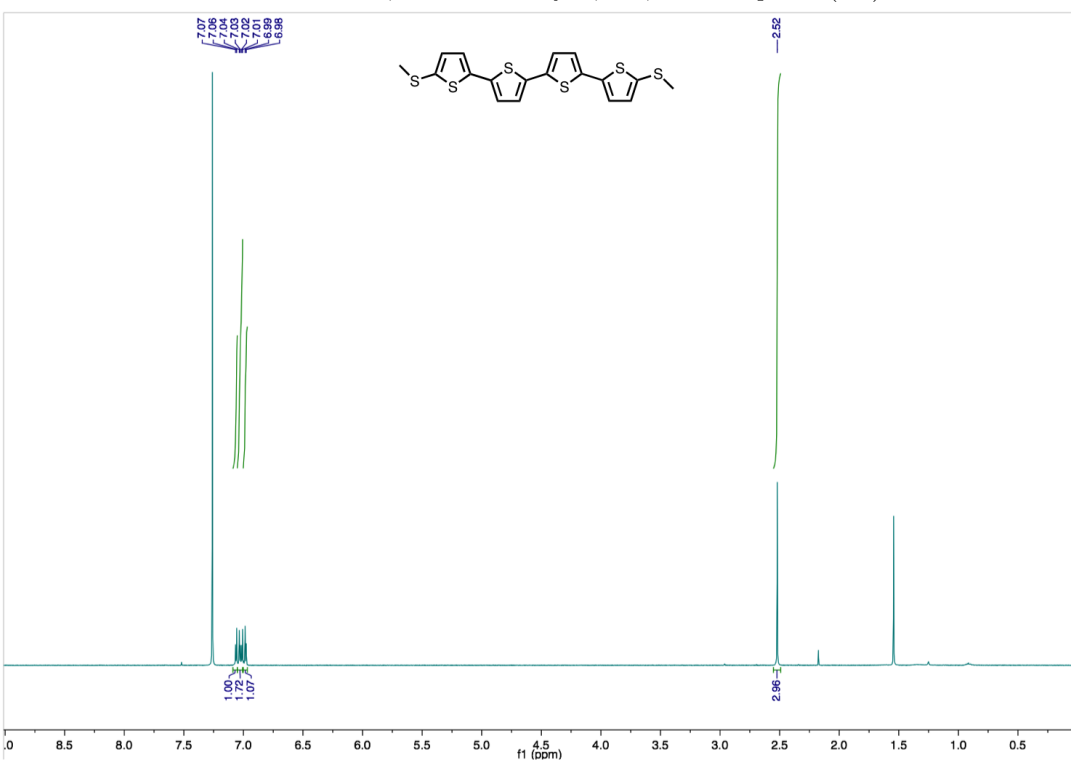


<sup>1</sup>H NMR of 5,5' bisthiomethyl 3,3' dimethyl 2,2' bithiophene (**T2-twist**)

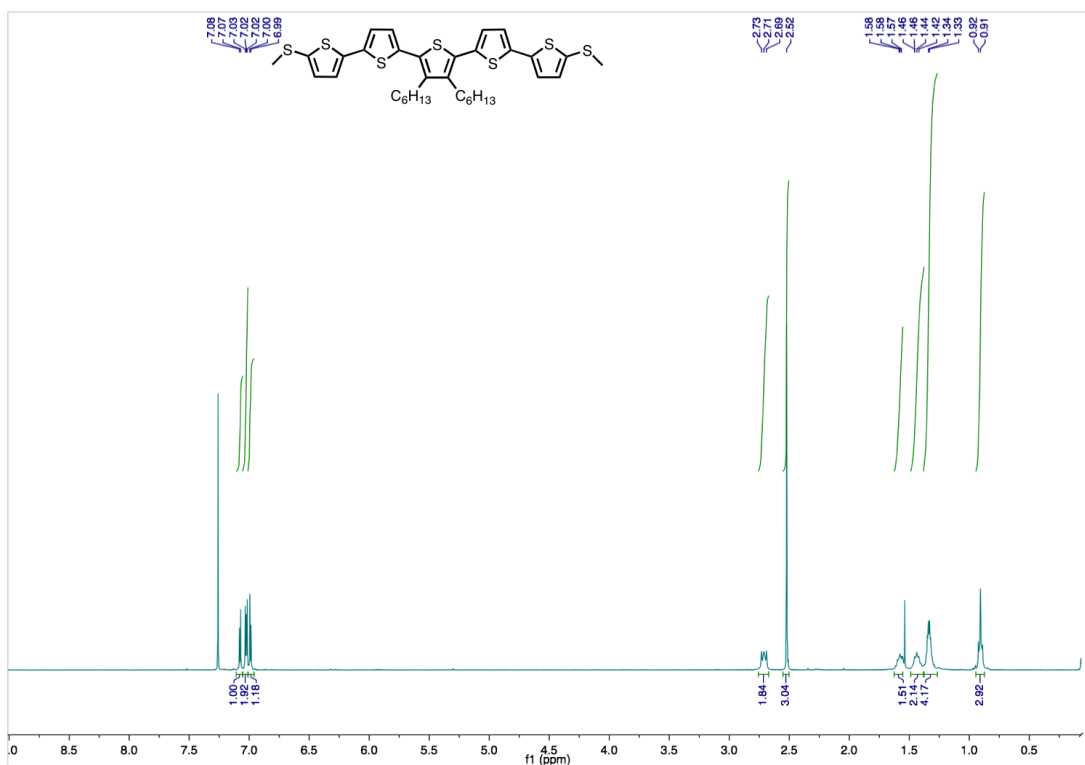




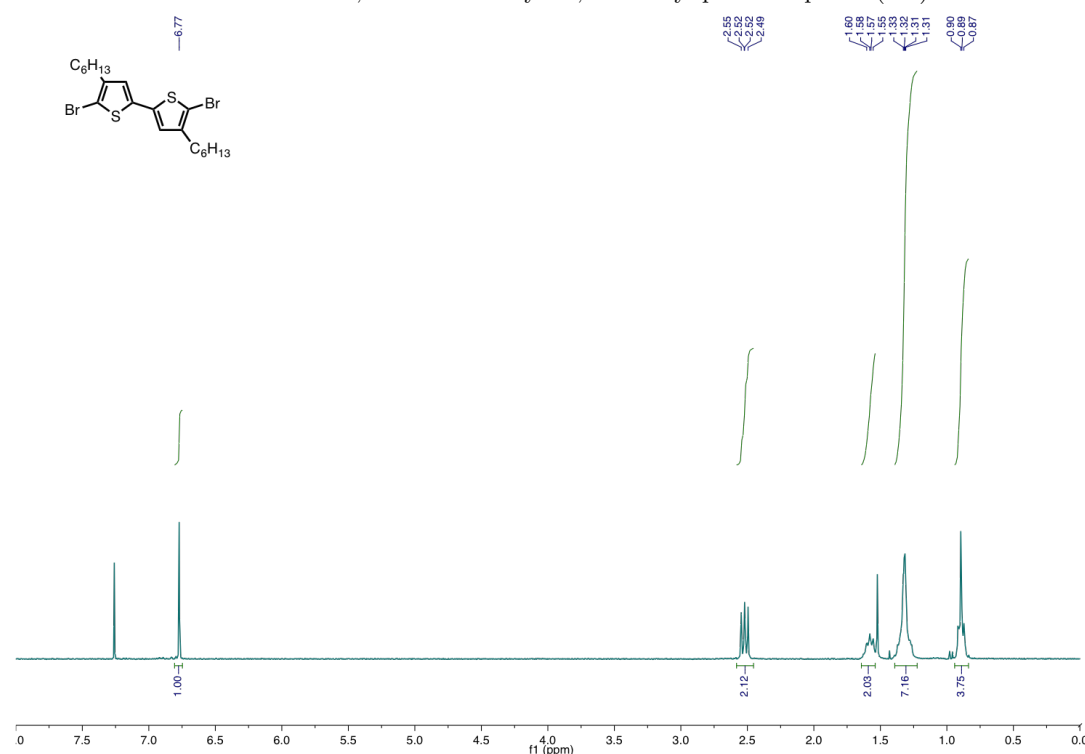
$^1\text{H}$  NMR of 5,5'' bis(thiomethyl)-2,2':5',2''-terthiophene (**T3**)



$^1\text{H}$  NMR of 5,5'' bis(thiomethyl)-quaterthiophene (**T4**)



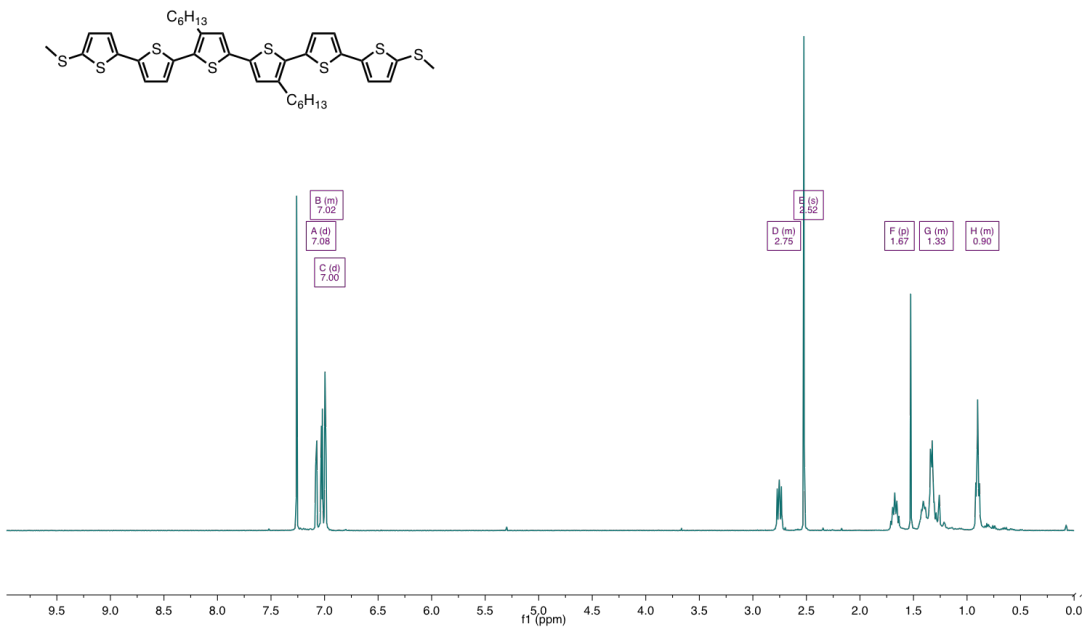
$^1\text{H}$  NMR of 5,5'''-dithiomethyl-3'',4''-dihexyl-pentathiophene (**T5**)



$^1\text{H}$  NMR of 5,5'-dibromo-4,4'-dihexyl-2,2'-bithiophene (**3.3**)



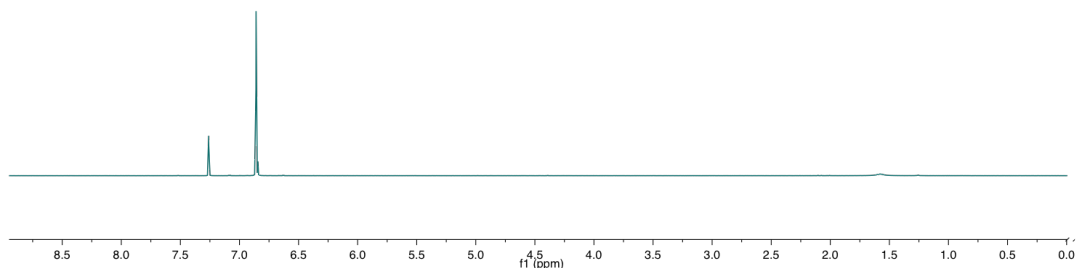
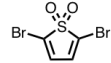
<sup>1</sup>H NMR (400 MHz, Chloroform-d) δ 7.08 (d, *J*=3.8 Hz, 1H), 7.06 – 7.01 (m, 2H), 7.00 (d, *J*=1.0 Hz, 2H), 2.80 – 2.71 (m, 2H), 2.52 (s, 3H), 1.67 (p, *J*=7.8, 7.4 Hz, 2H), 1.46 – 1.25 (m, 8H), 0.95 – 0.86 (m, 3H).



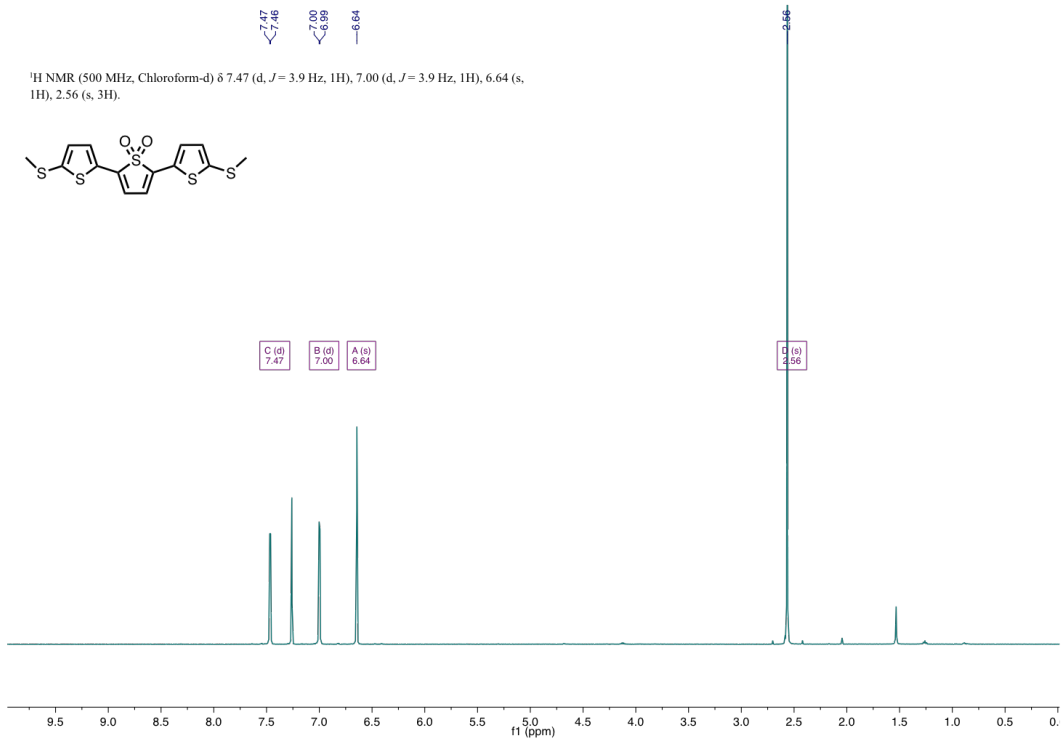
<sup>1</sup>H NMR of 3'',4''-dihexyl-5,5'''- bis(methylthio)-sexithiophene (**T6**)

<sup>1</sup>H NMR (400 MHz, CDCl<sub>3</sub>) δ 6.86.

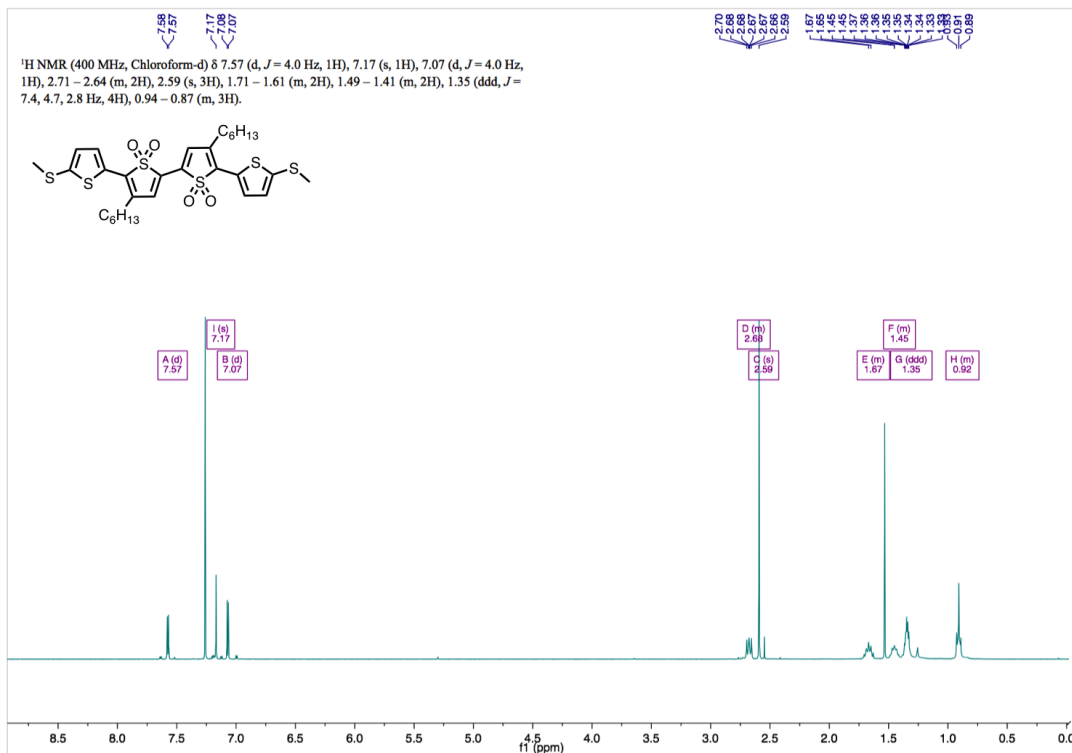
— 6.86



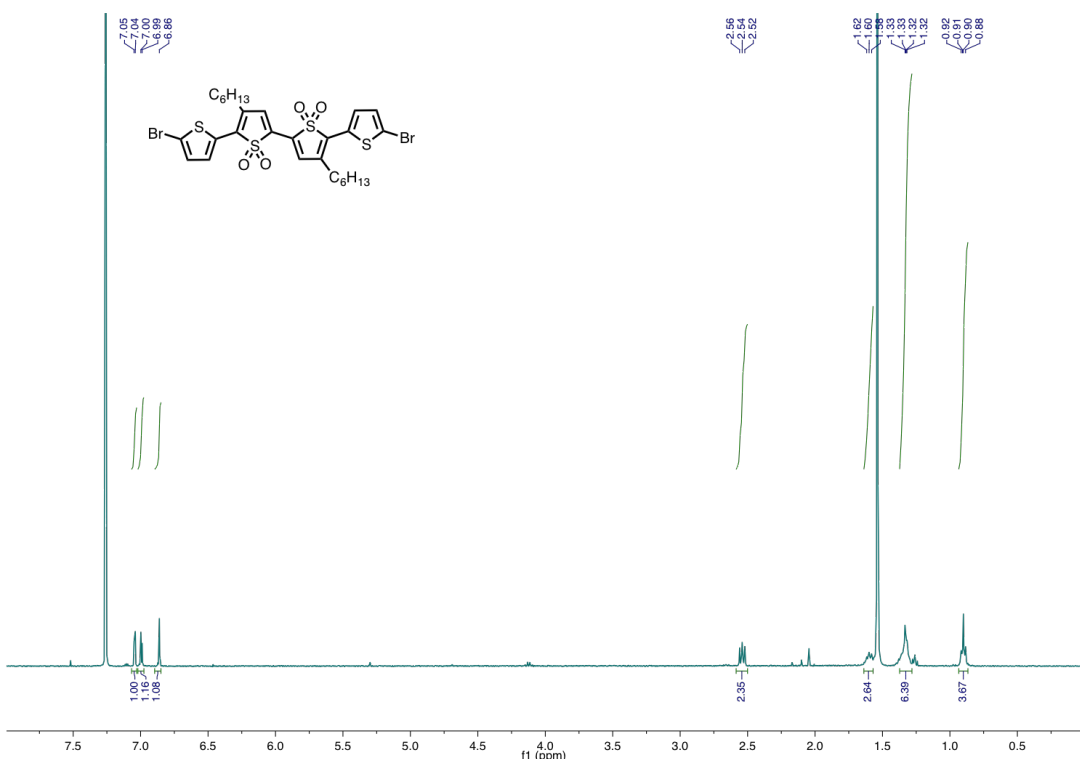
<sup>1</sup>H NMR of 2,5-dibromothiophene-1,1-dioxide (**4.1**)



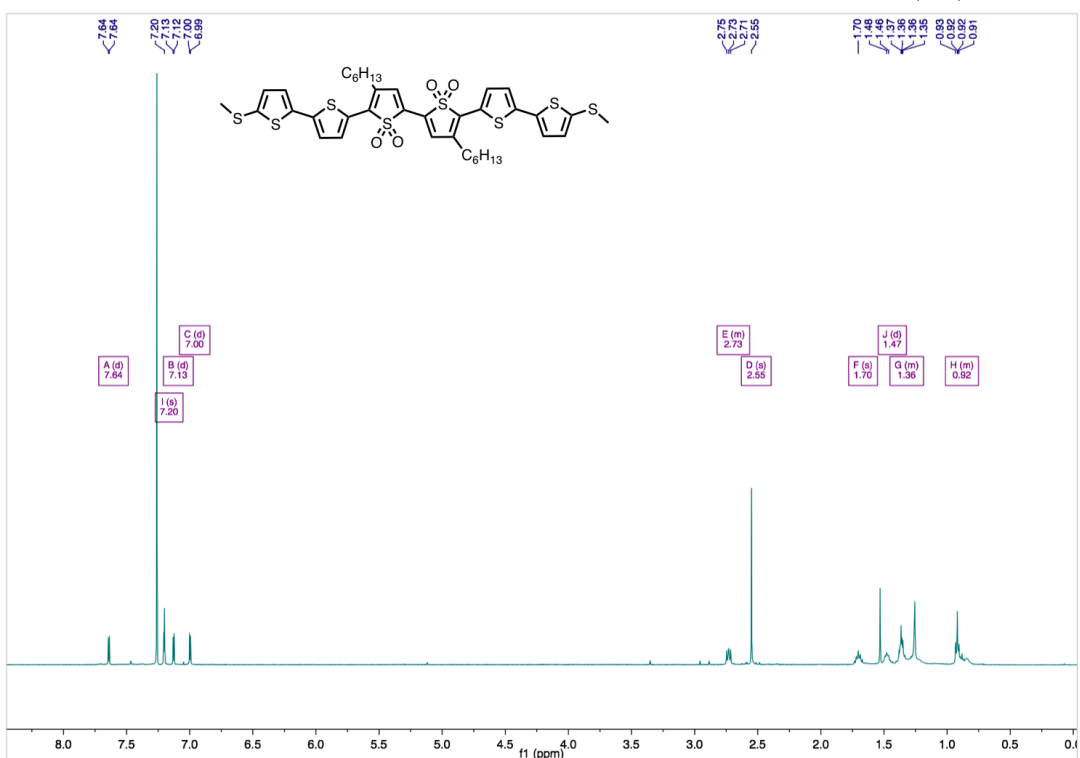
<sup>1</sup>H NMR of 5,5''-bis(methylthio)-terthiophene-dioxide (**TDO1**)



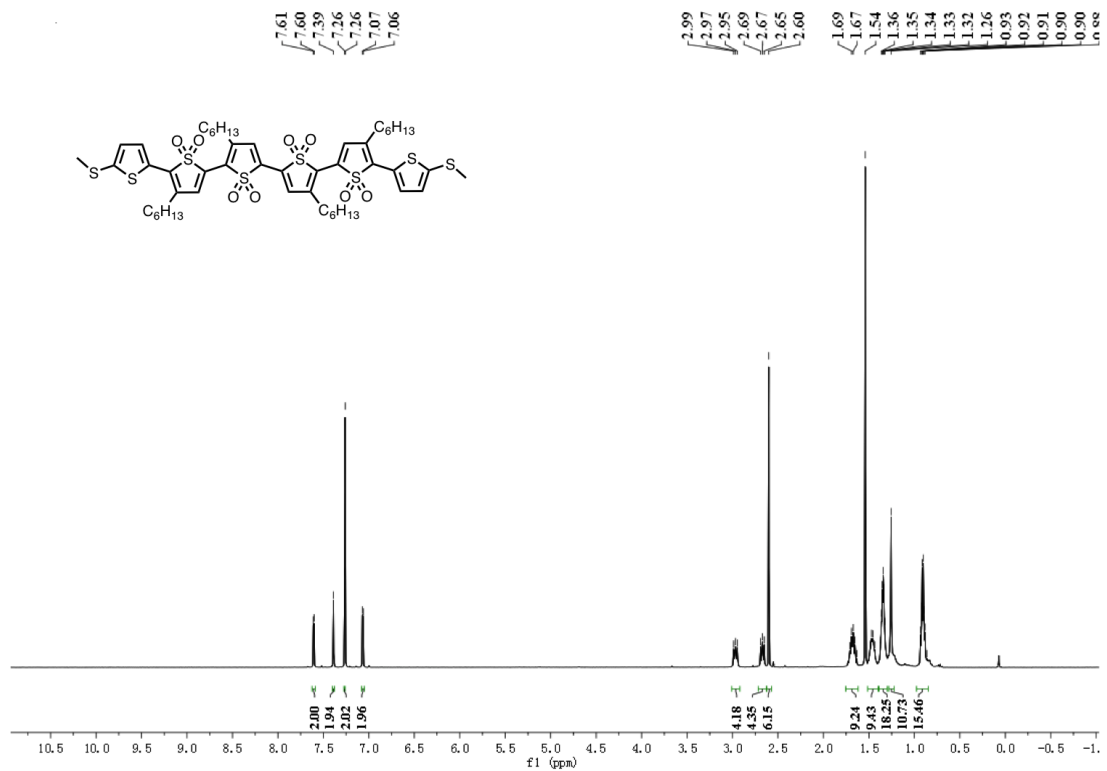
<sup>1</sup>H NMR of 3',4''-dihexyl-5,5''-bis(methylthio)-quaterthiophene-tetraoxide (**TDO2**)



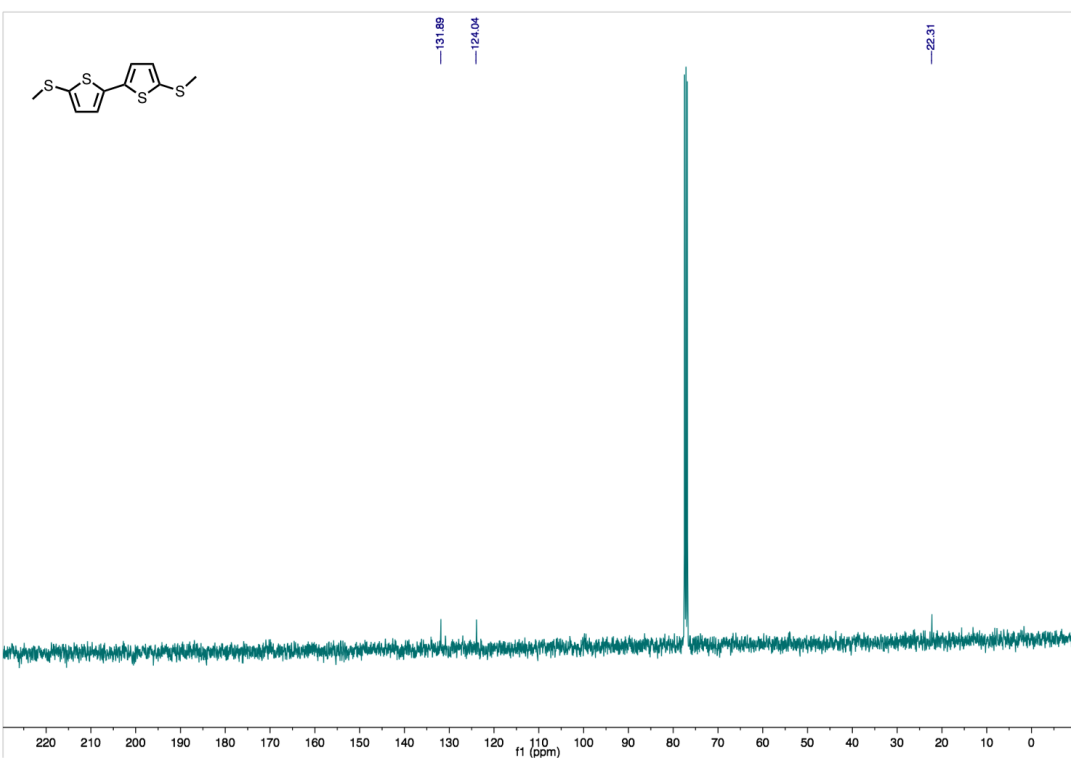
$^1\text{H}$  NMR of 5,5''-dibromo-3',4''-dihexyl- quaterthiophene -tetraoxide (**4.2**)



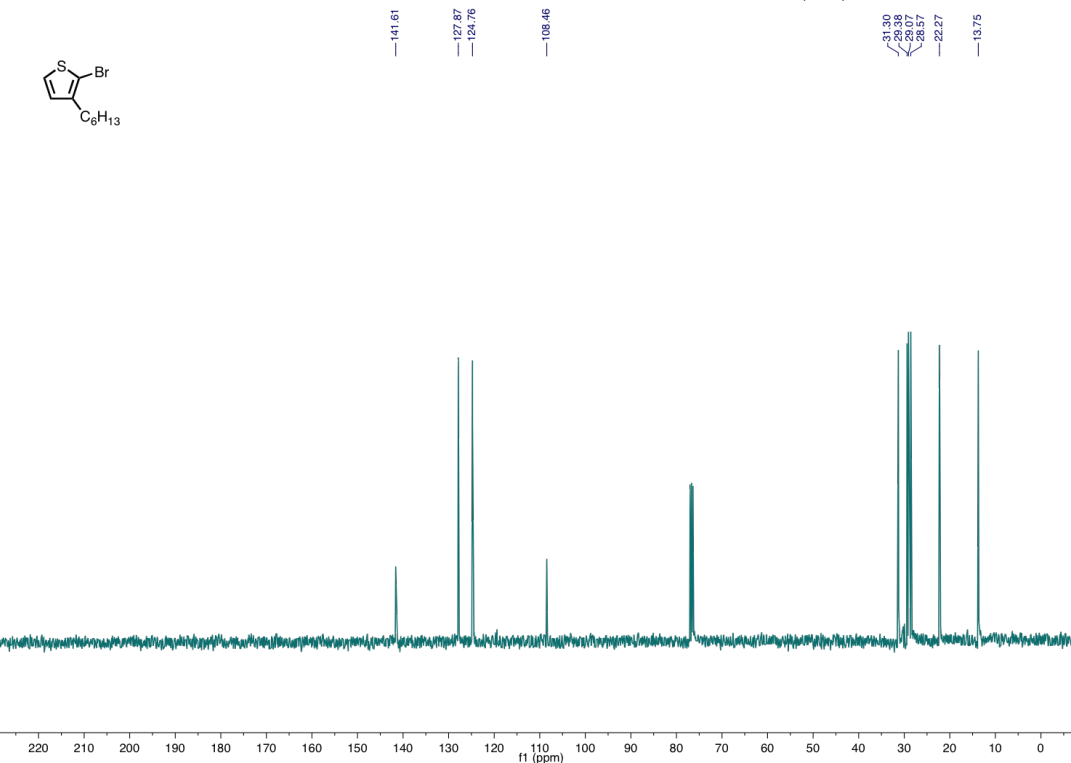
$^1\text{H}$  NMR of 3'',4''-dihexyl-5,5'''-bis(methylthio) -sexithiophene-tetraoxide (**4.3**)



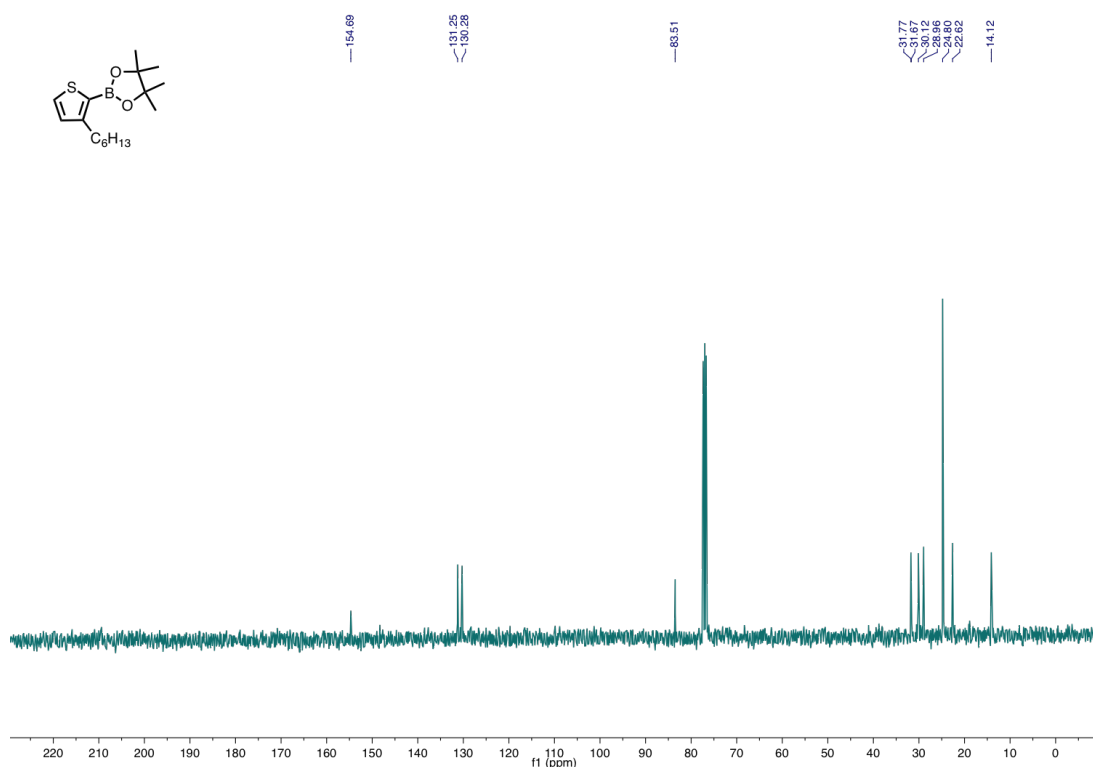
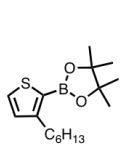
<sup>1</sup>H NMR of 3',3'',4'',4'''-tetrahexyl-bis(methylthio)-sexithiophene-octaoxide (**TDO4**)



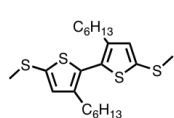
$^{13}\text{C}$  NMR of 5,5'-bisthiomethyl 2,2'-bithiophene (**T2**)



$^{13}\text{C}$  NMR of 2-bromo, 3-hexyl thiophene (**2.1**)

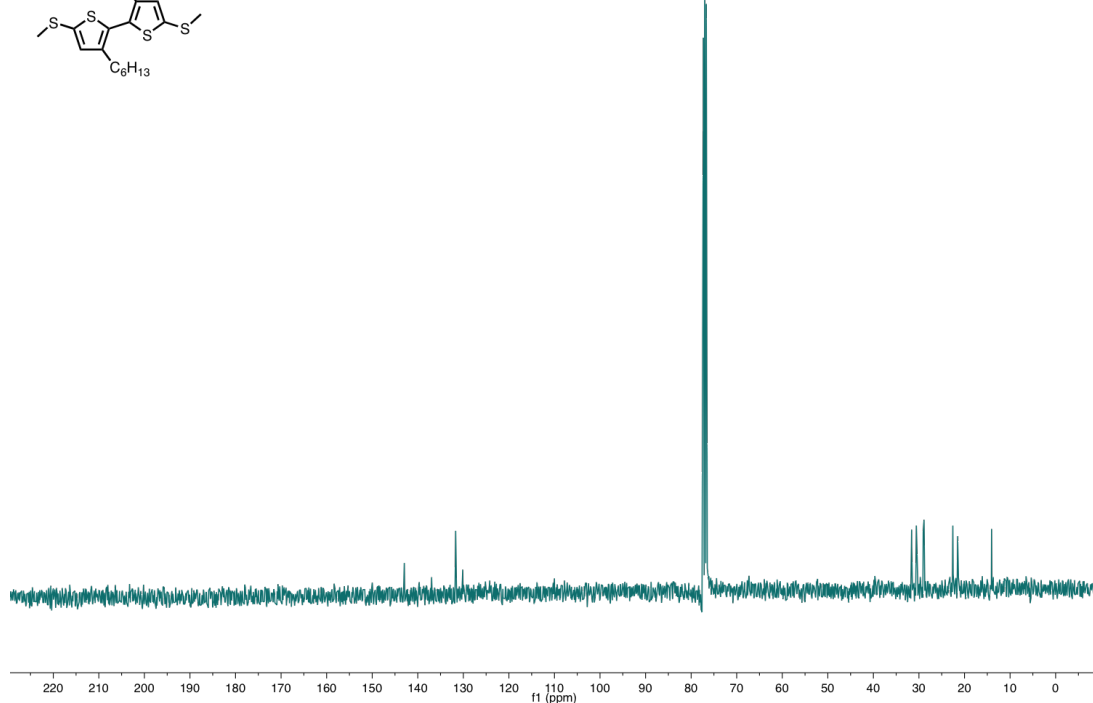


$^{13}\text{C}$  NMR of 3-hexyl thiophene-2-boronic acid pinacol (**2.2**)

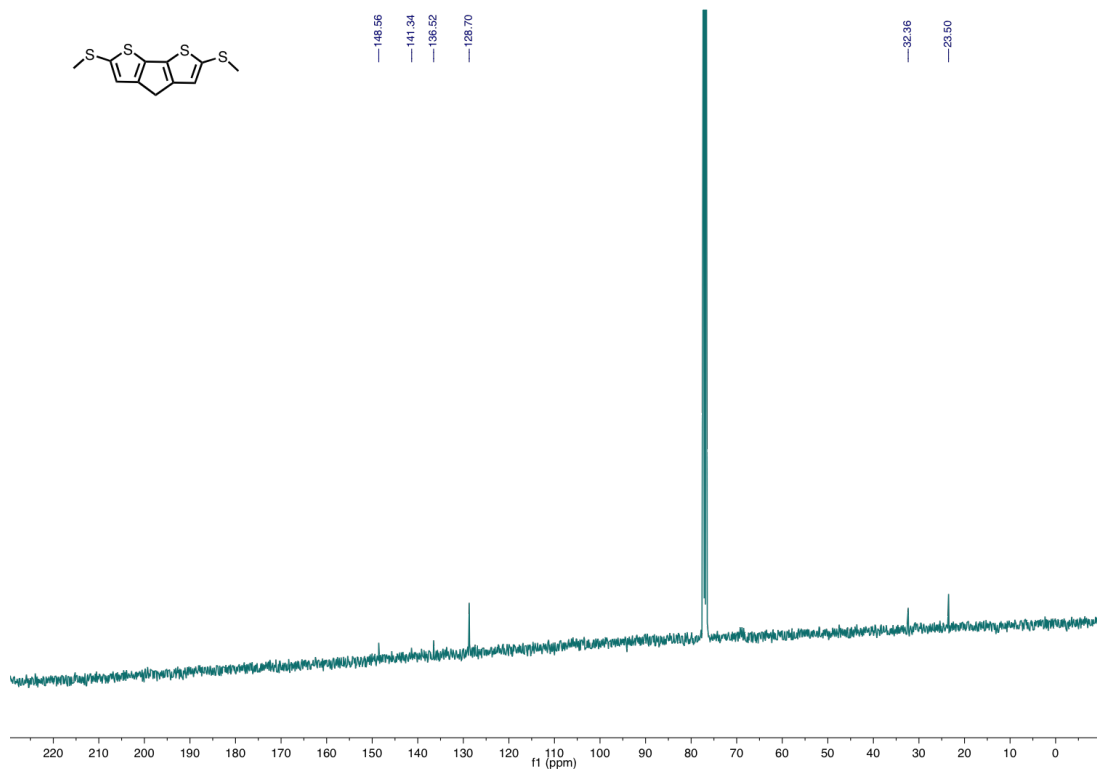


-143.03    -137.03    -131.68    -130.07

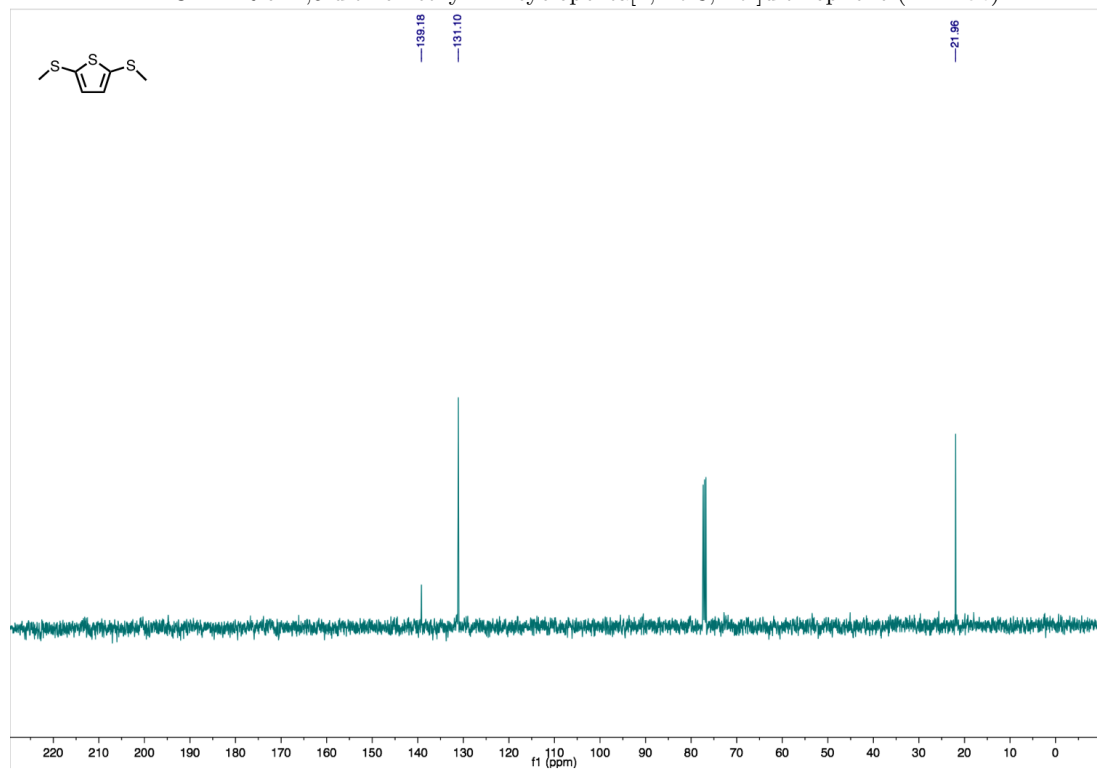
-31.61    -30.56    -29.06    -28.88  
-22.56    -21.51    -14.07



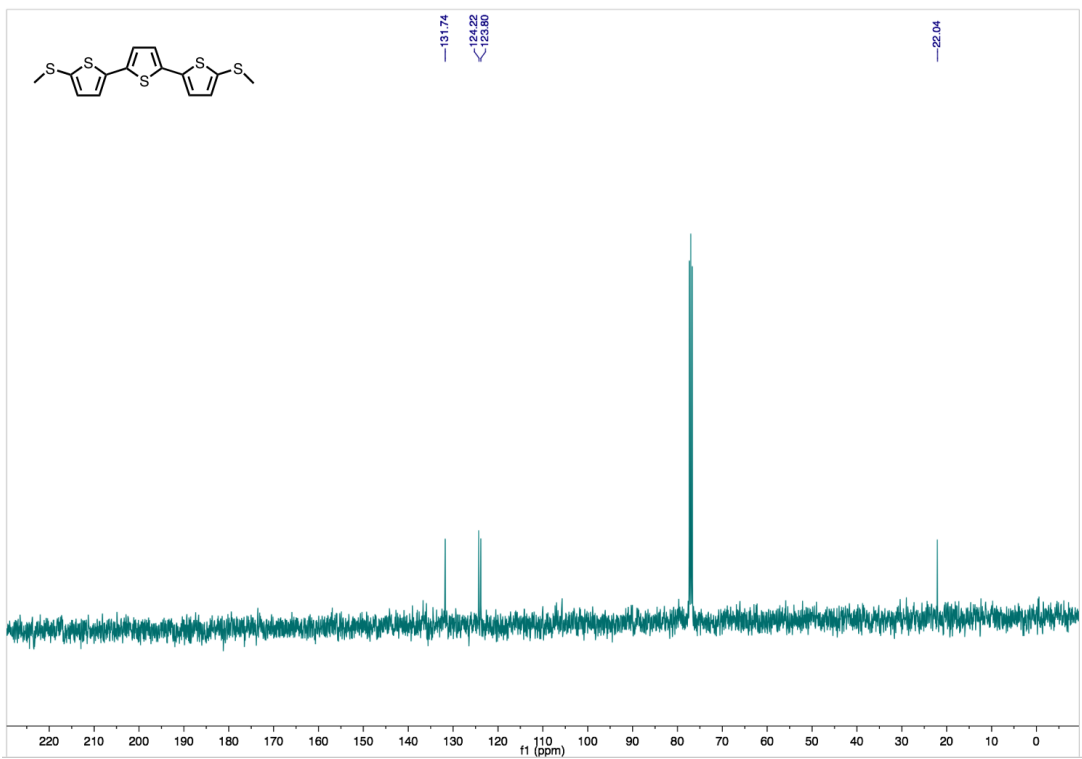
$^{13}\text{C}$  NMR of 5,5' bisthiomethyl 3,3' dimethyl 2,2' bithiophene (**T2-twist**)



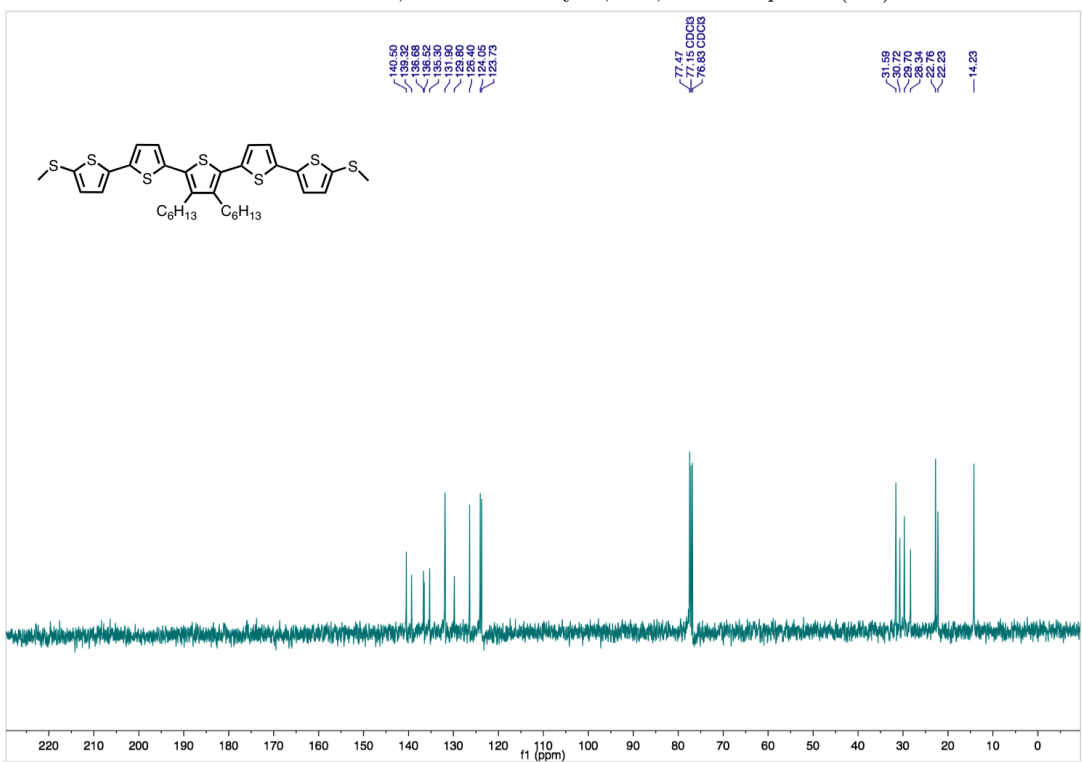
$^{13}\text{C}$  NMR of 2,6-dithiomethyl-4H-cyclopenta[2,1-b:3,4-b']dithiophene (**T2-flat**)



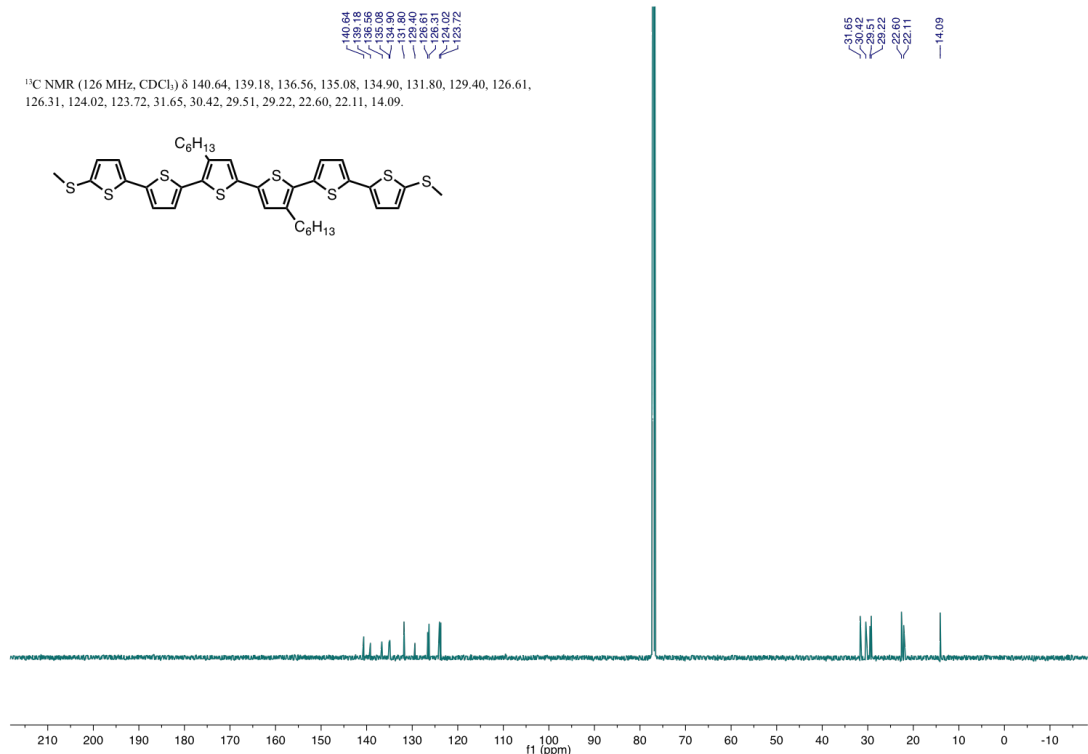
$^{13}\text{C}$  NMR of 2,5-bisthiomethylthiophene (**T1**)



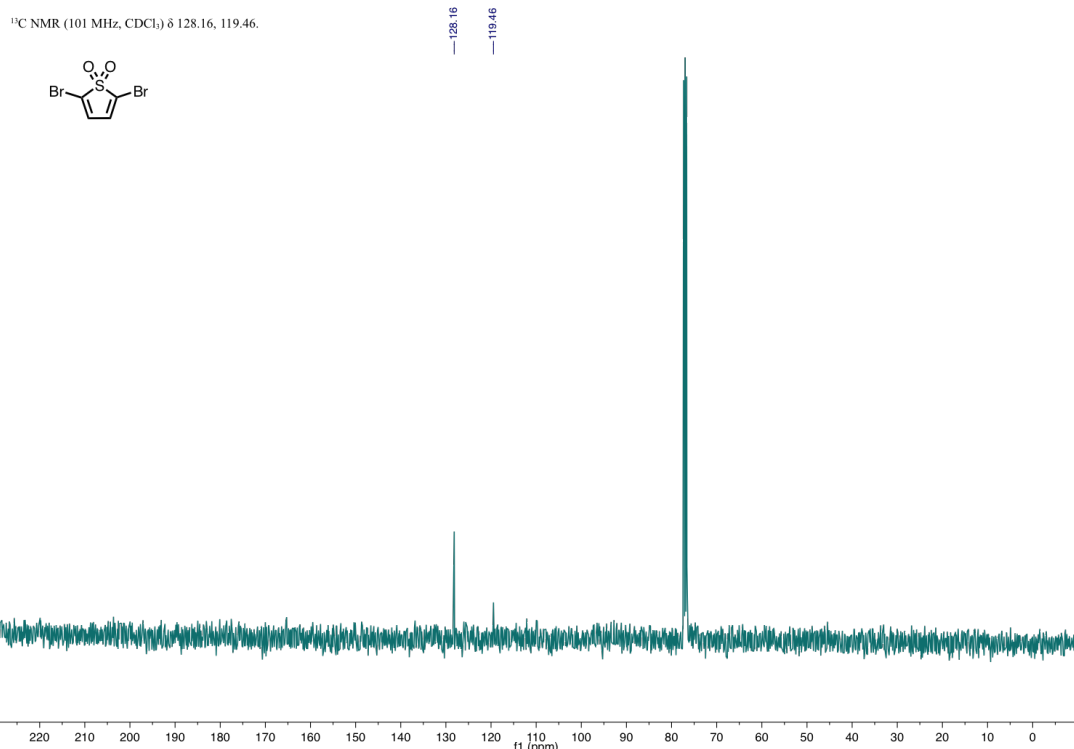
<sup>13</sup>C NMR of 5,5''-bisthiomethyl-2,2':5',2''-terthiophene (T3)



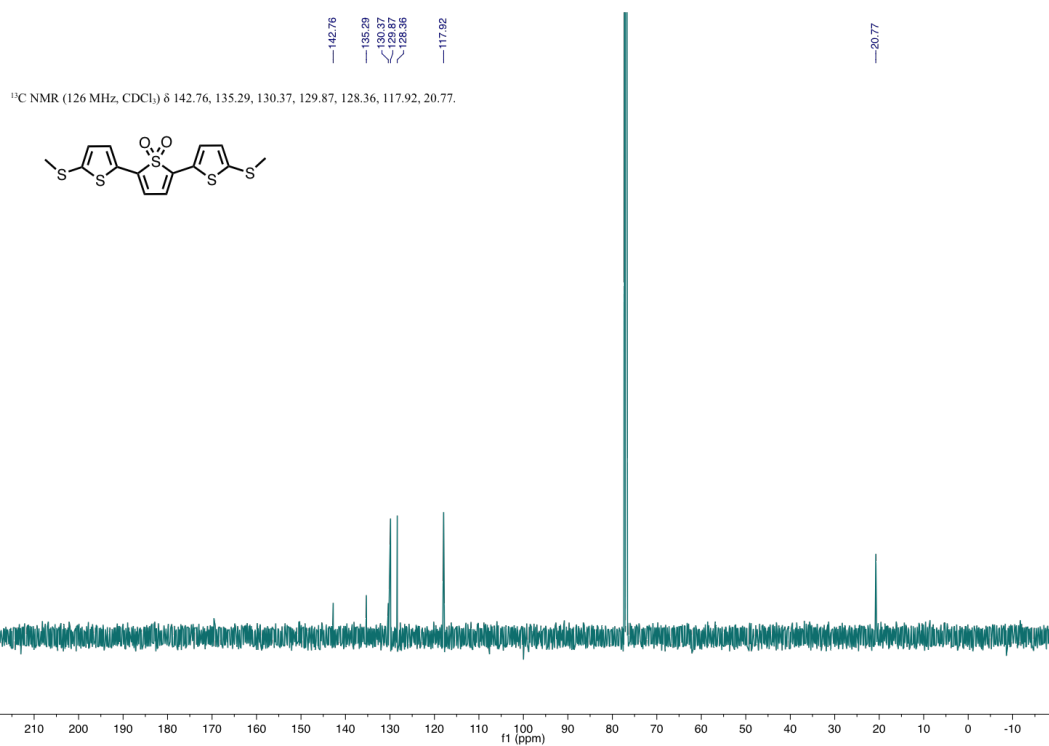
<sup>13</sup>C NMR of 5,5'''-dithiomethyl-3'',4''-dihexyl-pentathiophene (T5)



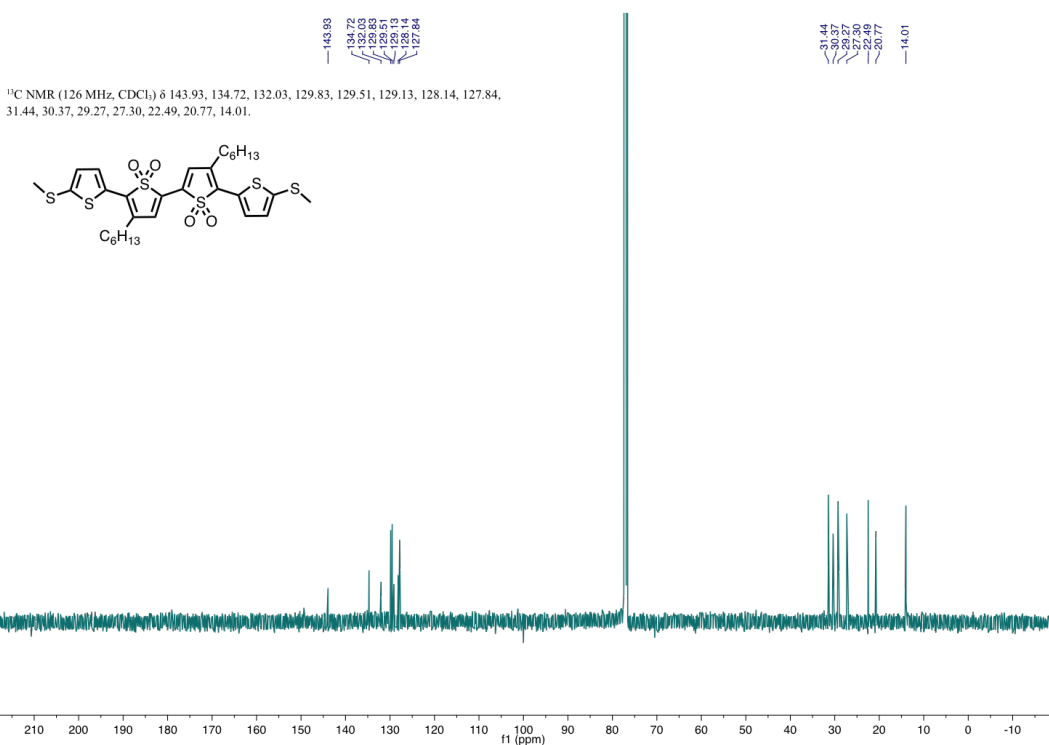
$^{13}\text{C}$  NMR of 3'',4''-dihexyl-5,5'''- bis(methylthio)- sexithiophene (**T6**)



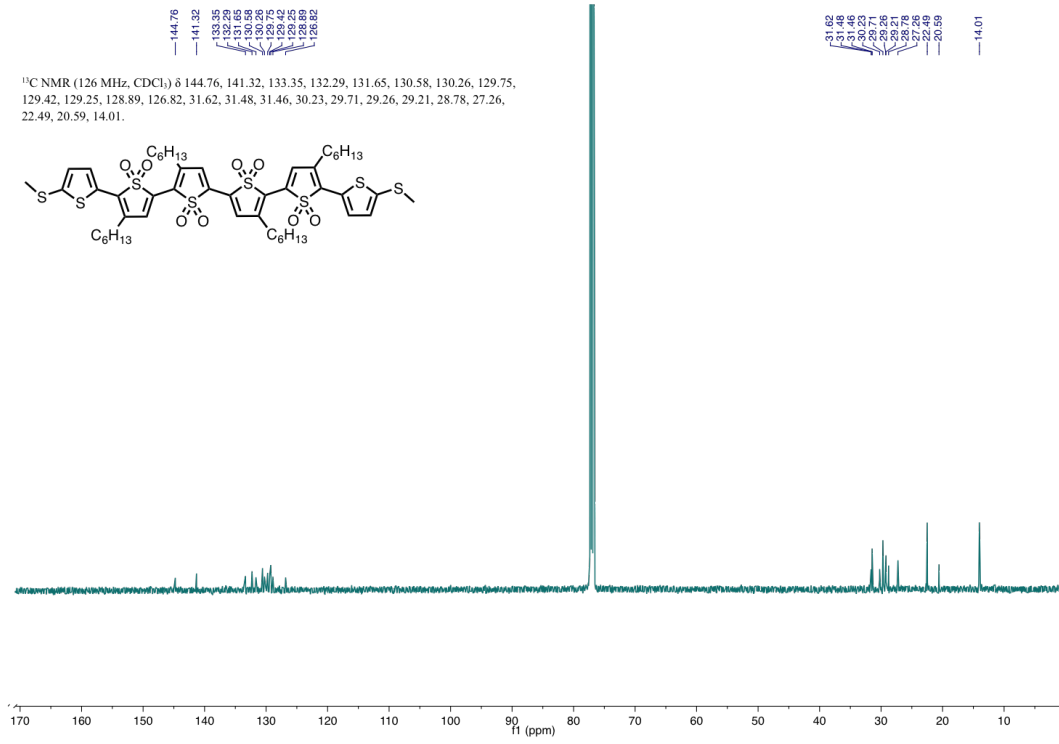
$^{13}\text{C}$  NMR of 2,5-dibromothiophene-1,1-dioxide (**4.1**)



<sup>13</sup>C NMR of 5,5"-bis(methylthio)-terthiophene-1,1-dioxide (**TDO1**)



<sup>13</sup>C NMR of 3',4"-dihexyl-5,5"-bis(methylthio)-quaterthiophene-tetraoxide (**TDO2**)



<sup>13</sup>C NMR of 3',3'',4'',4'''-tetrahexyl-bis(methylthio)-sexithiophene-octaoxide (**TD04**)

## Bibliography

- [1] K. S. Novoselov, A. K. Geim, S. V. Morozov, D. Jiang, Y. Zhang, S. V. Dubonos, I. V. Grigorieva, and A. A. Firsov. Electric field effect in atomically thin carbon films. *Science*, 306(5696):666–669, 2004.
- [2] R. Rossetti, S. Nakahara, and L. E. Brus. Quantum size effects in the redox potentials, resonance raman-spectra, and electronic-spectra of cds crystallites in aqueous-solution. *Journal of Chemical Physics*, 79(2):1086–1088, 1983.
- [3] G. E. Moore. *Electronics Magazine*, 38(8), 1965.
- [4] H. S. P. Wong. Beyond the conventional transistor. *Ibm Journal of Research and Development*, 46(2-3):133–168, 2002.
- [5] A. Aviram and M. A. Ratner. Molecular rectifiers. *Chemical Physics Letters*, 29(2):277–283, 1974.
- [6] M. Fuechsle, S. Mahapatra, F. A. Zwanenburg, M. Friesen, M. A. Eriksson, and M. Y. Simmons. Spectroscopy of few-electron single-crystal silicon quantum dots. *Nature Nanotechnology*, 5(7):502–505, 2010.
- [7] K. Moth-Poulsen and T. Bjornholm. Molecular electronics with single molecules in solid-state devices. *Nature Nanotechnology*, 4(9):551–556, 2009.
- [8] G. C. Solomon, C. Herrmann, T. Hansen, V. Mujica, and M. A. Ratner. Exploring local currents in molecular junctions. *Nature Chemistry*, 2(3):223–228, 2010.
- [9] W. Haiss, C. S. Wang, I. Grace, A. S. Batsanov, D. J. Schiffrin, S. J. Higgins, M. R. Bryce, C. J. Lambert, and R. J. Nichols. Precision control of single-molecule electrical junctions. *Nature Materials*, 5(12):995–1002, 2006.
- [10] F. Chen, J. Hihath, Z. F. Huang, X. L. Li, and N. J. Tao. Measurement of single-molecule conductance. *Annual Review of Physical Chemistry*, 58:535–564, 2007.
- [11] B. Q. Xu and N. J. J. Tao. Measurement of single-molecule resistance by repeated formation of molecular junctions. *Science*, 301(5637):1221–1223, 2003.
- [12] L. Venkataraman, J. E. Klare, C. Nuckolls, M. S. Hybertsen, and M. L. Steigerwald. Dependence of single-molecule junction conductance on molecular conformation. *Nature*, 442(7105):904–907, 2006.
- [13] A. D. Zhao, Q. X. Li, L. Chen, H. J. Xiang, W. H. Wang, S. Pan, B. Wang, X. D. Xiao, J. L. Yang, J. G. Hou, and Q. S. Zhu. Controlling the kondo effect of an adsorbed magnetic ion through its chemical bonding. *Science*, 309(5740):1542–1544, 2005.
- [14] J. Reichert, R. Ochs, D. Beckmann, H. B. Weber, M. Mayor, and H. von Lohneysen. Driving current through single organic molecules. *Physical Review Letters*, 88(17), 2002.
- [15] X. D. Cui, A. Primak, X. Zarate, J. Tomfohr, O. F. Sankey, A. L. Moore, T. A. Moore, D. Gust, G. Harris, and S. M. Lindsay. Reproducible measurement of single-molecule conductivity. *Science*, 294(5542):571–574, 2001.

- [16] S. N. Yaliraki, M. Kemp, and M. A. Ratner. Conductance of molecular wires: Influence of molecule-electrode binding. *Journal of the American Chemical Society*, 121(14):3428–3434, 1999.
- [17] F. Moresco, L. Gross, M. Alemani, K. H. Rieder, H. Tang, A. Gourdon, and C. Joachim. Probing the different stages in contacting a single molecular wire. *Physical Review Letters*, 91(3), 2003.
- [18] I. F. Perepichka and D. F. Perepichka. *Handbook of thiophene-based materials: applications in organic electronics and photonics*. Wiley, Chichester, U.K., 2009.
- [19] G. Dennler, M. C. Scharber, and C. J. Brabec. Polymer-fullerene bulk-heterojunction solar cells. *Advanced Materials*, 21(13):1323–1338, 2009.
- [20] H. Sirringhaus, N. Tessler, and R. H. Friend. Integrated optoelectronic devices based on conjugated polymers. *Science*, 280(5370):1741–1744, 1998.
- [21] H. Sirringhaus, P. J. Brown, R. H. Friend, M. M. Nielsen, K. Bechgaard, B. M. W. Langeveld-Voss, A. J. H. Spiering, R. A. J. Janssen, E. W. Meijer, P. Herwig, and D. M. de Leeuw. Two-dimensional charge transport in self-organized, high-mobility conjugated polymers. *Nature*, 401(6754):685–688, 1999.
- [22] J. Roncali. Conjugated poly(thiophenes) - synthesis, functionalization, and applications. *Chemical Reviews*, 92(4):711–738, 1992.
- [23] T. Yamamoto, K. Sanechika, and A. Yamamoto. Preparation of thermostable and electric-conducting poly(2,5-thienylene). *Journal of Polymer Science Part C-Polymer Letters*, 18(1):9–12, 1980.
- [24] G. Horowitz, D. Fichou, X. Z. Peng, Z. G. Xu, and F. Garnier. A field-effect transistor based on conjugated alpha-sexithienyl. *Solid State Communications*, 72(4):381–384, 1989.
- [25] R. D. McCullough, R. D. Lowe, M. Jayaraman, and D. L. Anderson. Design, synthesis, and control of conducting polymer architectures - structurally homogeneous poly(3-alkylthiophenes). *Journal of Organic Chemistry*, 58(4):904–912, 1993.
- [26] A. J. Heeger. Semiconducting polymers: the third generation. *Chemical Society Reviews*, 39(7):2354–2371, 2010.
- [27] V. Meyer. On a substance that accompanies benzene in coal tar. *Berichte der Deutschen chemischen Gesellschaft*, 16:1465–1478, 1883.
- [28] R. C. Haddon, A. S. Perel, R. C. Morris, T. T. M. Palstra, A. F. Hebard, and R. M. Fleming. C-60 thin-film transistors. *Applied Physics Letters*, 67(1):121–123, 1995.
- [29] F. Diedrich and P. J. Stang. *Metal Catalyzed Cross-coupling Reactions*. Wiley-VCH, 2006.
- [30] X. Y. Cai, M. W. Burand, C. R. Newman, D. A. da Silva, T. M. Pappenfus, M. M. Bader, J. L. Bredas, K. R. Mann, and C. D. Frisbie. N- and p-channel transport behavior in thin film transistors based on tricyanovinyl-capped oligothiophenes. *Journal of Physical Chemistry B*, 110(30):14590–14597, 2006.

- [31] Y. Y. Liang, D. Q. Feng, Y. Wu, S. T. Tsai, G. Li, C. Ray, and L. P. Yu. Highly efficient solar cell polymers developed via fine-tuning of structural and electronic properties. *Journal of the American Chemical Society*, 131(22):7792–7799, 2009.
- [32] C. R. Newman, C. D. Frisbie, D. A. da Silva, J. L. Bredas, P. C. Ewbank, and K. R. Mann. Introduction to organic thin film transistors and design of n-channel organic semiconductors. *Chemistry of Materials*, 16(23):4436–4451, 2004.
- [33] B. Q. Xu, X. L. Li, X. Y. Xiao, H. Sakaguchi, and N. J. Tao. Electromechanical and conductance switching properties of single oligothiophene molecules. *Nano Letters*, 5(7):1491–1495, 2005.
- [34] R. Yamada, H. Kumazawa, T. Noutoshi, S. Tanaka, and H. Tada. Electrical conductance of oligothiophene molecular wires. *Nano Letters*, 8(4):1237–1240, 2008.
- [35] E. Leary, H. Hobenreich, S. J. Higgins, H. van Zalinge, W. Haiss, R. J. Nichols, C. M. Finch, I. Grace, C. J. Lambert, R. McGrath, and J. Smerdon. Single-molecule solvation-shell sensing. *Physical Review Letters*, 102(8), 2009.
- [36] G. Barbarella, L. Favaretto, G. Sotgiu, M. Zambianchi, L. Antolini, O. Pudova, and A. Bongini. Oligothiophene-s,s-dioxides. synthesis and electronic properties in relation to the parent oligothiophenes. *Journal of Organic Chemistry*, 63(16):5497–5506, 1998.
- [37] G. Barbarella, O. Pudova, C. Arbizzani, M. Mastragostino, and A. Bongini. Oligothiophene-s,s-dioxides: a new class of thiophene-based materials. *Journal of Organic Chemistry*, 63(5):1742–1745, 1998.
- [38] G. Barbarella, L. Favaretto, G. Sotgiu, M. Zambianchi, V. Fattori, M. Cocchi, F. Cacialli, G. Gigli, and R. Cingolani. Modified oligothiophenes with high photo- and electroluminescence efficiencies. *Advanced Materials*, 11(16):1375–1379, 1999.
- [39] K. Tanaka, S. L. Wang, and T. Yamabe. Electronic-structures of substituted derivatives of polythiophene - design of narrow-band-gap polymers. *Synthetic Metals*, 30(1):57–65, 1989.
- [40] C. Arbizzani, G. Barbarella, A. Bongini, L. Favaretto, M. Mastragostino, P. Ostoja, O. Pudova, and M. Zambianchi. Oligothiophene-s,s-dioxides: towards n-type semiconductor oligothiophenes? *Optical Materials*, 9(1-4):43–45, 1998.
- [41] E. Amir and S. Rozen. Synthesis of [all]-s,s-dioxide oligothiophenes using hof.ch3cn. *Angewandte Chemie-International Edition*, 44(45):7374–7378, 2005.
- [42] S. Potash and S. Rozen. New conjugated oligothiophenes containing the unique arrangement of internal adjacent [all]-s,s-oxygenated thiophene fragments. *Chemistry-a European Journal*, 19(17):5289–5296, 2013.
- [43] J. R. Widawsky, P. Darancet, J. B. Neaton, and L. Venkataraman. Simultaneous determination of conductance and thermopower of single molecule junctions. *Nano Letters*, 12 (1):354–358, 2012.

- [44] J. R. Widawsky, W. Chen, H. Vazquez, T. Kim, R. Breslow, M. S. Hybertsen, and L. Venkataraman. Length-dependent thermopower of highly conducting au-c bonded single molecule junctions. *Nano Letters*, 13(6):2889–2894, 2013.
- [45] E. J. Dell, B. Capozzi, K. H. DuBay, T. C. Berkelbach, J. R. Moreno, D. R. Reichman, L. Venkataraman, and L. M. Campos. Impact of molecular symmetry on single-molecule conductance. *Journal of the American Chemical Society*, 135(32):11724–11727, 2013.
- [46] Y. Q. Xue and M. A. Ratner. Microscopic theory of single-electron tunneling through molecular-assembled metallic nanoparticles. *Physical Review B*, 68(23), 2003.
- [47] S. H. Ke, H. U. Baranger, and W. T. Yang. Molecular conductance: Chemical trends of anchoring groups. *Journal of the American Chemical Society*, 126(48):15897–15904, 2004.
- [48] K. H. Muller. Effect of the atomic configuration of gold electrodes on the electrical conduction of alkanedithiol molecules. *Physical Review B*, 73(4), 2006.
- [49] J. M. Beebe, V. B. Engelkes, L. L. Miller, and C. D. Frisbie. Contact resistance in metal-molecule-metal junctions based on aliphatic sams: Effects of surface linker and metal work function. *Journal of the American Chemical Society*, 124(38):11268–11269, 2002.
- [50] Y. B. Hu, Y. Zhu, H. J. Gao, and H. Guo. Conductance of an ensemble of molecular wires: A statistical analysis. *Physical Review Letters*, 95(15), 2005.
- [51] H. Basch, R. Cohen, and M. A. Ratner. Interface geometry and molecular junction conductance: Geometric fluctuation and stochastic switching. *Nano Letters*, 5(9):1668–1675, 2005.
- [52] S. Y. Quek, M. Kamenetska, M. L. Steigerwald, H. J. Choi, S. G. Louie, M. S. Hybertsen, J. B. Neaton, and L. Venkataraman. Mechanically controlled binary conductance switching of a single-molecule junction. *Nature Nanotechnology*, 4(4):230–234, 2009.
- [53] Y. S. Park, J. R. Widawsky, M. Kamenetska, M. L. Steigerwald, M. S. Hybertsen, C. Nuckolls, and L. Venkataraman. Frustrated rotations in single-molecule junctions. *Journal of the American Chemical Society*, 131(31):10820–+, 2009.
- [54] A. Mishchenko, D. Vonlanthen, V. Meded, M. Burkle, C. Li, I. V. Pobelov, A. Bagrets, J. K. Viljas, F. Pauly, F. Evers, M. Mayor, and T. Wandlowski. Influence of conformation on conductance of biphenyl-dithiol single-molecule contacts. *Nano Letters*, 10(1):156–163, 2010.
- [55] Y. S. Park, A. C. Whalley, M. Kamenetska, M. L. Steigerwald, M. S. Hybertsen, C. Nuckolls, and L. Venkataraman. Contact chemistry and single-molecule conductance: A comparison of phosphines, methyl sulfides, and amines. *Journal of the American Chemical Society*, 129(51):15768–+, 2007.
- [56] S. Tanaka, S. Tamba, D. Tanaka, A. Sugie, and A. Mori. Synthesis of well-defined head-to-tail-type oligothiophenes by regioselective deprotonation of 3-substituted thiophenes and nickel-catalyzed cross-coupling reaction. *Journal of the American Chemical Society*, 133(42):16734–16737, 2011.

- [57] N. Miyaura, K. Yamada, and A. Suzuki. New stereospecific cross-coupling by the palladium-catalyzed reaction of 1-alkenylboranes with 1-alkenyl or 1-alkynyl halides. *Tetrahedron Letters*, 20(36):3437–3440, 1979.
- [58] K. H. DuBay, M. L. Hall, T. F. Hughes, C. J. Wu, D. R. Reichman, and R. A. Friesner. Accurate force field development for modeling conjugated polymers. *Journal of Chemical Theory and Computation*, 8(11):4556–4569, 2012.
- [59] K. J. Bowers, R. O. Dror, and D. E. Shaw. The midpoint method for parallelization of particle simulations. *Journal of Chemical Physics*, 124(18), 2006.
- [60] B. Capozzi, E. J. Dell, T. C. Berkelbach, D. R. Reichman, L. Venkataraman, and L. M. Campos. Length-dependent conductance of oligothiophenes. *Journal of the American Chemical Society*, 136(29):10486–10492, 2014.
- [61] S. K. Lee, R. Yamada, S. Tanaka, G. S. Chang, Y. Asai, and H. Tada. Universal temperature crossover behavior of electrical conductance in a single oligothiophene molecular wire. *Acs Nano*, 6(6):5078–5082, 2012.
- [62] Y. Le, M. Endou, S. K. Lee, R. Yamada, H. Tada, and Y. Aso. Completely encapsulated oligothiophenes: Synthesis, properties, and single-molecule conductance. *Angewandte Chemie-International Edition*, 50(50):11980–11984, 2011.
- [63] D. Milstein and J. K. Stille. Palladium-catalyzed coupling of tetraorganotin compounds with aryl and benzyl halides - synthetic utility and mechanism. *Journal of the American Chemical Society*, 101(17):4992–4998, 1979.
- [64] M. Takahashi, K. Masui, H. Sekiguchi, N. Kobayashi, A. Mori, M. Funahashi, and N. Tamaoki. Palladium-catalyzed c-h homocoupling of bromothiophene derivatives and synthetic application to well-defined oligothiophenes. *Journal of the American Chemical Society*, 128(33):10930–10933, 2006.
- [65] R. S. Klausen, J. R. Widawsky, M. L. Steigerwald, L. Venkataraman, and C. Nuckolls. Conductive molecular silicon. *Journal of the American Chemical Society*, 134(10):4541–4544, 2012.
- [66] V. B. Engelkes, J. M. Beebe, and C. D. Frisbie. Length-dependent transport in molecular junctions based on sams of alkanethiols and alkanedithiols: Effect of metal work function and applied bias on tunneling efficiency and contact resistance. *Journal of the American Chemical Society*, 126(43):14287–14296, 2004.
- [67] W. B. Chen, J. R. Widawsky, H. Vazquez, S. T. Schneebeli, M. S. Hybertsen, R. Breslow, and L. Venkataraman. Highly conducting pi-conjugated molecular junctions covalently bonded to gold electrodes. *Journal of the American Chemical Society*, 133(43):17160–17163, 2011.
- [68] C. Li, I. Pobelov, T. Wandlowski, A. Bagrets, A. Arnold, and F. Evers. Charge transport in single au vertical bar alkanedithiol vertical bar au junctions: Coordination geometries and conformational degrees of freedom. *Journal of the American Chemical Society*, 130(1):318–326, 2008.

- [69] M. S. Hybertsen, L. Venkataraman, J. E. Klare, A. CWhalley, M. L. Steigerwald, and C. Nuckolls. Amine-linked single-molecule circuits: systematic trends across molecular families. *Journal of Physics-Condensed Matter*, 20(37), 2008.
- [70] A. Salomon, D. Cahen, S. Lindsay, J. Tomfohr, V. B. Engelkes, and C. D. Frisbie. Comparison of electronic transport measurements on organic molecules. *Advanced Materials*, 15(22):1881–1890, 2003.
- [71] J. He, F. Chen, J. Li, O. F. Sankey, Y. Terazono, C. Herrero, D. Gust, T. A. Moore, A. L. Moore, and S. M. Lindsay. Electronic decay constant of carotenoid polyenes from single-molecule measurements. *Journal of the American Chemical Society*, 127(5):1384–1385, 2005.
- [72] W. B. Davis, W. A. Svec, M. A. Ratner, and M. R. Wasielewski. Molecular-wire behaviour in p-phenylenevinylene oligomers. *Nature*, 396(6706):60–63, 1998.
- [73] J. S. Meisner, M. Kamenetska, M. Krikorian, M. Steigerwald, L. Venkataraman, and C. Nuckolls. Single-molecule potentiometer: Oligoene functional materials. *Abstracts of Papers of the American Chemical Society*, 242, 2011.
- [74] Z. L. Cheng, R. Skouta, H. Vazquez, J. R. Widawsky, S. Schneebeli, W. Chen, M. S. Hybertsen, R. Breslow, and L. Venkataraman. In situ formation of highly conducting covalent au-c contacts for single-molecule junctions. *Nature Nanotechnology*, 6(6):353–357, 2011.
- [75] M. D. Curtis, J. Cao, and J. W. Kampf. Solid-state packing of conjugated oligomers: from pi-stacks to the herringbone structure. *Journal of the American Chemical Society*, 126(13):4318–4328, 2004.
- [76] G. Horowitz, B. Bachet, A. Yassar, P. Lang, F. Demanze, J. L. Fave, and F. Garnier. Growth and characterization of sexithiophene single-crystals. *Chemistry of Materials*, 7 (7):1337–1341, 1995.
- [77] T. Siegrist, R. M. Fleming, R. C. Haddon, R. A. Laudise, A. J. Lovinger, H. E. Katz, P. Bridenbaugh, and D. D. Davis. The crystal-structure of the high-temperature polymorph of alpha-hexathienyl. *Journal of Materials Research*, 10(9):2170–2173, 1995.
- [78] P. Leclerc, M. Surin, P. Viville, R. Lazzaroni, A. F. M. Kilbinger, O. Henze, W. J. Feast, M. Cavallini, F. Biscarini, A. P. H. J. Schenning, and E. W. Meijer. About oligothiophene self-assembly: From aggregation in solution to solid-state nanostructures. *Chemistry of Materials*, 16(23):4452–4466, 2004.
- [79] S. Ellinger, U. Ziener, U. Thewalt, K. Landfester, and M. Moller. Synthesis and self-organization of alpha,omega-substituted oligothiophenes with long, branched alkyl substituents. *Chemistry of Materials*, 19(5):1070–1075, 2007.
- [80] A. B. Nepomnyashchii, R. J. Ono, D. M. Lyons, J. L. Sessler, C. W. Bielawski, and A. J. Bard. Oligothiophene nanoparticles: Photophysical and electrogenerated chemiluminescence studies. *Journal of Physical Chemistry Letters*, 3(15):2035–2038, 2012.

- [81] M. Kamenetska, M. Koentopp, A. C. Whalley, Y. S. Park, M. L. Steigerwald, C. Nuckles, M. S. Hybertsen, and L. Venkataraman. Formation and evolution of single-molecule junctions. *Physical Review Letters*, 102(12), 2009.
- [82] H. Vazquez, R. Skouta, S. Schneebeli, M. Kamenetska, R. Breslow, L. Venkataraman, and M. S. Hybertsen. Probing the conductance superposition law in single-molecule circuits with parallel paths. *Nature Nanotechnology*, 7(10):663–667, 2012.
- [83] K. Yoshizawa, T. Tada, and A. Staykov. Orbital views of the electron transport in molecular devices. *Journal of the American Chemical Society*, 130(29):9406–9413, 2008.
- [84] C. C. Chi, I. F. Pai, and W. S. Chung. Thermal and microwave assisted reactions of 2,5-disubstituted thienosultines with [60]fullerene: non-kekule biradicals and self-sensitized oxygenation of the cycloadduct. *Tetrahedron*, 60(48):10869–10876, 2004.
- [85] E. J. Dell, B. Capozzi, J. L. Xia, L. Venkataraman, and L. M. Campos. Molecular length dictates the nature of charge carriers in single-molecule junctions of oxidized oligothiophenes. *Nature Chemistry*, 7(3):209–214, 2015.
- [86] H. A. Ho, H. Brisset, E. H. Elandaloussi, P. Frere, and J. Roncali. Thiophene-based conjugated oligomers and polymers with high electron affinity. *Advanced Materials*, 8(12):990–994, 1996.
- [87] P. M. Beaujuge and J. M. J. Fréchet. Molecular design and ordering effects in pi-functional materials for transistor and solar cell applications. *Journal of the American Chemical Society*, 133(50):20009–20029, 2011.
- [88] E. J. Dell and L. M. Campos. The preparation of thiophene-s,s-dioxides and their role in organic electronics. *Journal of Materials Chemistry*, 22(26):12945–12952, 2012.
- [89] M. S. Raasch, P. H. Benders, D. N. Reinhoudt, and W. P. Trompenaars. *Chemistry of Heterocyclic Compounds*. Wiley & Sons, New York, 1985.
- [90] S. Rozen and M. Kol. Olefin epoxidation using elemental fluorine. *Journal of Organic Chemistry*, 55(17):5155–5159, 1990.
- [91] S. Rozen. Elemental fluorine and hof.ch3cn in service of general organic chemistry. *European Journal of Organic Chemistry*, 5(12):2433–2447, 2005.
- [92] S. Rozen and Y. Bareket. Oxidation of sulfur-containing compounds with hof.ch3cn. *Journal of Organic Chemistry*, 62(5):1457–1462, 1997.
- [93] G. Li, V. Shrotriya, J. S. Huang, Y. Yao, T. Moriarty, K. Emery, and Y. Yang. High-efficiency solution processable polymer photovoltaic cells by self-organization of polymer blends. *Nature Materials*, 4(11):864–868, 2005.
- [94] P. Sonar, E. L. Williams, S. P. Singh, and A. Dodabalapur. Thiophene-benzothiadiazole-thiophene (d-a-d) based polymers: effect of donor/acceptor moieties adjacent to d-a-d segment on photophysical and photovoltaic properties. *Journal of Materials Chemistry*, 21(28):10532–10541, 2011.

- [95] L. E. Bolivar Martinez, M. C. dos Santos, and D. S. Galvao. Electronic structure of push-pull molecules based on thiophene oligomers. *Journal of Physical Chemistry*, 100(26):11029–11032, 1996.
- [96] I. Visoly-Fisher, K. Daie, Y. Terazono, C. Herrero, F. Fungo, L. Otero, E. Durantini, J. J. Silber, L. Sereno, D. Gust, T. A. Moore, A. L. Moore, and S. M. Lindsay. Conductance of a biomolecular wire. *Proceedings of the National Academy of Sciences of the United States of America*, 103(23):8686–8690, 2006.
- [97] Y. Q. Xue, S. Datta, and M. A. Ratner. Charge transfer and "band lineup" in molecular electronic devices: A chemical and numerical interpretation. *Journal of Chemical Physics*, 115(9):4292–4299, 2001.
- [98] G. Heimel, L. Romaner, J. L. Bredas, and E. Zojer. Interface energetics and level alignment at covalent metal-molecule junctions: pi-conjugated thiols on gold. *Physical Review Letters*, 96(19), 2006.
- [99] L. Venkataraman, J. E. Klare, I. W. Tam, C. Nuckolls, M. S. Hybertsen, and M. L. Steigerwald. Single-molecule circuits with well-defined molecular conductance. *Nano Letters*, 6(3):458–462, 2006.
- [100] A. Mishchenko, L. A. Zotti, D. Vonlanthen, M. Burkle, F. Pauly, J. C. Cuevas, M. Mayor, and T. Wandlowski. Single-molecule junctions based on nitrile-terminated biphenyls: A promising new anchoring group. *Journal of the American Chemical Society*, 133(2):184–187, 2011.
- [101] C. A. Martin, D. Ding, J. K. Sorensen, T. Bjornholm, J. M. van Ruitenbeek, and H. S. J. van der Zant. Fullerene-based anchoring groups for molecular electronics. *Journal of the American Chemical Society*, 130(40):13198–13199, 2008.
- [102] A. Facchetti, M. Mushrush, H. E. Katz, and T. J. Marks. n-type building blocks for organic electronics: A homologous family of fluorocarbon-substituted thiophene oligomers with high carrier mobility. *Advanced Materials*, 15(1):33–+, 2003.
- [103] Y. N. Li, S. P. Singh, and P. Sonar. A high mobility p-type dpp-thieno[3,2-b]thiophene copolymer for organic thin-film transistors. *Advanced Materials*, 22(43):4862–+, 2010.
- [104] J. E. Anthony, A. Facchetti, M. Heeney, S. R. Marder, and X. W. Zhan. n-type organic semiconductors in organic electronics. *Advanced Materials*, 22(34):3876–3892, 2010.
- [105] M. H. Yoon, S. A. DiBenedetto, A. Facchetti, and T. J. Marks. Organic thin-film transistors based on carbonyl-functionalized quaterthiophenes: High mobility n-channel semiconductors and ambipolar transport. *Journal of the American Chemical Society*, 127(5):1348–1349, 2005.
- [106] A. Facchetti, M. H. Yoon, C. L. Stern, G. R. Hutchison, M. A. Ratner, and T. J. Marks. Building blocks for n-type molecular and polymeric electronics. perfluoroalkyl- versus alkyl-functionalized ligothiophenes (nts; n=2-6). systematic synthesis, spectroscopy, electrochemistry, and solid-state organization. *Journal of the American Chemical Society*, 126(41):13480–13501, 2004.

- [107] Y. Ie, M. Nitani, M. Ishikawa, K. Nakayama, H. Tada, T. Kaneda, and Y. Aso. Electronegative oligothiophenes for n-type semiconductors: Difluoromethylene-bridged bithiophene and its oligomers. *Organic Letters*, 9(11):2115–2118, 2007.
- [108] Y. Le, Y. Umemoto, M. Okabe, T. Kusunoki, K. I. Nakayama, Y. J. Pu, J. Kido, H. Tada, and Y. Aso. Electronegative oligothiophenes based on difluorodioxocyclopentene-annelated thiophenes: Synthesis, properties, and n-type fet performances. *Organic Letters*, 10(5):833–836, 2008.
- [109] N. Camaioni, G. Ridolfi, V. Fattori, L. Favaretto, and G. Barbarella. Oligothiophene-s,s-dioxides as a class of electron-acceptor materials for organic photovoltaics. *Applied Physics Letters*, 84(11):1901–1903, 2004.
- [110] S. J. Wei, J. L. Xia, E. J. Dell, Y. V. Jiang, R. Song, H. Lee, P. Rodenbough, A. L. Briseno, and L. M. Campos. Bandgap engineering through controlled oxidation of polythiophenes. *Angewandte Chemie-International Edition*, 53(7):1832–1836, 2014.
- [111] M. C. Scharber, D. Wuhlbacher, M. Koppe, P. Denk, C. Waldauf, A. J. Heeger, and C. L. Brabec. Design rules for donors in bulk-heterojunction solar cells - towards 10 *Advanced Materials*, 18(6):789–+, 2006.
- [112] J. L. Bredas, R. Silbey, D. S. Boudreaux, and R. R. Chance. Chain-length dependence of electronic and electrochemical properties of conjugated systems - polyacetylene, polyphenylene, polythiophene, and polypyrrole. *Journal of the American Chemical Society*, 105(22):6555–6559, 1983.
- [113] V. D. Parker. Problem of assigning values to energy changes of electrode-reactions. *Journal of the American Chemical Society*, 96(17):5656–5659, 1974.
- [114] M. Paulsson and S. Datta. Thermoelectric effect in molecular electronics. *Physical Review B*, 67(24), 2003.
- [115] J. A. Malen, P. Doak, K. Baheti, T. D. Tilley, R. A. Segalman, and A. Majumdar. Identifying the length dependence of orbital alignment and contact coupling in molecular heterojunctions. *Nano Letters*, 9(3):1164–1169, 2009.
- [116] K. Baheti, J. A. Malen, P. Doak, T. D. Tilley, A. Majumdar, and R. A. Segalman. Probing the chemistry of molecular heterojunctions using thermoelectricity. *Abstracts of Papers of the American Chemical Society*, 235, 2008.
- [117] P. Reddy, S. Y. Jang, R. A. Segalman, and A. Majumdar. Thermoelectricity in molecular junctions. *Science*, 315(5818):1568–1571, 2007.
- [118] C. Evangelisti, K. Gillemot, E. Leary, M. T. Gonzalez, G. Rubio-Bollinger, C. J. Lambert, and N. Aguirre. Engineering the thermopower of c-60 molecular junctions. *Nano Letters*, 13(5):2141–2145, 2013.